Space-Time Processing for the Wideband-CDMA System

by

Kazi A. Zahid

Thesis submitted to the faculty of the
Virginia Polytechnic Institute and State University
in partial fulfillment of the requirements for the degree of

MASTER OF SCIENCE

in

Electrical Engineering

Approved:

Dr. Jeffrey H. Reed	Dr. William H. Tranter
Dr. Brian D. Woerner	Dr. Robert J. Boyle

January, 2001
Blacksburg, Virginia

Keywords: Beamforming, RAKE receiver, 2-D RAKE, Spatio-temporal channel, W-CDMA

Copyright 2000, Kazi A. Zahid

Space-Time Processing for the Wideband-CDMA System

by

Kazi A. Zahid

(Abstract)

Deployment of antenna arrays is a very promising solution to reduce the Multiple Access Interference (MAI) from high data rate users in the Wideband Code Division Multiple Access (W-CDMA) system. Combining the antenna array with a RAKE receiver, both of which exploits multipath diversity, can significantly improve the system performance. In this research, we investigate the performance of these beamformer-RAKE receivers, also known as two-dimensional (2-D) RAKE receiver, for the reverse link of the W-CDMA system. We consider three different Pilot Symbol Assisted (PSA) beamforming techniques, Direct Matrix Inversion (DMI), Least-Mean Square (LMS) and Recursive Least Square (RLS) adaptive algorithms. Two different Geometrically Based Single Bounce (GBSB) statistical channel models are considered, one, which is more suitable for array processing, and the other is conductive to RAKE combining. The performances of the 2-D RAKE receivers are evaluated in these two channel models as a function of the number of antenna elements and RAKE fingers. It is shown that, in both the cases, the 2-D RAKE receiver outperforms the conventional RAKE receiver and the conventional beamformer by a significant margin. Also, the output SINR expression of a 2-D RAKE receiver with the general optimum beamformer is derived.

ACKNOWLEDGEMENTS

First of all I would like to express my gratitude to my academic advisor, Dr. Jeffrey H. Reed, for the invaluable support, guidance and encouragement he has provided over the duration of this research. I thank him for presenting me the opportunity to work in a research topic like this, which I enjoyed every moment. I also thank my committee members, Dr. William H. Tranter, Dr. Brian D. Woerner and Dr. Robert J. Boyle for carefully reviewing my thesis and providing valuable suggestions.

I wish to thank Raqibul Mostafa for his continuous encouragement and fruitful discussion over the course of this research. He advised and guided me like his younger brother. I also thank Fakhrul Alam and James Hicks for their valuable suggestions in simulation and analysis of our proposed system.

I would like to thank Dr. Jong H. Kim of LG Electronics for some crucial suggestions he provided in the design of the PSA 2-D RAKE receiver for W-CDMA. I also thank Jai Tsai for his critical discussion, which helped me to understand many aspects of space-time processing for W-CDMA. I also thank Saffet Bayram for his continuous encouragement in my research.

I wish to thank US Navy's NAVCITTI program, LG Electronics, Raytheon and Texas Instruments for providing the financial support for this work.

Most of all, I would like to thank my parents, my brother and my sister for their love and emotional support. I couldn't have come up to this point in my life without their unfathomable and everlasting care for me.

TABLE OF CONTENTS

1 Introduction **1**

2 Overview of Space-time processing for CDMA **5**

2.1 Space-time Combining Schemes 6

2.1.1 Space-time RAKE Receiver for CDMA 7

2.1.2 Generic architecture of 2-D RAKE Receiver 10

2.1.2.1 Beam-space beamforming 11

2.1.2.2 Bearing estimation beamforming 12

2.1.2.3 Eigenfilter beamforming 12

2.1.3 Antenna diversity in IS-95 CDMA 13

2.2 2-D RAKE receiver structures 14

2.2.1 Pilot symbol Assisted (PSA) 2-D RAKE structures 14

2.2.2 Blind 2-D RAKE structures 15

2.3 Summary 17

3 Spatio-temporal Channel Models **18**

3.1 Geometrically Based Single Bounce Elliptical Model 19

3.1.1 Introduction 19

3.1.2 Assumptions 19

3.1.3 Geometry and Notation 20

3.1.4 Mathematical Formulation 20

3.1.5 Generation of Samples of the Elliptical Channel Model 22

3.2 Geometrically Based Single Bounce Circular Model 24

3.2.1 Introduction 24

3.2.2 Assumptions 24

3.2.3 Geometry and Notation 25

3.2.4 Mathematical Formulation 26

3.2.5 Generation of Samples of the Circular Channel Model 27
3.3 Channel parameters from the W-CDMA system perspective 28
3.3.1 Power-delay profile 28
3.3.2 Angle Spread 30
3.3.3 Range of channel parameters for uplink W-CDMA 33
3.4 Summary 34
4 Overview of Uplink W-CDMA Standard 35
4.1 Uplink Physical Channels 36
4.1.1 Dedicated Uplink Physical Channels 36
4.1.2 Common Uplink Physical channels 38
4.2 Spreading and Modulation of Uplink DPDCH and DPCCH 38
4.3 Uplink Code generation and allocation 39
4.3.1 Channelization Codes 39
4.3.1.1 Properties of channelization codes 40
4.3.2 Scrambling Codes 41
4.3.2.1 Uplink long scrambling code 41
4.3.2.2 Properties of Uplink Long Scrambling Code 43
4.4 Channel Coding 43
4.4.1 Error Detection 44
4.4.2 Error Correction 44
4.5 Summary 45
5 System Modeling and Analysis 46
5.1 Transmitter Model 47
5.2 Channel Description 48
5.3 Receiver Model 50
5.3.1 Direct Matrix Inversion (DMI) beamforming 53
5.3.2 Least Mean Square (LMS) Adaptive beamforming 55
5.3.3 Recursive Least-Square (RLS) Adaptive Beamforming 56
5.4 Generalized Optimum Output SINR Analysis 58
5.5 Summary 60
6 Simulation Results and Discussion 61

6.1 Simulation Set Up 62
6.1.1 Transmitter Specifications 62
6.2 Multipath Channel Generation 64
6.2.1 Microcellular Environment 64
6.2.2 Macrocellular Environment 65
6.3 Receiver Operational Block 66
6.4 Simulation Environment 68
6.5 Simulation Results 68
6.5.1 BER performance Versus Number of Users 68
6.5.1.1 Macrocellular Circular Channel Environment 69
6.5.1.1.1 LMS Beamforming 69
6.5.1.1.2 DMI beamforming 71
6.5.1.1.3 RLS beamforming 73
6.5.1.2 Microcellular Elliptical Channel Environment 75
6.5.1.2.1 LMS Beamforming 75
6.5.1.2.2 DMI Beamforming 78
6.5.1.2.3 RLS beamforming 80
6.5.2 BER performance vs. Eb/No 82
6.5.2.1 Macrocellular Circular Channel Environment 82
6.5.2.1.1 LMS beamforming 82
6.5.2.1.2 DMI beamforming 87
6.5.2.1.3 RLS beamforming 90
6.5.2.2 Microcellular Elliptical Channel Environment 94
6.5.2.2.1 LMS beamforming 94
6.5.2.2.2 DMI beamforming 97
6.5.2.2.3 RLS beamforming 99
6.6 Summary 102
7 Conclusions and Future Work **103**
7.1 Future Work 104
References **105**
Vita **109**

LIST OF FIGURES

Figure 2.1.1: Block Diagram of a RAKE Receiver 7
Figure 2.1.2: A RAKE Receiver Structure for CDMA system 8
Figure 2.1.3: 1-D RAKE Receiver Figure 2.1.3(b): 2-D RAKE Receiver 10
Figure 2.1.4: A generic 2-D RAKE receiver architecture 11
Figure 2.1.5: Block diagram of the base station receiver in IS-95 13
Figure 2.2.1: Pilot Symbol Assisted (PSA) coherent 2-D RAKE receiver structure 14
Figure 2.2.2: Block Diagram of a 2-D RAKE Receiver for the Base station of IS-95 16
Figure 3.1.1: Geometry of the GBSB elliptical channel model 20
Figure 3.2.1: Geometry of the Circular Scattering Channel Model 25
Figure 3.3.1: Power-Delay profile for elliptical model with different BS to mobile distance 29
Figure 3.3.2: Power-delay profile for elliptical model with different BS to mobile distance 30
Figure 3.3.3: Angle spread for the elliptical model with different BS to mobile distance 31
Figure 3.3.4: Angle spread for the circular model with different BS to mobile distance 32
Figure 3.3.5: Power-delay profile of ETSI's vehicular A outdoor channel model 33
Figure 4.1.1: Frame Structure for Uplink DPDCH/DPCCH 37
Figure 4.2.1: Spreading and modulation for uplink DPDCH and DPCCH 38
Figure 4.3.1: Code Tree for Generation of OVSF Codes 39
Figure 4.3.2(a): Auto-correlation of a Figure 4.3.2(b): Cross-correlation of two 40
Figure 5.1.1: W-CDMA uplink transmitter model 47
Figure 5.3.1: Base station antenna array receiver model 50
Figure 6.2.1: Multipath propagation scenario for microcellular environments 64
Figure 6.2.2: Multipath propagation model for macrocellular environment 66
Figure 6.3.1: Block diagram of a PSA 2-D RAKE receiver used for simulation 67
Figure 6.5.1: BER performance of a 2-D RAKE receiver with 2-element LMS beamformer 69

Figure 6.5.2: BER performance of a 2-D RAKE receiver with 4-element LMS beamformer 70
Figure 6.5.3: BER performance of a 2-D RAKE receiver with 6-element LMS beamformer 71
Figure 6.5.4: BER performance of a 2-D RAKE receiver with 2-element DMI beamformer..... 72
Figure 6.5.5: BER performance of a 2-D RAKE receiver with 4-element DMI beamformer..... 72
Figure 6.5.6: BER performance of a 2-D RAKE receiver with 6-element DMI beamformer..... 73
Figure 6.5.7: BER performance of a 2-D RAKE receiver with 2-element RLS beamformer 74
Figure 6.5.8: BER performance of a 2-D RAKE receiver with 4-element RLS beamformer 74
Figure 6.5.9: BER performance of a 2-D RAKE receiver with 6-element RLS beamformer 75
Figure 6.5.10: BER performance of a 2-D RAKE receiver with 2-element LMS beamformer ... 76
Figure 6.5.11: BER performance of a 2-D RAKE receiver with 4-element LMS beamformer ... 77
Figure 6.5.12: BER performance of a 2-D RAKE receiver with 6-element LMS beamformer ... 77
Figure 6.5.13: BER performance of a 2-D RAKE receiver with 2-element DMI beamformer.... 78
Figure 6.5.14: BER performance of a 2-D RAKE receiver with 4-element DMI beamformer.... 79
Figure 6.5.15: BER performance of a 2-D RAKE receiver with 6-element DMI beamformer.... 79
Figure 6.5.16: BER performance of a 2-D RAKE receiver with 2-element RLS beamformer 80
Figure 6.5.17: BER performance of a 2-D RAKE receiver with 4-element RLS beamformer 81
Figure 6.5.18: BER performance of a 2-D RAKE receiver with 6-element RLS beamformer 81
Figure 6.5.19: BER vs. Eb/No for a 2-element LMS 2-D RAKE receiver with 2-user scenario . 83
Figure 6.5.20: BER vs. Eb/No for a 2-element LMS 2-D RAKE receiver with 4-user scenario . 83
Figure 6.5.21: BER vs. Eb/No for a 4-element LMS 2-D RAKE receiver with 4-user scenario . 84
Figure 6.5.22: BER vs. Eb/No for a 4-element LMS 2-D RAKE receiver with 8-user scenario . 85
Figure 6.5.23: BER vs. Eb/No for a 6-element LMS 2-D RAKE receiver with 6-user scenario . 86
Figure 6.5.24: BER vs. Eb/No for a 6-element LMS 2-D RAKE receiver with 12-user scenario 86
Figure 6.5.25: BER vs. Eb/No for a 2-element DMI 2-D RAKE receiver with 2-user scenario .. 87
Figure 6.5.26: BER vs. Eb/No for a 2-element DMI 2-D RAKE receiver with 4-user scenario .. 88
Figure 6.5.27: BER vs. Eb/No for a 4-element DMI 2-D RAKE receiver with 4-user scenario .. 88
Figure 6.5.28: BER vs. Eb/No for a 4-element DMI 2-D RAKE receiver with 8-user scenario .. 89
Figure 6.5.29: BER vs. Eb/No for a 6-element DMI 2-D RAKE receiver with 6-user scenario .. 89
Figure 6.5.30: BER vs. Eb/No for a 6-element DMI 2-D RAKE receiver with 12-user scenario 90
Figure 6.5.31: BER vs. Eb/No for a 2-element RLS 2-D RAKE receiver with 2-user scenario .. 91
Figure 6.5.32: BER vs. Eb/No for a 2-element RLS 2-D RAKE receiver with 4-user scenario .. 91

Figure 6.5.33: BER vs. Eb/No for a 4-element RLS 2-D RAKE receiver with 4-user scenario .. 92
Figure 6.5.34: BER vs. Eb/No for a 4-element RLS 2-D RAKE receiver with 8-user scenario .. 92
Figure 6.5.35: BER vs. Eb/No for a 6-element RLS 2-D RAKE receiver with 6-user scenario .. 93
Figure 6.5.36: BER vs. Eb/No for a 6-element RLS 2-D RAKE receiver with 12-user scenario 93
Figure 6.5.37: BER vs. Eb/No for a 2-element LMS 2-D RAKE receiver with 2-user scenario . 94
Figure 6.5.38: BER vs. Eb/No for a 2-element LMS 2-D RAKE receiver with 4-user scenario . 95
Figure 6.5.39: BER vs. Eb/No for a 4-element LMS 2-D RAKE receiver with 4-user scenario . 96
Figure 6.5.40: BER vs. Eb/No for a 4-element LMS 2-D RAKE receiver with 8-user scenario . 96
Figure 6.5.41: BER vs. Eb/No for a 2-element DMI 2-D RAKE receiver with 2-user scenario .. 97
Figure 6.5.42: BER vs. Eb/No for a 2-element DMI 2-D RAKE receiver with 4-user scenario .. 98
Figure 6.5.43: BER vs. Eb/No for a 4-element DMI 2-D RAKE receiver with 4-user scenario .. 98
Figure 6.5.44: BER vs. Eb/No for a 4-element DMI 2-D RAKE receiver with 8-user scenario .. 99
Figure 6.5.45: BER vs. Eb/No for a 2-element RLS 2-D RAKE receiver with 2-user scenario 100
Figure 6.5.46: BER vs. Eb/No for a 2-element RLS 2-D RAKE receiver with 4-user scenario 100
Figure 6.5.47: BER vs. Eb/No for a 4-element RLS 2-D RAKE receiver with 4-user scenario 101
Figure 6.5.48: BER vs. Eb/No for a 4-element RLS 2-D RAKE receiver with 8-user scenario 101

Chapter 1

Introduction

Wideband direct sequence Code Division Multiple Access (W-CDMA) has been widely accepted as the radio access scheme for the third generation (3G) wireless system known as International Mobile Telecommunications-2000 (IMT-2000). One of the major objectives of IMT-2000 is to support high and widely variable data rate users with high quality and achieve enhanced system coverage and capacity. For example, the target specified by IMT-2000 for minimum user data rate is 144 kbps in vehicular environments and 384 kbps in pedestrian environments [Oli99]. But in a Direct Sequence CDMA (DS-CDMA) system where all the users communicate simultaneously within the same frequency band, the high data rate users may cause large Multiple Access Interference (MAI) due to their increased transmission power. This problem is particularly severe in the uplink (mobile to base station) where the users transmit asynchronously, producing the well known near-far problem. In addition to MAI, the received signal is also subjected to multipath fading due to the relative motion between the mobile and the local scatterers. Also, distance dependent path loss and long term fading (shadowing) exist. All of these significantly degrade the uplink system capacity. A promising technique to reduce the MAI and thereby increase the uplink system capacity is to employ an adaptive antenna array [Lib96], [Nag94a], [Nag94b].

An adaptive antenna array is capable of forming a beam towards the desired user and directing the nulls towards the interferers, which is commonly known as beamforming. By doing so, it can reduce the co-channel interference from the other users within its own cell as well as in the neighboring cells, thereby increasing the system capacity. There exist many adaptive antenna array algorithms or beamforming techniques, both blind and Pilot Symbol Assisted (PSA) that

offer different advantages for different environments. However, for a CDMA type system where the users are differentiated by specific code sequences, the performance of a beamforming algorithm depends on the cross-correlation property of the desired user's code sequence. In addition, many beamforming techniques are not applicable for an overloaded system like CDMA, i.e., where the number of users is usually much higher than number of antenna elements. Furthermore, an adaptive array must track fast changes in channel conditions and it's element separation is usually such that fading in different elements are strongly correlated. In practice even though an adaptive array minimizes the MAI to improve the Signal to Interference Ratio (SIR), its performance is limited by multipath fading.

Traditionally, a combination of fast transmit power control and the RAKE receiver is employed for the uplink of a practical CDMA base station [Ada96]. Transmit power control is used to combat the near-far problem by keeping the received Signal power to Interference plus background Noise power Ratio (SINR) for each user at a prescribed target level. The RAKE receiver exploits the frequency selective multipath diversity structure of a channel by combining signals of the desired user propagating along different but resolvable paths. In doing so, it tracks the instantaneous changes in channel conditions and thereby mitigates the effect of fading. However, the performance of a RAKE receiver also depends on how well the desired user's signal is extracted from the interference, which again is determined by the cross-correlation property of the desired user's code sequence and the level of interference. Hence, the performance of a RAKE receiver is interference limited even though by offering fading reduction capability it improves the Signal to Noise Ratio (SNR).

It follows then, that the most obvious way to achieve both MAI suppression and fading reduction is to combine an adaptive antenna array with a RAKE receiver. Such a receiver is commonly known as a space-time or two-dimensional (2-D) RAKE receiver due to the fact that both the spatial and the temporal processing are used to estimate the user's transmitted data. A 2-D RAKE receiver is composed of a beamformer connected to each finger of the subsequent RAKE combiner. The beamformer in a particular RAKE finger tries to direct the beam in the direction of a desired user's multipath component to which the finger is synchronized and steer nulls to the other signals. In doing so, it improves the overall SINR and outperforms both the plain adaptive array and the conventional RAKE receiver.

In this research, we consider the 2-D RAKE receiver for the uplink of the W-CDMA system. Our approach is to combine different PSA adaptive beamforming algorithms with a coherent Maximal Ratio Combining (MRC) RAKE receiver. The reason we concentrate on the PSA beamforming techniques is that the W-CDMA standard specifies pilot symbols in the uplink. These pilot symbols can be used for both beamformer weight calculation and channel estimation required for subsequent coherent RAKE combining. We consider the Direct Matrix Inversion (DMI), Least Mean Square (LMS) and Recursive Least Square (RLS) based adaptive beamforming techniques, which use the pilot symbols as the reference signal. We simulate these PSA based beamformer-RAKE receivers with the W-CDMA reverse link transmitted signal using the Geometrically Based Single Bounce (GBSB) statistical channel models. Our objective is to compare the performance of these 2-D RAKE receivers with the conventional RAKE receiver and the conventional beamformer. We look into the BER and capacity performance of a 2-D RAKE receiver with varying number of antenna elements and RAKE fingers. We also look into the performance tradeoff between antenna array and RAKE in channel conditions that suit beamforming over RAKE combining and vice versa. The performance of different beamforming techniques used in the 2-D RAKE receiver are also compared. Finally, we develop a mathematical formulation for the output SINR of a 2-D RAKE receiver.

The thesis is organized as follows. In Chapter 2, we present a brief overview of the space-time processing intended for the CDMA system. We introduce conventional RAKE and 2-D RAKE receivers, the generic architecture of a 2-D RAKE receiver, PSA and blind 2-D RAKE structures. We also review the antenna diversity implemented in IS-95 base stations. Chapter 3 describes two GBSB spatio-temporal channel models that we use in our simulation. We discuss in detail the generation of channel parameters and their meaningful range for the W-CDMA. The channel models are also characterized qualitatively in terms of multipath power-delay profile and angle spread. In Chapter 4, we introduce the current W-CDMA uplink standard used to simulate the transmitted signal. We briefly present the uplink physical channel format, modulation and spreading, scrambling and spreading code generation and allocation. In Chapter 5, we develop a detailed mathematical description of the overall system. We formulate the W-CDMA uplink transmitter model, a spatio-temporal parametric channel and perform a detailed analysis of a PSA 2-D RAKE receiver. We also derive the output SINR expression for a generalized 2-D RAKE receiver. Chapter 6 describes the simulation environments and presents the simulation

results. A detailed performance comparison of the various PSA 2-D RAKE receivers in the two proposed GBSB channel models is provided in this chapter. Finally, a brief summary and conclusion are provided in chapter 7 along with some suggestions for future work.

Chapter 2

Overview of Space-time Processing for CDMA

A space-time processing system operates simultaneously on multiple antennas by processing signal samples in both spatial and temporal domain. In the receive side, space-time processing can increase the array gain, exploit spatial and temporal diversity effectively and reduce the cochannel and intersymbol interference. On the transmit side the space-time processor can increase the array gain, improve diversity and reduce the generation of cochannel and inter-symbol interference. In a CDMA system where there are a large number of interfering signals, space-time processing techniques have the potential to be very effective. This is due to the fact that, space-time processing can reduce the interference from users within its own cells and from the neighboring cells resulting in better coverage area, BER performance, transmitted mobile power and system capacity [Pau97], [Tho96].

In this chapter, we focus on the space-time processing techniques for the receive side in reverse link of CDMA system. The main focus is on the two-dimensional (2-D) RAKE receivers, which integrate the array processing (beamforming) with a conventional RAKE receiver. The chapter is organized as follows: Section 2.1 provides a brief overview of the different space-time combining schemes, 2-D RAKE receiver architecture and the current antenna diversity approach for IS-95 CDMA systems. In Section 2.2, we explain the structural details of several of these 2-D RAKE receivers. Finally, we summarize the chapter in Section 2.3.

2.1 Space-time Combining Schemes

Two generic approaches for space-time processing in the receiver are commonly considered [Bern96]. They are

1. Cascaded spatio-temporal processing
2. Joint domain spatio-temporal processing

The cascaded spatio-temporal processor consists of a spatial processor whose output is fed into a succeeding temporal processor or it can be the other way around. The processing may be the typical diversity combining techniques such as coherent Maximal Ratio Combining (MRC), noncoherent Equal Gain Combining (EGC). It can also be an optimum combining scheme based on the well-known optimization criteria such as Minimum Mean Squared Error (MMSE), Maximum Signal to Interference plus Noise Ratio (Maximum SINR) and Maximum Likelihood (ML). Both the domains can employ the same processing technique, i.e., either the diversity combining or the optimum combining. Alternately, individual domains can have their unique processing techniques. In this respect, the cascaded space-time processors can be categorized as below

1. Cascaded spatial-diversity temporal-diversity
2. Cascaded spatial-diversity temporal-optimum
3. Cascaded spatial-optimum temporal-diversity
4. Cascaded spatial-optimum temporal-optimum

All of these configurations have their relative merits and demerits in terms of the SINR performance and implementation complexity. It can be expected, that due to its interference suppression capability, an optimum-combining configuration will give a better signal to interference ratio (SIR) performance than a diversity-combining configuration. Alternately, exploitation of the multipath diversity structure in either domain will definitely improve the signal to noise ratio (SNR). The diversity techniques rely on the estimation of various channel parameters such as multipath channel gain and phase, angle of arrivals, etc. The way in which these parameters are estimated determines the required amount of computation. In some cases, noncoherent combining may offer lower complexity structures than coherent combining. In the case of optimum combining, the algorithm that is used to compute the coefficients/weights

necessary for combining determines the computational complexity. Various adaptive techniques are developed to calculate the optimum weights based on the performance criteria as mentioned above [Hay91].

In joint domain processing, the samples in both the spatial domain and the temporal domain are processed simultaneously. The processor in this case computes the overall combiner coefficients/weight vectors by processing signals jointly in both the spatial and the temporal domains.

Again, both the approaches have their relative merits and demerits in terms of SINR performance and system complexity. Cascaded spatio-temporal processors are attractive with respect to complexity for implementation but they give sub-optimum performance. On the other hand, joint domain processing can perform very close to the optimum, but suffers from large computational burden.

2.1.1 Space-time RAKE Receiver for CDMA

In a frequency selective fading environment, the delay spread of the multipath is large compared to the symbol period. CDMA systems can be employed in such a rich multipath environment to exploit the temporal diversity available with multipath. The wider the bandwidth of the spread spectrum signal, the more resolvable the individual multipath components in time. Appropriate combinations of these independently fading paths can reduce the effect of signal strength fluctuation due to fading. Thus intersymbol interference (ISI) is not a problem in a CDMA system since multipaths separated by more than one chip period in time can easily be resolved after matched filtering and despreading. A popular single-user receiver structure for a multipath environment is the RAKE combiner first proposed by Price and Green in [Pri58]. The block diagram in Figure 2.1.1 shows the basic operation of a simplified RAKE receiver [Nag96a].

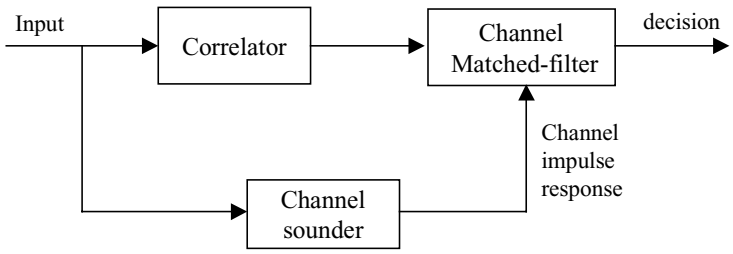

Figure 2.1.1: Block Diagram of a RAKE Receiver

The input spread spectrum signal is first despread by a correlator (matched filter), which is matched to the known (user specific) spreading sequence. The waveform at the output of the correlator will have peaks at instants, which coincide the propagation delays of different multipath components. A succeeding linear transversal filter matched to channel impulse response determined by a channel sounder then constructively combines the contribution from these various peaks. For coherent combining, the channel-matched filter obtains the channel phase information through pilot signals transmitted concurrently with the data signals. In the case when only noncoherent detection is possible, the channel sounder does not provide the phase information and a different combining scheme is usually implemented by the channel-matched filter.

The structure of a RAKE receiver consists of several correlators, each synchronized to a multipath component associated with a particular delay. An implementation of the RAKE receiver is shown in Figure 2.1.2 [Nag96a].

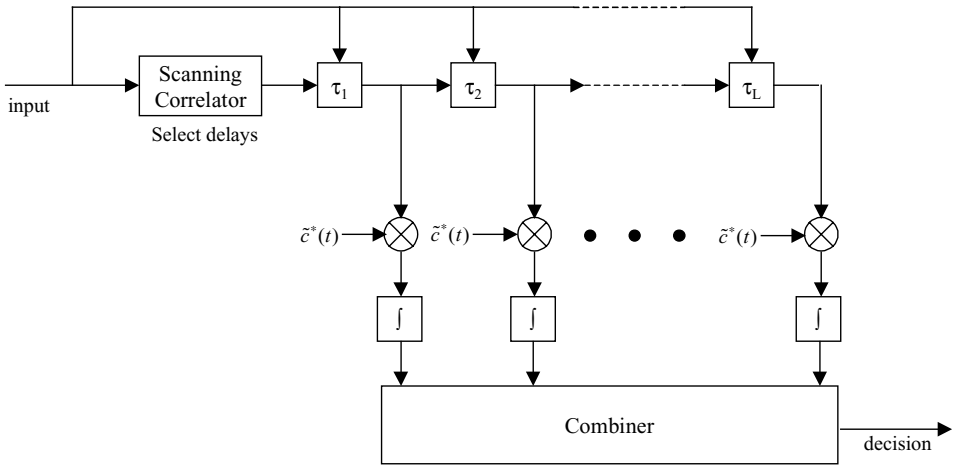

Figure 2.1.2: A RAKE Receiver Structure for CDMA system

The scanning correlator identifies the delays, τ_l, l=1,2…L for the L multipath components. As can be predicted, the performance of the receiver is determined by the number of correlators used. The outputs of the correlators are combined to maximize the SNR. If the combining weights are matched to the discrete channel gain coefficients corresponding to the respective multipath components, it is called Maximal Ratio Combining (MRC), which is also a coherent RAKE receiver. For noncoherent combining, all the weights are set equal and this is termed as Equal Gain Combining (EGC). It is also possible to set the combining weights such that SINR instead of SNR is maximized.

In a conventional CDMA receiver, the channel impulse response parameters (amplitude, phase and delay) for the multipath components separated by more than a chip period are estimated by temporal code filtering. For this purpose either the user's spreading code or a pilot sequence can be used. The signal is then passed through a RAKE correlator that is matched to the channel output and subsequently combined either in a coherent or noncoherent fashion. Since in this case only the temporal structure of the received multipath signals are exploited, it is termed as the one dimensional (1-D) or temporal RAKE receiver. Detailed discussion on the structure and performance of such a RAKE receiver can be found in [Pro95], [Gro90], [Kan90], [Hig93].

In general, the multipath components arrive at the receiver not only with different time delays but also with different angle of arrivals (AOA). A single omni-directional antenna receiver cannot take advantage of this spatial structure of the multipath signals. But with an antenna array, the receiver can exploit this spatial diversity by doing either a diversity combining or an optimum combining which is otherwise known as beamforming. Thus, the so-called space-time RAKE receiver structure consists of a spatial combiner for each of the multipath components considered followed by a standard 1-D RAKE. As mentioned in section 2.1, the spatial combiner may be a diversity combiner of MRC or EGC type. Alternately, it can be a selection diversity type in which case the receiver selects the signal from the appropriate antenna element and feeds it to the RAKE combiner. An excellent treatment of the performance analysis of such space-time combining schemes can be found in [Mon99]. In the case of an optimum combiner/beamformer it tries to match the desired path's array response vector by optimizing some performance criterion. Typically in literature, a cascade of a *beamformer* and a RAKE receiver is known as 2-D RAKE receiver. Figure 2.1.3(a) and (b) draw a comparison between the 1-D and 2-D RAKE receiver structures.

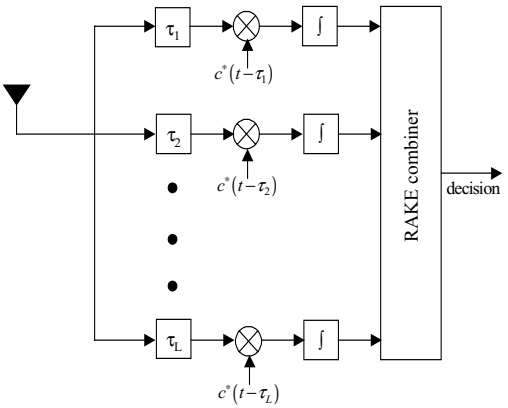

Figure 2.1.3: 1-D RAKE Receiver

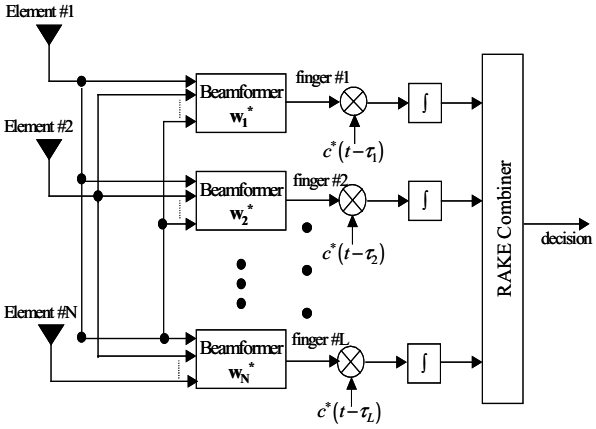

Figure 2.1.3(b): 2-D RAKE Receiver

2.1.2 Generic architecture of 2-D RAKE Receiver

Recently, a number of novel and effective beamformer-RAKE combinations have been proposed for the emerging W-CDMA standard of IMT-2000. Several of these schemes take advantage of the user dedicated control channel to estimate various channel parameters required for the beamformer and the RAKE combiner. There are also schemes that use blind channel identification techniques for these purposes. In both cases, the receiver usually exploits the unique properties of the users' spreading code sequence to extract the multipath channel information. The difference in the two approaches comes from the fact the in the first case, the user specific control information transmitted via the dedicated control channel is exploited whereas in the second case the receiver has to demodulate the unknown modulated data signal to recover the information. For both cases, a typical architecture usually consists of a front-end searcher that searches for the spatio-temporal multipaths from the desired user. Basically, the searcher operates by correlating the user's dedicated spreading code sequence with the received signal to get a measure of the multipath power-delay profile. This power-delay profile is then extensively examined to estimate the number of multipath components in the signal, their propagation delays and the angle of arrivals. A generic 2-D RAKE architecture is shown in Figure 2.1.4.

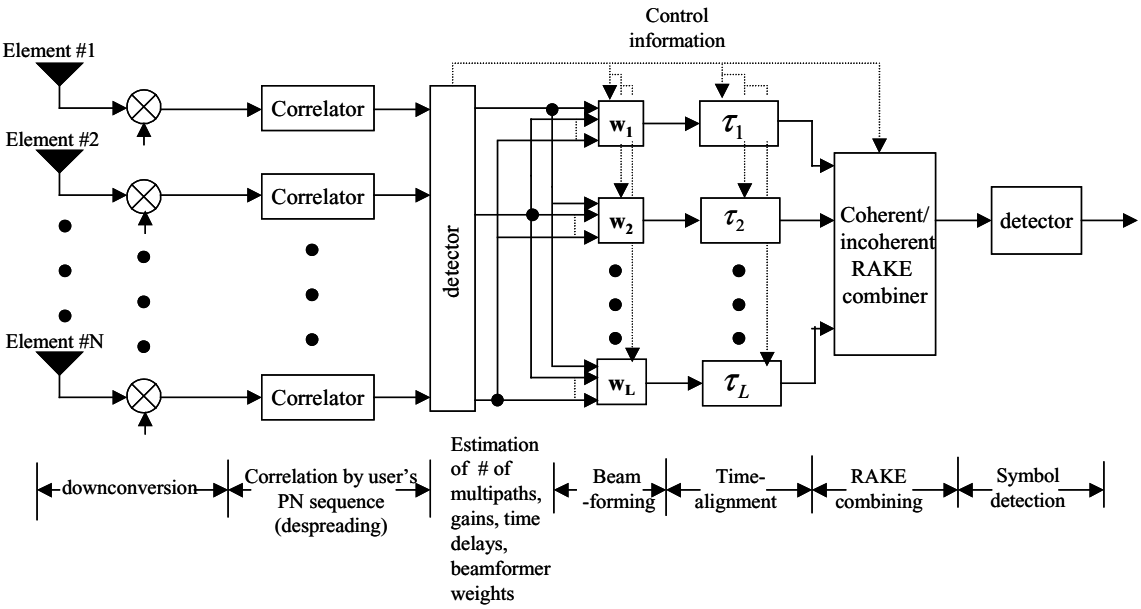

Figure 2.1.4: A generic 2-D RAKE receiver architecture

Basically, the 2-D RAKE architecture consists of a number of beamformers, each of which is intended for a specific multipath from the desired user. The front-end searcher, shown as a bank of correlators followed by a detector in Figure 2.4, assigns each beamformer a vector multipath component based on some channel estimation approach. Thus, the receiver detects the strongest multipath components and selects/adjusts the beamformer weight vectors accordingly based on some performance criterion. The outputs of all the beamformers are then combined in a conventional RAKE combiner and subsequently fed into a decision device. A number of different beamforming techniques can be applied to improve the receiver performance while at the same time reducing the complexity. Most of them are based on estimating the array covariance matrix over a length of time in which the channel parameters do not change substantially. A general classification of the beamforming techniques is given below [Tho96].

2.1.2.1 Beam-space beamforming

In this case, the received signal is passed through a bank of beamformers each with a fixed weight vector. Based on the measured average power at the beamformer outputs, the receiver takes a decision on which beamforming technique should be used. One approach is the well-known switched beam beamformer, in which case the receiver chooses the beamformer with the largest output power to pick out the desired signal [Lit96].

2.1.2.2 Bearing estimation beamforming

Bearing estimation is a technique that is based on the assumption that the received signal is composed of a number of spatially separated multipath components. Different direction of arrival (DOA) estimation techniques can be applied to the array covariance matrix in order to pick out the major directional components. There are some high resolution subspace based DOA estimation techniques such as MUSIC and ESPIRIT, which performs very well in the underloaded case i.e., when the number of signal components are less than the number of array elements. But in a dense urban environment where the multipath components are highly correlated they performance degrades rapidly [Kri96].

2.1.2.3 Eigenfilter beamforming

Eigenfilter beamforming techniques are based on the eigen-decomposition of the array covariance matrix. Provided that the SINR is large enough, the eigenvectors corresponding to the largest eigenvalue of the array covariance matrix provide an estimate of the array response vector. Then this estimate can be used to form efficient beamformer based on the well-known optimum performance criteria such as MMSE, Maximum SINR and ML [Sau93].

Among these techniques, the beamspace and the bearing estimation techniques basically direct one or more narrow beams to the incoming signals from the mobile. This is optimal only when the multipath angle spread is small. In the case of large angular spread, the eigenfilter method should give better performance since the beamformer weights are calculated to maximize some performance criterion. For a detailed description on various beamforming techniques refer to [Vee88], [Lit96], [Ert98b], [God97].

The RAKE combiner in a 2-D RAKE receiver may be either coherent or noncoherent type. In coherent combining the estimation of the multipath phase, amplitude and delay is required. Usually, a known pilot sequence needs to be transmitted for each user to estimate the channel phase. This has the effect of reducing the overall power efficiency. This is due to the fact that the power of the unmodulated pilot portion is greater than the power of the modulated data portion of the transmitted signal. For such cases, noncoherent detection schemes with either differential phase shift keying (DPSK) that do not require phase coherence or with M-ary orthogonal modulation signals that is used in IS-95 can be good alternatives [Nag96a].

2.1.3 Antenna diversity in IS-95 CDMA

In IS-95 CDMA, the base station uses dual antenna diversity in each sector to exploit the spatial diversity structure of the multipath channel. Thus, for a three-sectored cell-site, the base station has six antenna elements, which are widely spaced so that the fading is independent at each element. The block diagram of the base station receiver is shown in Figure 2.1.5 [Nag96a].

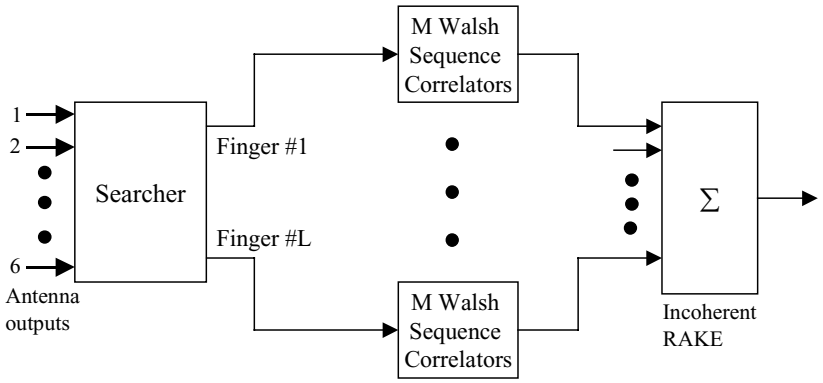

Figure 2.1.5: Block diagram of the base station receiver in IS-95

The receiver consists of a front-end searcher followed by a bank of M Walsh sequence correlators and a noncoherent RAKE combiner. The front-end searcher is implemented by a large number of scanning correlators that continuously search all the six antenna outputs for multipath signals coming from the mobile. The received multipath signals are then ordered in accordance to their energy, and the L strongest ones are chosen for RAKE combining, where L is the number of RAKE fingers. Since no pilot symbols are transmitted in the uplink, noncoherent combining is used for the L RAKE fingers. The front-end searcher also provides the necessary time delay information for the M-Walsh sequence correlators. This form of diversity is commonly known as the selection diversity. A detailed discussion on implementation of antenna diversity in IS-95 can be found in [Qua92], [Pad94].

The main drawback of this approach is that the base station treats all the diversity channels equally. That is, it cannot distinguish among the multipath components received in different elements. Furthermore, the same multipath components received in different channels are treated as different multipath components due to the wide separation of antenna elements. In short, as it is not doing any beamforming, it cannot efficiently exploit spatial diversity structure of the multipath channel [Nag96a].

2.2 2-D RAKE receiver structures

2.2.1 Pilot symbol Assisted (PSA) 2-D RAKE structures

A pilot symbol assisted (PSA) coherent 2-D RAKE receiver utilizes the transmitted pilot symbols for both channel estimation and beamforming. In other words, the pilot symbol assisted channel estimation is performed for coherent RAKE combining and the beamformer weights are calculated using some non-blind (pilot symbols assisted) beamforming techniques. By doing the array processing it can suppresses the Multi-user Access Interference (MAI) by directing the nulls towards the interfering users with the assumption that the changes in the angles of arrival of the interfering signals are slow. The RAKE combiner tracks the instantaneous temporal changes of the channel conditions and combines the multipath signals to maximize the signal to interference plus noise ratio (MRC combining). Since the W-CDMA standard has specified pilot symbols in the uplink, these PSA 2-D receivers will be attractive for implementing in a W-CDMA base station. A simplified diagram of a PSA coherent 2-D RAKE receiver is shown in Figure 2.2.1 [Tan97].

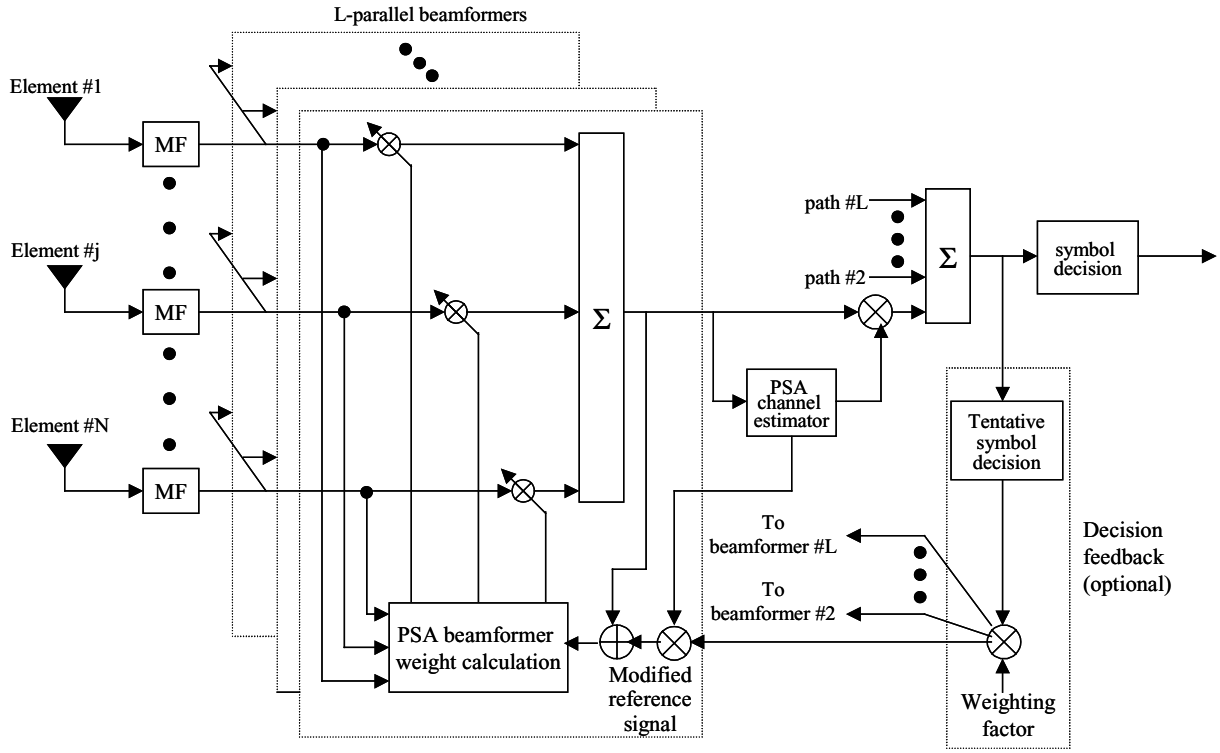

Figure 2.2.1: Pilot Symbol Assisted (PSA) coherent 2-D RAKE receiver structure

The receiver portion shown in Figure 2.2.1 is intended to detect a single user's received signal. As can be seen, the receiver consists of a matched filter (MF), beamformer and pilot symbol assisted (PSA) coherent RAKE combiner. The received signal at each element is downconverted, lowpass filtered and subsequently digitized by an A/D converter. The baseband digital signal at each element is fed into the MF, which resolves the temporal multipath components. At each MF, the signal is first despread i.e., multiplied by a locally generated replica of the desired user's spreading code whose timing is synchronized to the time delay of one of the resolvable multipaths. The resulting despread signal is then integrated over the symbol interval by an Integrate and Dump (I&D) filter thereby collapsing the wideband chip sequence into the original narrowband symbol samples. The post correlation signals (output of the matched filter) at all the elements are then used in conjunction with the known pilot sequence and some in cases with the decision directed data sequence to calculate the beamformer weight vector. Usually for non-blind beamforming, MMSE based Least Mean Square (LMS) adaptive beamforming or the Recursive Least Square (RLS) adaptive beamforming is employed [Hay91]. At each element, the calculated beamformer weight is used to multiply the corresponding matched filter output. The resultant signals at all the elements are then combined to form the beamformed signal dedicated for that specific multipath. Each of the RAKE finger has such a beamformer connected to it. The outputs of the all the beamformer are then combined coherently in the subsequent MRC RAKE combiner. For more details of such PSA coherent 2-D RAKE receiver refer to [Tan97], [Tan00].

2.2.2 Blind 2-D RAKE structures

A blind 2-D RAKE receiver uses a blind beamfoming technique coupled with a channel estimation technique that does not use the reference/pilot signal. Direction-finding based beamforming techniques such as MUSIC, ESPIRIT and property restoral based techniques such as Constant Modulus Algorithm (CMA) are some of the examples of blind beamforming [Kri96], [Lit96]. However, in a CDMA type system, where the number of users is much more than the number of antenna elements these algorithms, are not effective. In this case, the code filtering approach which estimates the channel vector by *correlating* the input signal with the desired user's spreading code is a much more efficient way [Nag96a], [Kha94], [Kha93]. That is the channel parameters for the user are estimated by exploiting the code structure of the spread

signal. After getting a good estimation of both the spatial and temporal channel structures, the resolvable multipaths can be combined spatio-temporally to improve the output SINR. In short, the code filtering approach implements the Maximum SINR beamformer by obtaining a good estimate of the desired user's channel gain and the array response vector. The block diagram of a noncoherent 2-D RAKE receiver that is based on code filtering approach is shown in Figure 2.2.2 [Nag96b]. This sort of blind 2-D RAKE structure is a good candidate for the base station antenna array receiver in IS-95. Again, the receiver consists of a front-end beam-steering processor followed by a bank of Walsh correlators. The base band received signal vector and the post correlation signal vector are used to estimates the channel parameters for each path. The correlator outputs are then fed to an optimum beamformer followed by a noncoherent RAKE combiner. The beamformer weight vectors are calculated using the knowledge of the post correlation signal vector. The output of the RAKE combiner is then used to estimate the transmitted data. With the assumption that the channel parameters remain almost constant over several symbol periods, the output of the RAKE is also fed to the channel vector estimation algorithm to determine the winning post correlation signal vector, which corresponds to the actual transmitted Walsh symbols. For more details refer to [Nag96a], [Nag96b].

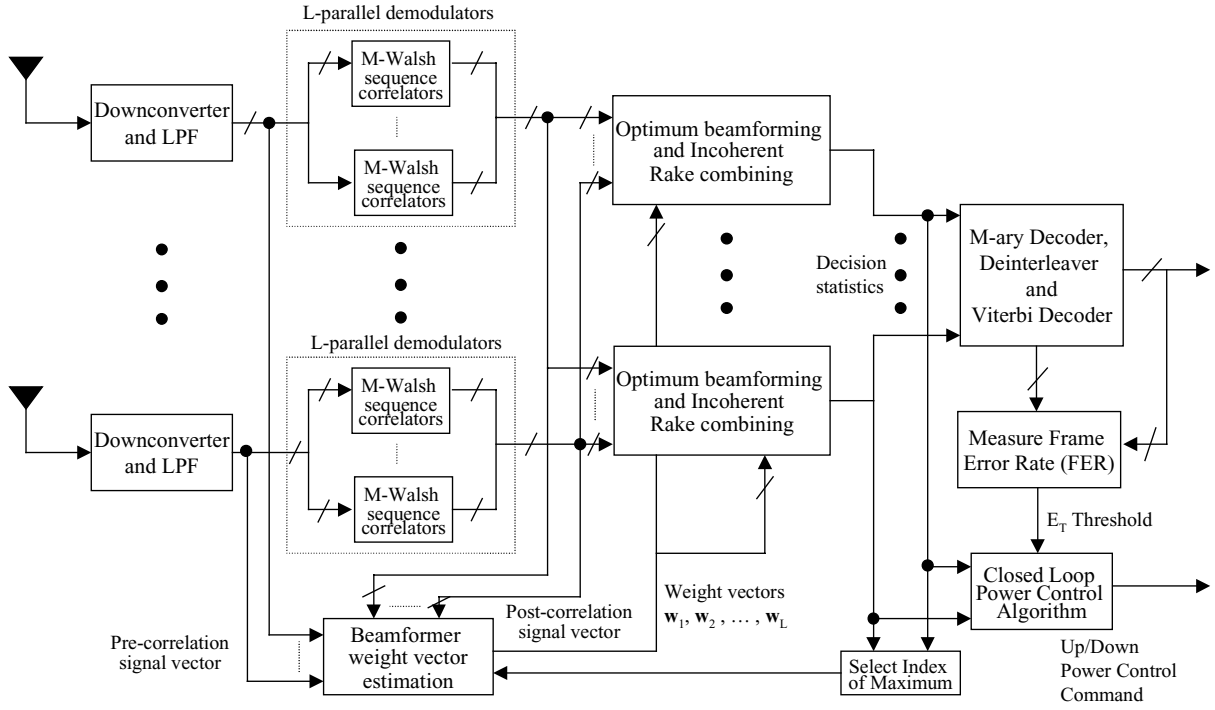

Figure 2.2.2: Block Diagram of a 2-D RAKE Receiver for the Base station of IS-95

2.3 Summary

In this chapter, we summarize the current and state of the art techniques for space-time processing for CDMA systems. Although the literature on antenna arrays for CDMA is vast and ever expanding, we focused our search mainly on 2-D RAKE receivers. These beamformer-RAKE structures have a vital role to play in the upcoming W-CDMA standard for IMT-2000. It is obvious that incorporation of antenna arrays with the conventional RAKE receiver will enhance the system performance manifold but the penalty is increased complexity. The added spatial dimension processing enables resolution of spatially separated multipaths induced that may not be resolvable in time. The extra spatial dimension will also help to reduce the near-far problem due to the imperfect orthogonality (partial correlation) and the asynchronous operation between the users in the uplink. In the following chapters we will quantify the performance of these 2-D RAKE structures through simulation in the W-CDMA environment.

Chapter 3

Spatio-temporal Channel Models

In a mobile radio communication system, multipaths can affect the system performance by causing destructive interference commonly known as fading. Antenna arrays are often used to mitigate the effect of fading and thereby increasing the system capacity. Application of antenna arrays may range from fixed directional spatial-filtering to adaptive beamforming. To test the performance of antenna arrays, an accurate description of the spatio-temporal channel model is required.

Classically, the rich scattering multipath environment is modeled as the Rayleigh fading phenomena [Cla68]. In this model, it is assumed that the signals are arriving uniformly along the azimuthal direction. However in more realistic scenarios, the angle of arrival (AOA) of the multipaths depends on a number of factors, such as the distance between the transmitter and receiver, location of scatterers, size of the receiving antenna etc. A number of channel models have been proposed in the literature based on both measurement data and statistical properties of the channel [Ert98a]. Some of these models are suited to the microcells typically set up in urban areas, while others are more applicable for the macrocells found in the rural and suburban areas. There are also channel models based on propagation statistics in the indoor environment [Sal87], [Spe97]. All these models provide multipath parameters including the AOA information essential to simulate an antenna array system.

In this chapter, two statistical channel models known as Geometrically Based Single Bounce (GBSB) elliptical and GBSB circular are described for micro and macrocellular environments [Ert98b]. In these models it is assumed that the multipath reflections are created by

random placement of scatterers inside a region defined by a specific geometry. From the position of the scatterers, multipath delays, AOA and power levels are determined. Thus these models provide a statistical description of the wideband spatio-temporal radio channel, which is useful in simulating a space-time processing system.

The chapter is organized as follows: Section 3.1 gives a brief description of the GBSB elliptical channel model and the method of generating the channel parameters for simulation purpose. Section 3.2 describes the GBSB circular channel model in a similar fashion. Finally in Section 3.3 the pros and cons of the two models are evaluated from the W-CDMA system perspective. Finally we draw a short chapter summary in section 3.4.

3.1 Geometrically Based Single Bounce Elliptical Model

3.1.1 Introduction

In a typical urban environment dense scattering coupled with abundance of reflection results in a rich multipath scenario. In this situation, the microcellular concept where the base-station has a relatively low antenna height is more appropriate. This implies that the multipath scatterers are located near the base station as well as near the mobile. Therefore, any spatial channel model that employs a geometrical scattering region around the mobile must also consider a similar scattering region around the base station. A particular channel model, which uses an elliptical scattering region surrounding the base station and the mobile has been proposed for the microcell environment [Ert98a]. This GBSB elliptical channel model is chosen for this research to describe a typical urban multipath propagation scenario.

3.1.2 Assumptions

The following assumptions are made in developing the elliptical channel model [Ert98a].

- The signals arriving at the base station are plane waves propagating along the horizon. As a consequence the AOA is calculated only in the azimuthal coordinates.
- The scatterers are omni-directional re-radiating elements having identical scattering coefficients.
- All scatterers are uncoupled. In other words, the signals reflected from each scatterer are not affected by the presence of the other scatterers.

- The received multipath signals are subjected to distance-dependent path loss characterized by a path loss exponent.

3.1.3 Geometry and Notation

In the GBSB elliptical channel model the scatterers are assumed to be uniformly distributed in an elliptical region. The base station and the mobile form the foci of the ellipse. The geometry of the elliptical model is shown in Figure 3.1.1.

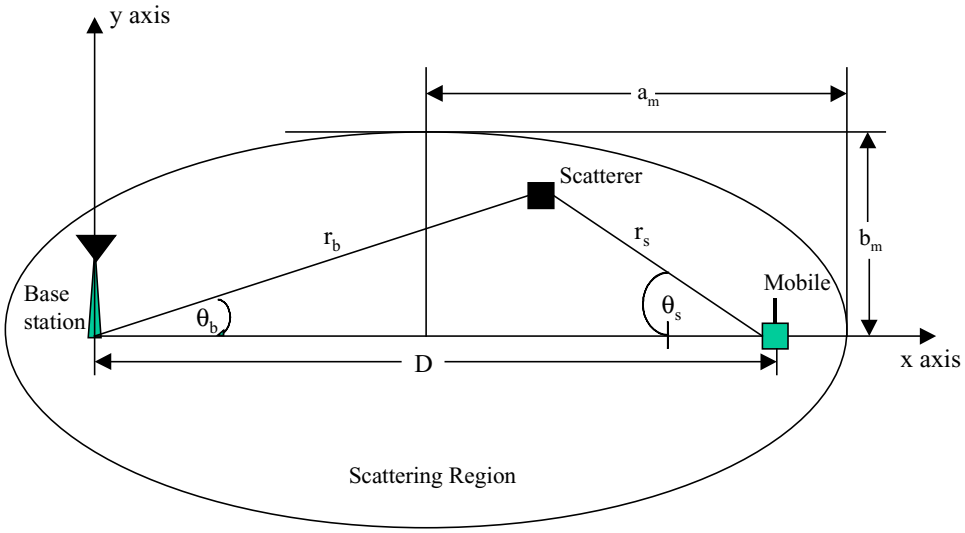

Figure 3.1.1: Geometry of the GBSB elliptical channel model

In Figure 3.1.1, the base station and the mobile are separated by a distance D, with the base station at the origin. All scatterers lie in a plane that includes the base station and the mobile, implying that the reflected multipath waves will appear to have the same elevation angle. The elliptical region is completely described by its semimajor axis, a_m and its semiminor axis, b_m. The choice of these parameters is determined by the maximum delay, τ_{max} of the multipaths. Larger values of τ_{max} imply greater path loss for the multipaths and, consequently, lower relative power compared to those with shorter delays. Hence, this model has a nice physical interpretation in that, changing the geometry of the ellipse can automatically adjust the various channel parameters, such as multipath amplitudes, delay spread and angle spread.

3.1.4 Mathematical Formulation

The semimajor axis, a_m and the semiminor axis, b_m are related to the maximum specified delay, τ_{max} as below

$$a_m = \frac{c\tau_{\max}}{2} \qquad b_m = \frac{1}{2}\sqrt{c^2\tau_{\max}^2 - D^2} \tag{3.1.4.1}$$

Where, D is the separation distance between the transmitter and the receiver and c is the speed of propagation ($3\text{x}10^8$ m/s). The equation of an ellipse in Cartesian coordinates

$$\begin{aligned} &\frac{\left(x - D/2\right)^2}{a_m^2} + \frac{y^2}{b_m^2} = 1 \\ \Rightarrow &\frac{\left(x - D/2\right)^2}{\left(\frac{c\tau_{\max}}{2}\right)^2} + \frac{y^2}{\left(\frac{\sqrt{c^2\tau_{\max}^2 - D^2}}{2}\right)^2} = 1 \end{aligned} \tag{3.1.4.2}$$

Substituting, $x = r_b\cos(\theta_b)$ and $y = r_b\sin(\theta_b)$, the equation of the ellipse in Polar coordinates

$$\frac{\left(r_b\cos\theta_b - D/2\right)^2}{\left(\frac{c\tau_{\max}}{2}\right)^2} + \frac{\left(r_b\sin\theta_b\right)^2}{\left(\frac{\sqrt{c^2\tau_{\max}^2 - D^2}}{2}\right)^2} = 1 \tag{3.1.4.3}$$

Where r_b is the distance from the base station of a scatterer located at the boundary of the ellipse and θ_b is the AOA at the base station. Any scatterer inside the ellipse can be viewed as an equivalent one located at the boundary of a smaller concentric ellipse. Equation (3.1.4.3) can then be solved for r_b for different values of the multipath propagation delay, $\tau \in [\tau_{min}, \tau_{max}]$. However an easier way is to utilize the coordinate location of the scatterer. Referring to Figure 3.1, the total propagation distance of a multipath ray from the mobile to the base-station

$$\begin{aligned} d &= r_b + r_s \\ &= r_b + \sqrt{\left(D - r_b\cos(\theta_b)\right)^2 + \left(r_b\cos(\theta_b)\right)^2} \\ &= r_b + \sqrt{D^2 + r_b^2 - 2Dr_b\cos(\theta_b)} \end{aligned} \tag{3.1.4.5}$$

Substituting $d = \tau c$ in (3.1.4.5) and solving for r_b yields

$$r_b = \frac{D^2 - \tau^2c^2}{2\left(D\cos(\theta_b) - \tau c\right)}; \quad \frac{D}{c} \le \tau \le \tau_m \tag{3.1.4.6}$$

Due to the symmetric nature of the scattering region, similar expressions can be derived with respect to the mobile. A detailed analysis on the pdf of multipath delays, AOA and power spectrum of the elliptical channel model can be found in [Ert98b].

3.1.5 Generation of Samples of the Elliptical Channel Model

The elliptical model described above can be used to generate various multipath signal parameters such as multipath delay τ_i, AOA θ_i, and power P_i of the i^{th} multipath component. Usually there are two ways to generate these parameters. In one method, the geometrical definition of the elliptical scattering region can be utilized to calculate the parameters. In the other method, the delay and AOA statistics are used to generate the channel samples. The first method is more computationally efficient and it will be described below in detail. The idea is first to define an ellipse corresponding to the maximum multipath delay, τ_m and uniformly place the scatterer inside the ellipse. The relevant signal parameters can then be calculated from the coordinates of the scatterers [Ert98b]. It is assumed that the number of multipaths (scatterers), L and the transmitter to receiver separation distance, D is known. The procedure is outlined below

- Choose a value of the maximum multipath propagation delay, τ_m.
- Generate samples of two uniformly distributed random variables, x_l and y_l, l=1,2…L over the interval [-1,1]. Thus, the points will be uniformly distributed in a square of arm length 2.
- Isolate the points that lie on and within a circle of unit radius centered at the origin. Translate them from the cartesian coordinates (x_l,y_l) to the polar coordinates (r_l,θ_l) according to the following relationships

$$r_l = \sqrt{x_l^2 + y_l^2}, \quad \phi_l = \tan^{-1}\left(\frac{y_l}{x_l}\right); \quad l = 1,2\ldots L \tag{3.1.5.1}$$

- Now, we have L samples of a random variable described by the polar coordinates (r_l,ϕ_l) that are uniformly distributed in a circle of unit radius. To translate these samples so that they are uniformly distributed in an ellipse, the following two transformations are performed

$$x_l = a_m r_l \cos(\phi_l) + \frac{D}{2}, \quad y_l = b_m r_l \sin(\phi_l); \quad l = 1,2\ldots L \tag{3.1.5.2}$$

Where, a_m and b_m are the semimajor and the semiminor axes of the ellipse respectively corresponding to the specified τ_m and are given by (3.1.4.1). The multipath propagation distance, d_l; l=1,2…L can be calculated as

$$d_l = \sqrt{x_l^2 + y_l^2} + \sqrt{(D - x_l)^2 + y_l^2}; \quad l = 1,2\ldots L \tag{3.1.5.3}$$

- The propagation delays of the multipaths, τ_l; l=1,2…L will be

$$\tau_l = \frac{d_l}{c}; \quad l = 1,2...L; \quad c = 3\times 10^8 \, m/s \tag{3.1.5.4}$$

- As the base station is located at the origin of the coordinate system, so the angle of arrivals (AOA) of the multipaths at the base station are given by

$$\theta_{b,l} = \tan^{-1}\left(\frac{y_l}{x_l}\right); \quad l = 1,2\ldots L \tag{3.1.5.5}$$

- The power of the direct path component (LOS) can be calculated as below

$$P_0(dBm) = P_{ref}(dBm) - 10n\log\left(\frac{D/c}{d_{ref}}\right) + G_t(\theta_d) + G_r(\theta_a) \tag{3.1.5.6}$$

where P_{ref} is the reference power measured at a distance d_{ref} from the transmitter using omni-directional antennas at the transmitter and the receiver. P_{ref} can be calculated using Friis' free space propagation model given by

$$P_{ref}(dBm) = P_T(dBm) - 20\log\left(\frac{4\pi d_{ref}}{\lambda}\right) \tag{3.1.5.7}$$

where P_T is the transmitted power and λ=c/f is the wavelength for a particular carrier frequency, f. The path loss exponent, n typically ranges from *3* to *4* in a microcell environment. $G_t(\theta_d)$ and $G_r(\theta_a)$ are the gains of the transmit and the receive antennas as functions of the angle of departure, θ_d and the angle of arrival, θ_a respectively. For the LOS component, θ_d and θ_a are both zero. The power of each of the multipath component can be calculated as below

$$P_l(dB) = P_0(dB) - 10n\log(d_l) - L_r + G_t(\theta_{d,l}) - G_t(0) + G_r(\theta_{a,l}) - G_r(0) \tag{3.1.5.8}$$

Where L_r is the path loss in dB.

- Assuming the phase of the multipath components, γ_l; l=1,2…L are uniformly distributed over the interval $[0,2\pi)$, the complex amplitudes of the multipath components are calculated as below

$$\alpha_l = 10^{(P_l - P_0)/20} e^{j\gamma_l}; \quad l = 1,2 \ldots L \tag{3.1.5.9}$$

3.2 Geometrically Based Single Bounce Circular Model

3.2.1 Introduction

A typical rural or suburban environment is characterized by local scatterers surrounding the mobile and no large reflectors away from the vicinity of the mobile is visible at the base station. In such environments, macrocellular concept where the base station antenna height is considered to be above the local clutter is a more appropriate selection. Thus, the multipath channel parameters in the propagation model for rural or suburban environment are essentially determined by the distribution of the scatterers around the mobile. A number of models have been proposed in the literature that defines the geometry and the underlying distribution of the scatterer region. In one of these models, it is assumed that the scatterers are uniformly distributed within a circle of predefined radius around the mobile [Pet96a]. This model known as Geometrically Based Single Bounce (GBSB) circular model is specially suited for macrocell environments and thus sufficient to represent a rural or suburban multipath propagation model.

3.2.2 Assumptions

A Geometrically Based Single Bounce circular model presupposes the following underlying assumptions [Pet96a], [Pet96b], [Ert98b].

- The signals received at the base station are plane waves propagating along the horizon. Thus only the azimuthal coordinates are required to represent the corresponding AOA. This is due to the fact that the separation distance between transmitter and receiver is large compared to the respective antenna heights.

- The scatterers are considered to be omni-directional re-radiating elements with identical scattering coefficients.

- Each multipath component at the base station have interacted with only a single scatterer and thus are not influenced by the other scatterers in the channel.

3.2.3 Geometry and Notation

The Geometrically Based Single Bounce (GBSB) circular model assumes that the scatterers are uniformly distributed within a circle of radius, R around the mobile. The geometry of the circular model is shown in Figure 3.2.1.

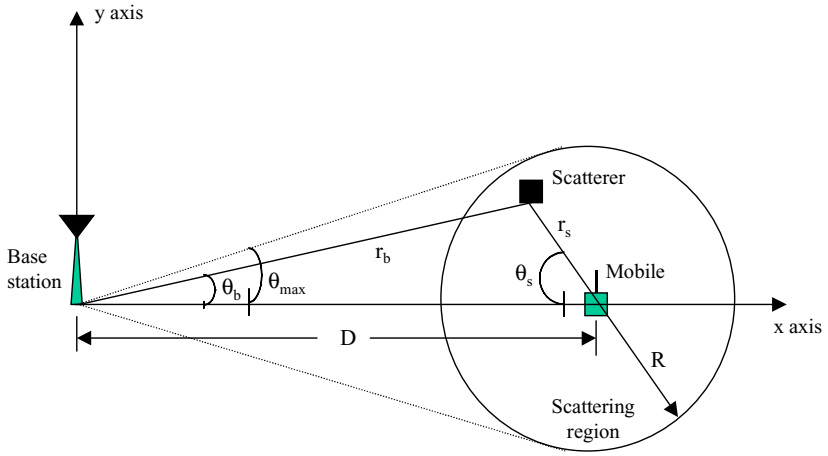

Figure 3.2.1: Geometry of the Circular Scattering Channel Model

In Figure 3.2.1, the base station and the mobile are separated by a distance *D*, with the base station at the origin of the coordinate system and the mobile is on the x-axis. The scatterers are uniformly placed in a circle of radius *R* with the mobile is at the center. Typically, $R < D$, so that there are no scatterers local to the base station as is the case in a macrocell region. For simplicity, the plane of the scatterer can be viewed as horizontal, which also includes the mobile and the base station. This will ensure that the angle of arrivals (AOA) of the received signal contains only azimuthal components. The AOA of the multipath components at the base station is denoted by θ_b and depends on two parameters: the angle of departure from the mobile and the position of the scatterer. The location of the scatterer is specified by its distance from the base station, r_b, and from the mobile, r_s, respectively. Since the scatterers are confined in a circle around the mobile, the AOA at the base station, θ_b, is limited by a maximum value denoted by, θ_{max}. Similarly, the AOA at the mobile, θ_s, depends on the angle of departure from the base station and the scatterer location. In this case, as the mobile is located inside the scattering region, the AOA can be any value in the interval $[0,2\pi)$.

The radius of the circular scattering region, R, is usually determined by equating the angle spread as predicted by the model with the measured angle spread. Typical values of angle spread in a macrocell environment ranges between one to six degrees for a transmitter to receiver separation distance of $D \approx 1$ km [Asz96]. Using the fact that the angle spread is inversely proportional to D, the measurement results suggest a radius of scatterer ranging from 30 to 200 m [Ert98a].

3.2.4 Mathematical Formulation

The region of scatterer in the Cartesian coordinates is given by

$$(x-D)^2 + y^2 \le R^2 \tag{3.2.4.1}$$

Substituting, $x = r_b \cos(\theta_b)$ and $y = r_b \sin(\theta_b)$ in (3.2.4.1) and expanding, the scattering region in polar coordinates

$$r_b^2 - 2 r_b D \cos(\theta_b) + D^2 \le R^2 \tag{3.2.4.2}$$

Referring to Figure 3.2, the total multipath propagation distance, d is given by

$$\begin{aligned} d &= r_b + r_s \\ &= r_b + \sqrt{\left(D - r_b \cos(\theta_b)\right)^2 + \left(r_b \sin(\theta_b)\right)^2} \\ &= r_b + \sqrt{D^2 + r_b^2 - 2 D r_b \cos(\theta_b)} \end{aligned} \tag{3.2.4.3}$$

Substituting $d = \tau c$ in (7), where τ is the total multipath propagation delay, the distance of the scatterer from the base station, r_b, can be expressed as

$$r_b = \frac{D^2 - \tau^2 c^2}{2\left(D\cos(\theta_b) - \tau c\right)} \tag{3.2.4.4}$$

As in the GBSB elliptical channel model, the symmetric nature of the scattering region allows similar expressions to be derived with respect to the mobile. A detailed analysis on the pdf of multipath delays, AOA and power spectrum of the circular channel model can be found in [Pet96b], [Ert98b].

3.2.5 Generation of Samples of the Circular Channel Model

As in the elliptical channel model, there are two ways to generate the multipath channel parameters using the circular channel model. Exploitation of the geometry of the scattering region, which will be described below, is a much more efficient method than the one that utilizes the statistics of the channel parameters (delay, AOA). Again, the basic idea is to define a uniform circular scattering surrounding the mobile with the radius corresponds to the maximum multipath delay, τ_m. The relevant signal parameters can then be calculated from the geometry of the scattering region [Ert98b]. As in the case of elliptical model, it will be assumed that number of multipaths, L and the transmitter to receiver separation distance, D is known. The procedure is described below.

- Choose a value of the maximum multipath delay, τ_m.
- Calculate the radius of the scattering region according to the following relationship

$$R_m = \frac{(c\tau_m - D)}{2} \tag{3.2.5.1}$$

  Where c is the speed of propagation.

- Generate samples of two uniform random variables, x_l and y_l, l=1,2…L over [-R_m,R_m] and isolate those that lie on and inside a circle of radius R_m. The coordinates of these points with respect to an origin at a distance D from the center of the circle is

$$x_c = x_l + D, \quad y_c = y_l; \quad l = 1,2,...,L \tag{3.2.5.2}$$

- The multipath propagation distance, d_l, l=1,2…L is then calculated as

$$d = \sqrt{x_c^2 + y_c^2} + \sqrt{(D - x_c)^2 + y_c^2} \tag{3.2.5.3}$$

- The propagation delay, τ_l and AOA at the base station (origin), θ_l, l=1,2…L are

$$\tau_l = \frac{d_l}{c}, \quad \theta_{b,l} = \tan^{-1}\left(\frac{y_c}{x_c}\right); \quad l = 1,2\ldots L \tag{3.2.5.4}$$

- As in the elliptical model, the power of the multipaths components are calculated as

$$P_l(dB) = P_0(dB) - 10n\log(d_l) - L_r + G_t(\theta_{d,l}) - G_t(0) + G_r(\theta_{a,l}) - G_r(0) \tag{3.2.5.5}$$

Where the terms have the same meanings as in Section 3.1.5.

- Then the complex gains of the multipaths components, α_l, l=1,2…L are given as

$$\alpha_l = 10^{(P_l - P_0)/20} e^{j\gamma_l}; \quad l = 1,2 \ldots L \tag{3.2.5.6}$$

With the assumption that the phases γ_l, l=1,2…L are uniformly distributed over [0,2π).

3.3 Channel parameters from the W-CDMA system perspective

In this section, the two scattering channel models are discussed with respect to the W-CDMA system. These channel models are used in our simulation and provide valuable insight into different channel parameters. The power-delay profile and the angle spread of these models will be evaluated using the geometry of the scattering region and AOA statistics that are already developed in [Ert98], [Lib96], [Pet96]. They will be compared under different conditions that determine the size and shape of the geometry, such as the maximum multipath delay, τ_m, and base station to mobile distance, D. The suitability of a channel model for an environment and the range of parameters for each model is also justified.

3.3.1 Power-delay profile

The power-delay profile of a multipath channel indicates the relative strength of the multipaths with respect to their time of arrivals and can be used to create an equivalent discrete finite impulse response (FIR) model of the channel. In a CDMA type wideband system where the channel is frequency selective, the power-delay profile indicates the time dispersiveness of the channel. The power-delay profile of the elliptical and the circular models can be generated using the procedure described in section (3.1.5) and (3.2.5) respectively. In generating these profiles, it is assumed that the line of sight (LOS) power is normalized to unity. Also only the distance dependent path loss is taken into account and no long term fading (shadowing) effect is considered. The antenna gains of both the transmitter and the receiver are assumed to be unity. The power-delay for a typical snapshot (a specific arrangement of scatterers) of the elliptical scattering channel model is shown in Figure 3.3.1.

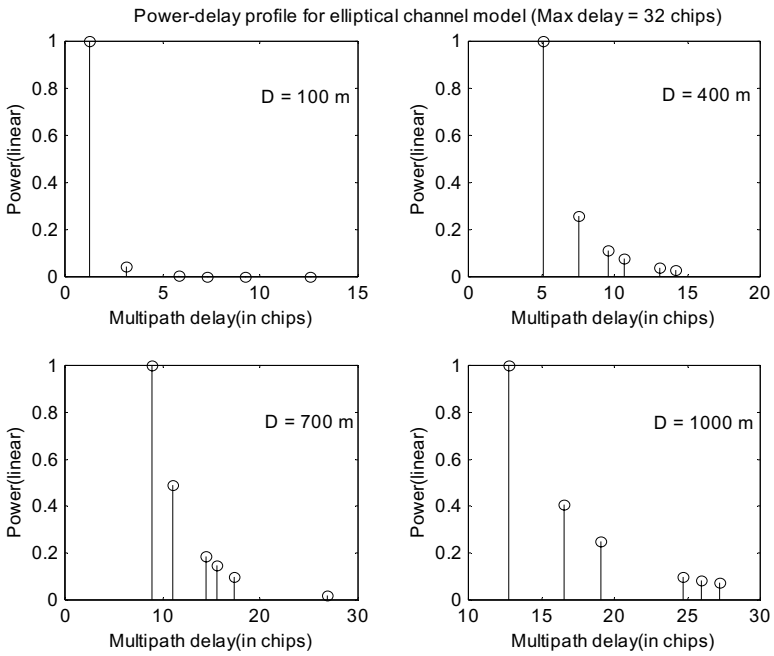

Figure 3.3.1: Power-Delay profile for elliptical model with different BS to mobile distance

In Figure 3.3.1, the boundary of the ellipse is defined by the maximum multipath delay, which is chosen to be 32 chips (~8 μs). The reason behind this is that in typical urban scenario where this elliptical model is applicable most of the multipath energy comes within 8 μs [Rap98]. Five scatterers are placed in the ellipse to form the reflected multipath rays. It can be seen that, as the distance *D* increases, the multipath components starts to arrive with a greater delay as expected, but their relative strength increases. This is due to the fact that as the outer boundary of the scattering region is fixed, the ellipse becomes more elongated with increasing *D*. Thus the difference in propagation distances between the line of sight path (LOS) and the other multipaths become closer and hence their relative power. In other words, as the distance increases, the multipaths become more specular (dominant in relative power with respect to each other).

Figure 3.3.2 shows the power-delay profile for a specific placement of five scatterers in the circular channel model. In this case, the maximum multipath delay is taken as 128 chips (~32 μs) in accordance with the rural and suburban macrocellular environment where this model is applicable. As can be seen, the curves follow the same pattern as those for elliptical channel model, i.e., the multipaths start to arrive at a later time with the increase of distance *D*, but with higher relative strength.

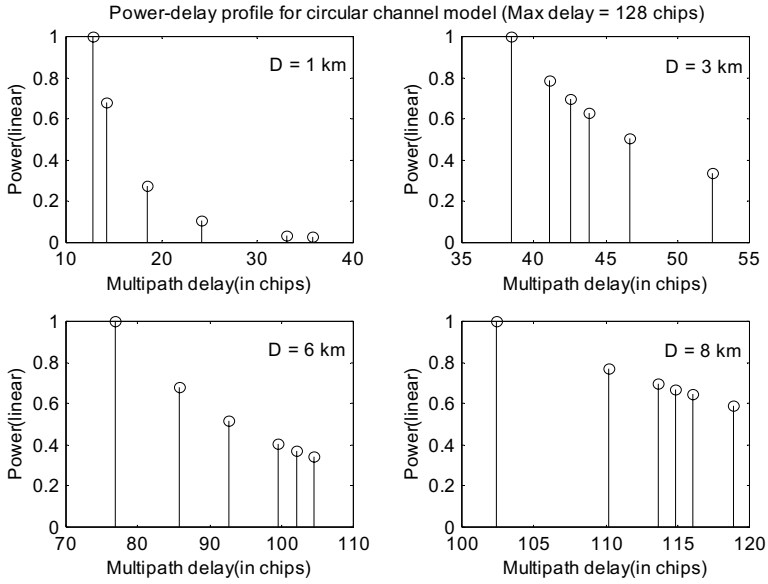

Figure 3.3.2: Power-delay profile for elliptical model with different BS to mobile distance

Comparing Figure 3.3.1 with Figure 3.3.2, it can be seen that the relative strengths of the multipaths in the power-delay profile of the elliptical channel model is not as high as those for circular channel model. This is obvious, since in the elliptical model the scatterers can be located far away from each other as opposed to the circular model, where the scatterer locations are relatively close by within a circular region surrounding the mobile. So, in dense urban environment where there are scatterers local to both base station and mobile, the elliptical channel model is more realistic. However, in rural places where the scatterers are mostly local to the mobile, the circular channel model is more applicable.

3.3.2 Angle Spread

The angle spread of a channel is a measure of the angular dispersiveness of the channel. In other words, angle spread when referred to the receive side is the spread of the AOA of the multipaths at the receive antenna. Likewise, angle spread refers to the transmit side is the spread of angle of departure (AOD) of the multipaths from the transmit antenna. There are two ways to define the angle spread, central moment angle spread and ensemble average angle spread [Lib96]. The central moment angle spread of a channel can be calculated when the measured channel impulse response is available. When the probability density functions (pdf) of the AOA/AOD of the multipaths are available, ensemble average delay spread can be used. We will

use the ensemble average angle spread using the pdf of AOA derived in [Ert98]. It is defined for AOA at the receiver (base-station) as below

$$\sigma_{\theta_b} = \sqrt{E\left\{\theta_b^{\,2}\right\} - E\left\{\theta_b\right\}^2} \tag{3.3.1.1}$$

where θ_b is the AOA at the base station and $E\{.\}$ is the expectation operator defined as

$$E\{x\} = \int_{-\infty}^{\infty} x f(x)\, dx \tag{3.3.1.2}$$

For the elliptical channel model, the AOA pdf is given by [Ert98]

$$f_{\theta_b}(\theta_b) = \frac{1}{8\pi a_m b_m}\left(\frac{\tau_m^2 c^2 - D^2}{\tau_m c - D\cos(\theta_b)}\right)^2; \quad -\pi \le \theta_b \le \pi \tag{3.3.1.3}$$

where the symbols have the same meaning as described in the earlier section. Using (3.3.1.2), it is found that the mean of AOA, $E\{\theta_b\}$ is zero, so the angle spread from (3.3.1.1) is

$$\sigma_{\theta_b} = \frac{\left(\tau_m^2 c^2 - D^2\right)}{8\pi a_m b_m}\int_{-\pi}^{\pi} \frac{\theta_b^2}{\left(\tau_m c - D\cos(\theta_b)\right)^2} d\theta_b \tag{3.3.1.4}$$

As this expression does not have a closed form solution, so it has to be evaluated numerically. A plot of angle spread vs. multipath delay for different base station to mobile distance, D is shown in Figure 3.3.3.

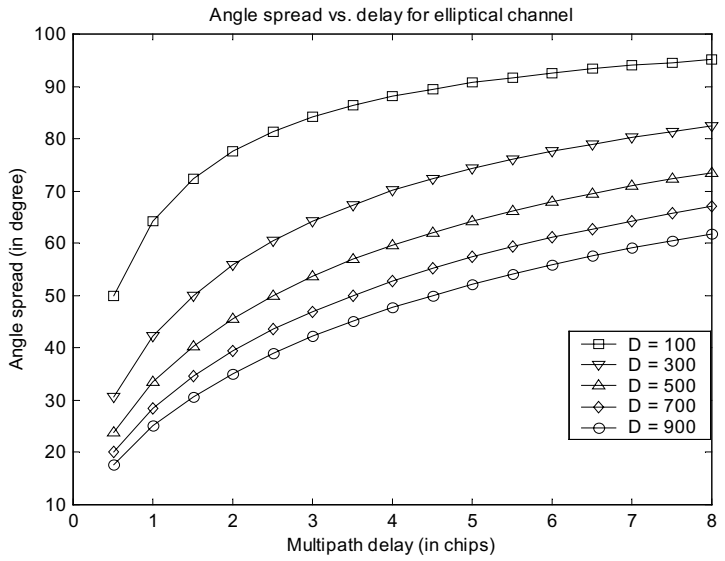

Figure 3.3.3: Angle spread for the elliptical model with different BS to mobile distance

In this plot, it is assumed that the maximum multipath delay can be of up-to eight W-CDMA chips. This is in accordance with a typical DPCH multipath searcher at the W-CDMA base station that uses a searching window of 8 chips (~2.5 μs). In terms of geometry, the multipath delay is related to the boundary of the ellipse and the distance, *D* corresponds to the major axis of the ellipse. As can be seen from Figure 3.5, for a particular *D*, the angle spread increases as the multipath delay increases. This is due to the fact that, a larger boundary of ellipse allows the multipaths to have a wide range of AOA and hence a large angle spread. However, the increase is not proportional with delay and the curves start to flatten out at higher delays. Again, for a particular delay, it can be seen that the angle spread decreases as *D* increases, indicating that ellipse is getting more elongated to have a wide range of AOA. Thus, the observation with the elliptical model is that, the bigger the scattering region the larger is the angle spread and the larger the distance from base station to the users the smaller is the angle spread.

Similarly, the ensemble average angle spread for the circular channel model can be found using the pdf of multipath AOA at the base station. However, a good fit for the angle spread curve is reported in [Ert98]. It is given as

$$\sigma_{\theta_b} = 31\frac{R_m}{D} \tag{3.3.1.5}$$

where the symbols bear the same meaning as described in the previous section. Substituting R_m from (3.2.5.1) in (3.3.1.5) with different values of maximum multipath delay, τ_m the angle spread curves can be plotted as shown in Figure 3.3.4.

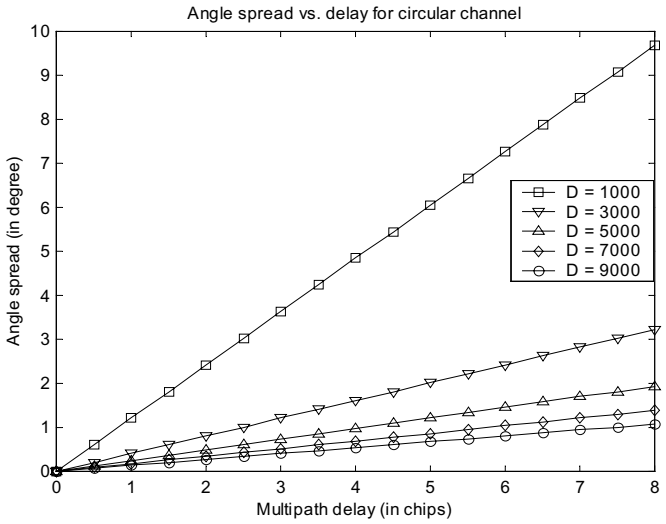

Figure 3.3.4: Angle spread for the circular model with different BS to mobile distance

As can be seen, the curves follow the same trends as those for the elliptical channel model, i.e., the angle spread increases with increase of multipath delay (circle radius) and decreases with distance from the base station. However, in this case the angle spread values are much smaller than those for the elliptical model. Also the curves are linear and do not flatten out at larger delays as was the case in the elliptical model.

3.3.3 Range of channel parameters for uplink W-CDMA

The GBSB channel models discussed in the previous sections are more applicable for an outdoor environment. Thus to generate meaningful ranges of multipath channel parameters using these channel models, they need to be compared with real measurement base outdoor channel models. One such channel model proposed for the W-CDMA is the ETSI's measurement-based vehicular A outdoor channel model. The power-delay profile of this channel model is shown in Figure 3.3.5 [ETS97].

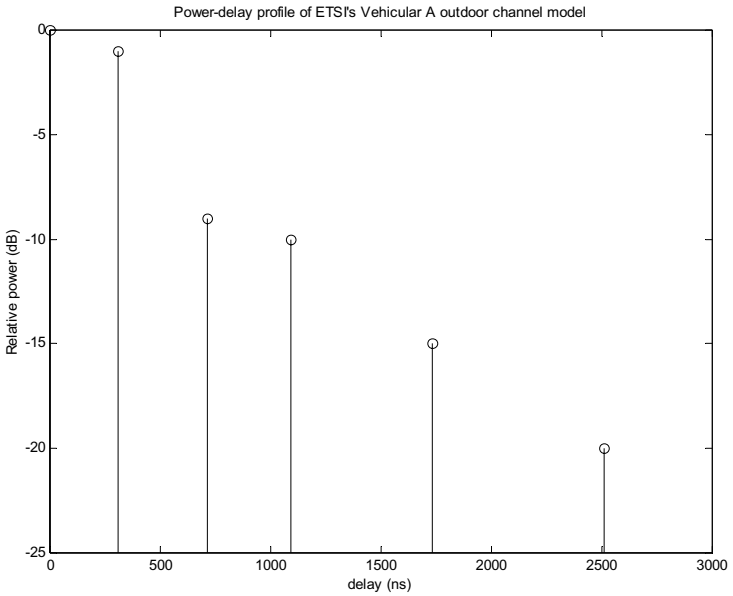

Figure 3.3.5: Power-delay profile of ETSI's vehicular A outdoor channel model

From Figure 3.3.5, the maximum multipath delay relative to the LOS path delay is ~ 2.5 μs, which corresponds to approx. eight W-CDMA chip periods (1chip period ≈ 0.3 μs). As already described in Sections 3.1.5 and 3.2.5, the shapes of the elliptical and the circular region are defined by the maximum multipath delay and the mobile to base station distance. Since the mobile to base station distance determines the LOS path delay, it follows that the maximum

multipath delay is equal to the LOS path delay plus the time period of 8 W-CDMA chips for both the channel. Also a practical Dedicated Physical Channel (DPCH) multipath searcher in the W-CDMA base station looks for the desired user's multipaths within a window of 8 chip periods. The range of the other channel parameters such as multipath power and AOA will be determined accordingly, once the boundaries of the geometrical regions are fixed. One good thing about the GBSB channel models is that the multipath parameters will change depending on the position of the scatterers and that is useful is simulating different channel environmenst. But, a measurement based channel model, like that in Figure 3.3.5 can only provide fixed channel parameters. In that respect the GBSB channel models are more useful in simulating a system like a space-time (2-D) RAKE receiver whose performance shows a space-time trade-off with the variation of spatial and temporal channel parameters.

3.4 Summary

In this chapter, we discussed two GBSB statistical channel models, which will be used as the spatio-temporal channels in our space-time processing simulation testbed. We described the geometrical configurations and mathematical formulations of these two models along with their implicit assumptions. We then outlined the procedure to generate the samples of the channel parameters in an efficient manner. These procedures will be followed extensively to simulate the multipath channel parameters. We then made a qualitative comparison between the two channel models with respect to two channel property indicators, namely, the power-delay profile and the angle spread. In doing so, we justified the proposition of which channel is suitable for which sort of environment and what range of values should be used for different channel parameters in these environments. These comparisons are made with the W-CDMA system perspective so that they will be more meaningful when we will simulate the spatio-temporal channel for our space-time processing system.

Chapter 4

Overview of Uplink W-CDMA Standard

Wideband Code Division Multiple Access (W-CDMA) radio interface has been chosen as the leading multiple access scheme for the third generation (3G) mobile cellular system. Based on the Radio Transmission Technology (RTT) proposal of the Universal Mobile communication System (UMTS), which is otherwise known as Universal Terrestrial Radio Access (UTRA), the W-CDMA system offers high multipath resolution capability, lower transmission power and support for high data rate users. Among the most prominent features of the W-CDMA is its backward compatibility with the already established Global System for Mobile Communication (GSM). Thus the network will support some attractive GSM features such as roaming. In addition, it will offer high service flexibility, inter-frequency and inter-system handover and support different performance enhancement features such as adaptive antennas, multi-user detection receiver and transmit diversity, etc [Dha98].

The W-CDMA system has a nominal bandwidth of 5MHz with a 200 kHz carrier raster and a chip rate of 3.84 Mchips/s. There are two different modes of operation: Frequency Division Duplex (FDD) and Time Division Duplex (TDD). In FDD mode the uplink and downlink transmission are carried over in two different frequency bands whereas in TDD mode only one frequency band is employed but with different synchronized time intervals. FDD is considered to be the main duplexing scheme and TDD is introduced mainly due to the asymmetric frequency bands designated by the International Telecommunication Union (ITU). Other key features are asynchronous base station operation in the FDD mode, plot symbol assisted coherent detection in both base station and mobile and fast closed loop power control [Zen99].

In this chapter, we elaborated briefly on the uplink transmission of W-CDMA in FDD mode. Our focus is on the uplink due to the fact that our space-time processing system is intended for the uplink receive at the base station. We will give brief descriptions of different uplink dedicated physical channels, proposed spreading, modulation and channel coding schemes for the uplink. We will also discuss uplink spreading and scrambling codes and their correlation properties. We tried to concentrate mainly on the information that is necessary to build up the simulation test-bed for our space-time processing system.

The chapter is organized as follows: In section 4.1, the uplink physical channels are described with a focus on the dedicated channels. Section 4.2 illustrates the uplink spreading and modulation techniques. Section 4.3 elaborates on the uplink spreading and scrambling code generation and their properties. Section 4.4 gives a brief introduction on uplink channel coding scheme. Finally the chapter summary is presented in section 4.5

4.1 Uplink Physical Channels

Physical channels are characterized by their carrier frequencies, radio frame structures, information streams they carry, channelization codes and the relative phase between the channels. The W-CDMA uplink physical channel structure consists of dedicated and common physical channels.

4.1.1 Dedicated Uplink Physical Channels

There are two types of dedicated uplink physical channels, which are I/Q code multiplexed within each W-CDMA radio frame [UMTSa]. These are

- Uplink Dedicated Physical Data Channel (Uplink DPDCH)

  This is used to carry the dedicated data generated at the Physical Layer and above in the form of the dedicated transport channel (DCH). Each radio link may be composed of zero, one or up to six uplink DPDCH.

- Uplink Dedicated Physical Control Channel (Uplink DPCCH)

  It is used to carry the control information generated at the Physical Layer. The control information consists of known pilot bits, transmit power-control (TPC) commands,

feedback information (FBI) and an optional transport-format combination indicator (TFCI). There is only one uplink DPCCH on each radio link.

The frame structures of the uplink DPDCH and DPCCH are shown in Figure 4.1.1. The frame length is 10 ms and it is divided into 15 slots of length 2560 chips, each corresponds to one power-control period.

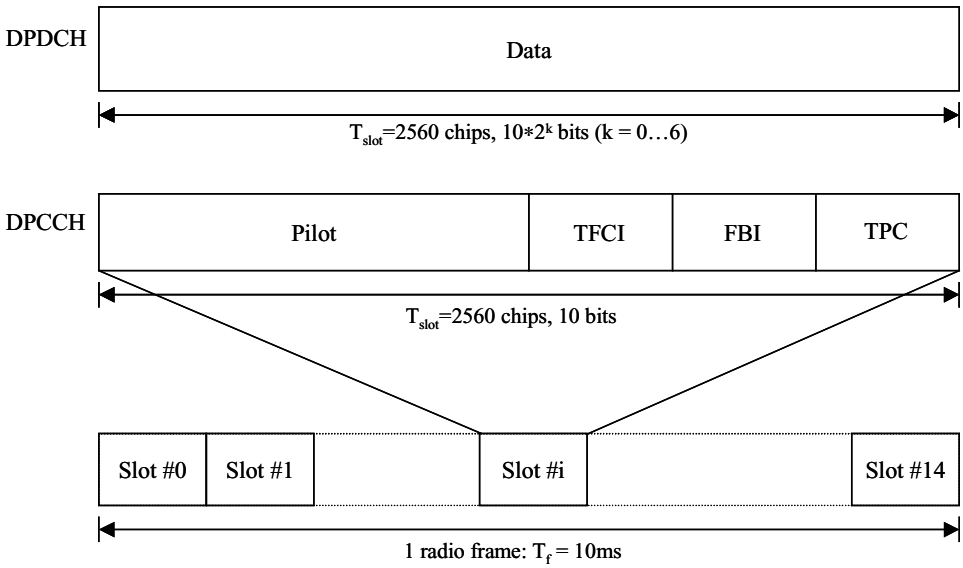

Figure 4.1.1: Frame Structure for Uplink DPDCH/DPCCH

The number of bits per uplink DPDCH/DPCCH slot is determined by the spreading factor (SF), defined as, $SF = 256/2^k$, k=0…6. For DPDCH, the spreading factor ranges from 4 to 256, while for DPCCH it is always equal to 256. The exact bit number of DPDCH and bit format of different DPCCH fields can be found in [UMTSa].

Pilot bits in the DPCCH field help channel estimation for coherent detection. They can also be used as reference signal for beamforming with multiple antenna elements. TFCI bits inform the receiver about the instantaneous transport format combination of the transport channels mapped to the simultaneously transmitted uplink DPDCH radio frame. FBI bits support techniques requiring feedback such as closed loop transmit diversity and site selection diversity transmission (SSDT). TPC bits are used for power control purposes [UMTSa].

4.1.2 Common Uplink Physical channels

Two common uplink physical channels are defined in W-CDMA. The Physical Random Access Channel (PRACH) is used to support the random access transmission based on a slotted ALOHA approach with fast acquisition indication. The Physical Common Packet Channel (PCPCH) is designated to carry the common packet channel.

4.2 Spreading and Modulation of Uplink DPDCH and DPCCH

The spreading and modulation of the uplink DPDCH and DPCCH is shown in Figure 4.2.1 [UMTSb].

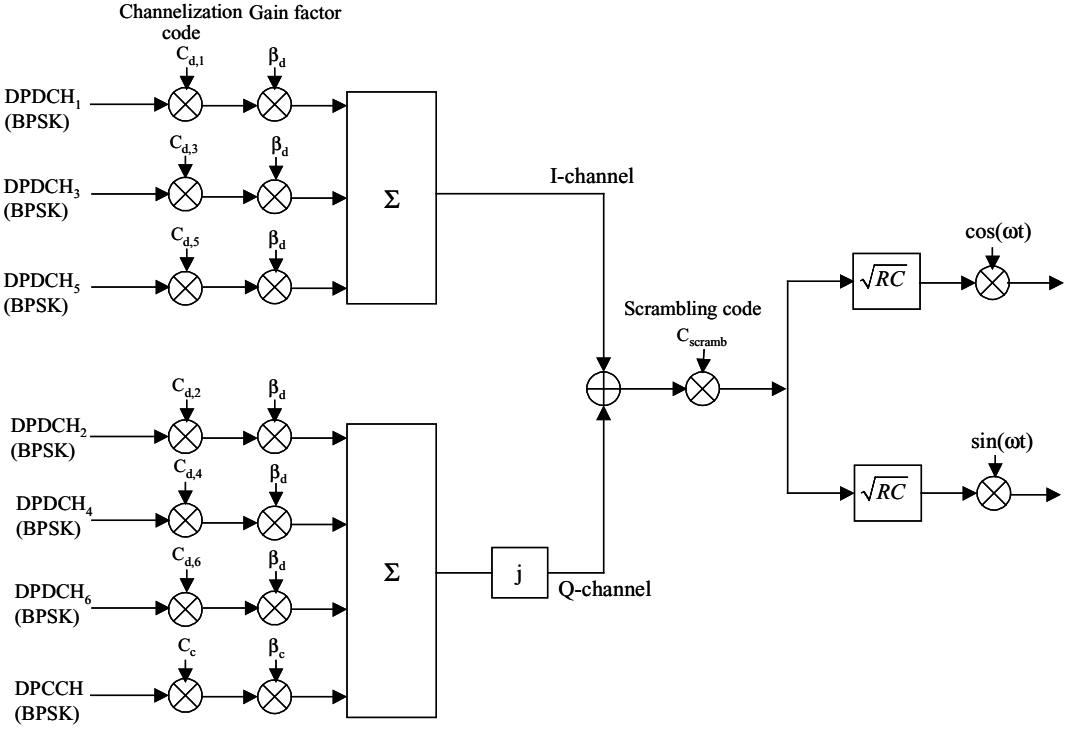

Figure 4.2.1: Spreading and modulation for uplink DPDCH and DPCCH

The binary DPCCH and DPDCHs are first mapped to bipolar bit sequences. The DPCCH is spread by the channelization code c_c, while the nth DPDCH is spread by the channelization code $c_{d,n}$, n=1,2…6. The spreaded DPDCH and DPCCH are then weighted by the gain factors β_c and β_d respectively and summed in quadrature to form the QPSK signal. A complex scrambling code, which is a unique signature of the mobile station (MS), then multiplies the QPSK signal

starting from the beginning of the frame. The scrambled signal is subsequently pulse shaped by a square-root raised cosine filter with a roll-off factor of 0.22 [UMTSb].

4.3 Uplink Code generation and allocation

4.3.1 Channelization Codes

The channelization codes that are used to spread the data to the chip rate of 3.84 Mcps are Orthogonal Variable Spreading Factor (OVSF) codes. The most important property of these codes is that they preserve the orthogonality between DPDCHs of an uplink user. The OVSF codes can be represented in a tree like structure as shown in Figure 4.3.1 [UMTSb].

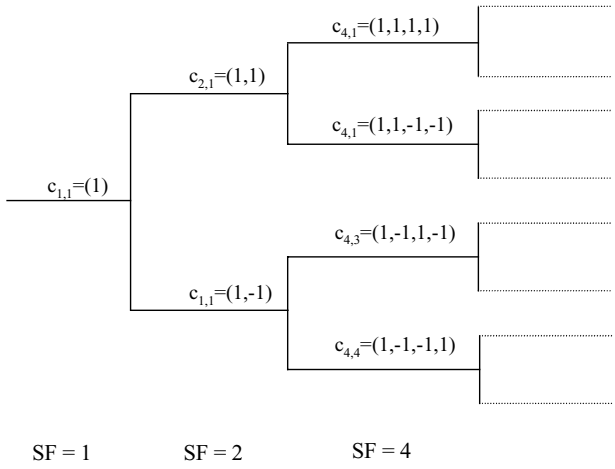

Figure 4.3.1: Code Tree for Generation of OVSF Codes

Each level of coding in the code tree corresponds to a particular SF. The number of codes in a particular level and the length of all the codewords in that level are both equal to the SF. A code in a particular level is orthogonal to another one in a different level if and only if one is not the mother of the other one. Thus, the number of available channelization codes is not fixed, but depends on the rate and the spreading factor of each physical channel. The generation method of the OVSF channelization code can be explained by the following equations.

$$C_{1,1} = 1$$

$$\begin{bmatrix} C_{2,1} \\ C_{2,2} \end{bmatrix} = \begin{bmatrix} C_{1,1} & C_{1,1} \\ C_{1,1} & -C_{1,1} \end{bmatrix} = \begin{bmatrix} 1 & 1 \\ 1 & -1 \end{bmatrix}$$

$$\bullet$$
$$\bullet$$

$$\begin{bmatrix} C_{2^{n+1},1} \\ C_{2^{n+2},1} \\ . \\ . \\ C_{2^{n+1},2^{n+1}-1} \\ C_{2^{n+1},2^{n+1}} \end{bmatrix} = \begin{bmatrix} C_{2^n,1} & C_{2^n,1} \\ C_{2^n,1} & -C_{2^n,1} \\ . & . \\ . & . \\ C_{2^n,2^n} & C_{2^n,2^n} \\ C_{2^n,2^n} & -C_{2^n,2^n} \end{bmatrix}$$

The channelization code for the DPCCH is always $C_{256,1}$. When only one DPDCH is to be transmitted, it is spread by the channelization code $C_{SF,(SF/4+1)}$. For example, the code, $C_{4,1}$ i.e., (1,1,-1-1) is used to spread a single DPDCH with an SF of 16. For multiple DPDCH transmission, all DPDCH will have SF of 4 and they are spread by the code $C_{4,k}$, where k=1 if $n \in \{1,2\}$, k=3 if $n \in \{3,4\}$ and k=2 if $n \in \{5,6\}$ [UMTSb].

4.3.1.1 Properties of channelization codes

The auto- and cross correlation properties of two OVSF codes of length 32 are shown in Figure 4.3.2(a) and 4.3.2(b) respectively.

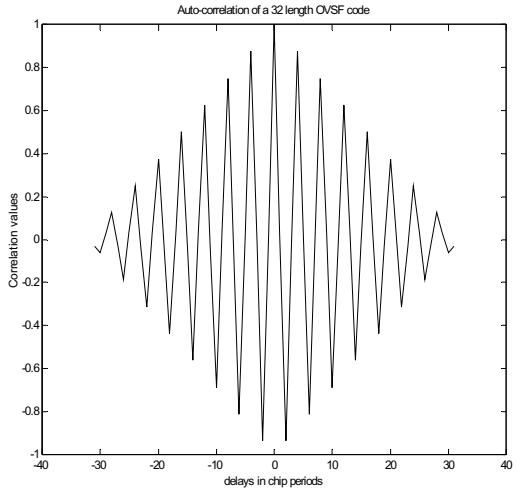

Figure 4.3.2(a): Auto-correlation of a length 32 OVSF code

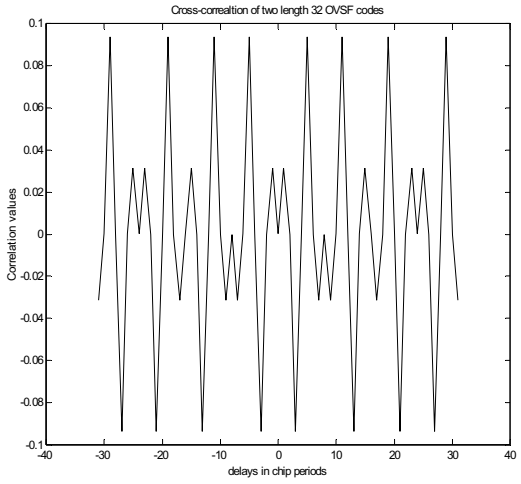

Figure 4.3.2(b): Cross-correlation of two length 32 OVSF codes

As can be seen form Figure 4.3.2(a), auto-correlation of the OVSF codes exhibit significant amount of correlation values at lags other than the zeroth lag. This implies that, when there is more than one multipath present from the desired user they will contribute significant amount of unwanted auto-correlation products to the desired multpath's correlator output. In Figure 4.3.2(b), the cross-correlation of two OVSF codes also shows high correlation values at the regular interval. Thus, if two users defined by two OVSF codes are not perfectly synchronous, then the unwanted cross-correlation products will also be significant.

4.3.2 Scrambling Codes

The uplink scrambling code can be either short or long. Short scrambling codes are generally used in cells in which the base station is equipped with an advanced receiver employing multiuser detection or interference cancellation. Long scrambling codes have better interference averaging properties and are preferred over the short scrambling code when the latter one does not give much gain in terms of implementation complexity. Both type of scrambling codes are complex numbers. Only the long scrambling code will be discussed here.

4.3.2.1 Uplink long scrambling code

The long scrambling code sequences $C_{long1,n}$ and $C_{long2,n}$ are constructed as the position wise modulo 2 sum of 38400 chip segments of two binary *m*-sequences [UMTSb]. The binary *m*-sequences are constructed from two generator polynomials of degree 25. This can be explained as below:

Let *x* and *y* be the two binary *m*-sequences constructed from the two primitive polynomials $X^{25} + X^3 + 1$ and $X^{25} + X^3 + X^2 + X + 1$, respectively.

Let $n_{23}\ldots n_0$ be the 24-bit binary representation of the scrambling code number *n* (decimal) with n_0 being the least significant bit (LSB). The *x* sequence depends on the scrambling code number *n* and is denoted as x_n. Furthermore, let $x_n(i)$ and $y(i)$ be the *i*th sequence of x_n and *y* respectively. Then the *m*-sequences x_n and *y* are constructed as

Initial conditions

$$\begin{aligned} &x_n(0) = n_0, x_n(1) = n_1, ..., = x_n(22) = n_{22}, x_n(23) = n_{23}, x_n(24) = 1 \\ &y(0) = y(1) = ... = y(23) = y(24) = 1 \end{aligned} \qquad (4.3.2.1.1)$$

The subsequent symbols are generated recursively as

$$\begin{aligned} x_n(i+25) &= x_n(i+3) + x_n(i) \ \text{ modulo 2, } \ i = 0 \ldots 2^{25} - 27 \\ y(i+25) &= y(i+3) + y(i+2) + y(i+1) + y(i) \ \text{ modulo 2, } \ i = 0 \ldots 2^{25} - 27 \end{aligned} \tag{4.3.2.1.2}$$

The binary gold sequence, z_n is defined as

$$z_n(i) = x_n(i) + y(i) \ \text{ modulo 2, } i = 0,1 \ldots 2^{25} - 2 \tag{4.3.2.1.3}$$

And is mapped to a bipolar sequence as

$$Z_n(i) = \begin{cases} +1; & z_n(i) = 0 \\ -1; & z_n(i) = 1 \end{cases}; \quad i = 0,1 \ldots 2^{25} - 2 \tag{4.3.2.1.4}$$

The real valued scrambling sequences $C_{long1,n}$ and $C_{long2,n}$ are defined as

$$\begin{aligned} C_{long1,n}(i) &= Z_n(i), i = 0,1 \ldots 2^{25} - 2 \\ C_{long2,n}(i) &= Z_n\left(\left(i + 16777232\right) \text{modulo} \left(2^{25} - 1\right)\right), i = 0,1 \ldots 2^{25} - 2 \end{aligned} \tag{4.3.2.1.5}$$

Finally the complex valued scrambling sequence $C_{long,n}$ is defined as

$$C_{long,n}(i) = c_{long1,n}(i)\left(1 + j(-1)^i c_{long2,n}\left(2\lfloor i/2 \rfloor\right)\right); i = 0,1 \ldots 2^{25} - 2 \tag{4.3.2.1.6}$$

Where $\lfloor . \rfloor$ is the floor operation (rounding to nearest lower integer). Figure 4.3.3 shows the equivalent shift register model of the uplink long scrambling generator [UMTSb].

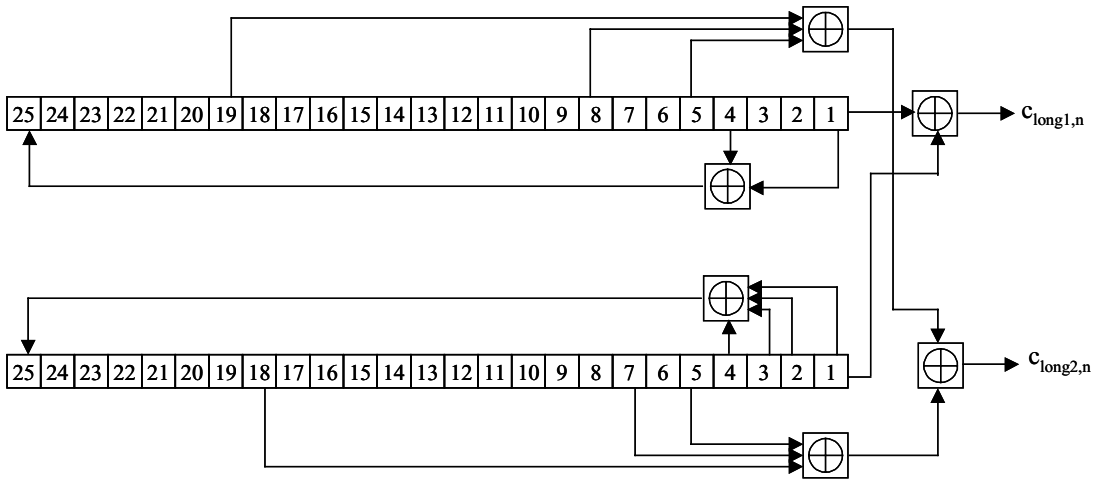

Figure 4.3.3: Shift Register Implementation of uplink long scrambling code generator

4.3.2.2 Properties of Uplink Long Scrambling Code

The auto- and cross-correlation properties of two uplink long scrambling codes are shown in Figure 4.3.3(a) and (b) respectively.

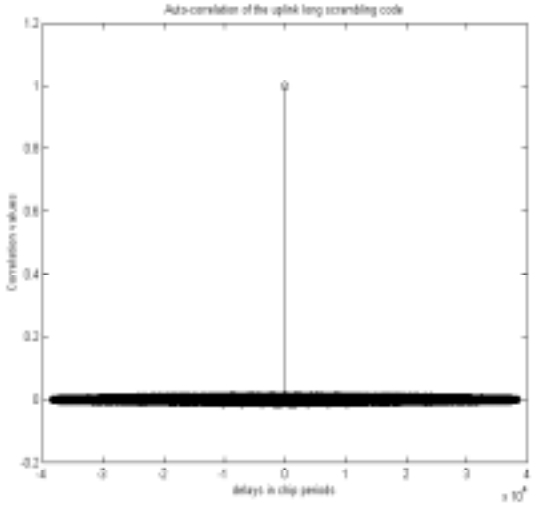

Figure 4.3.3(a): Auto-correlation of the uplink long scrambling code

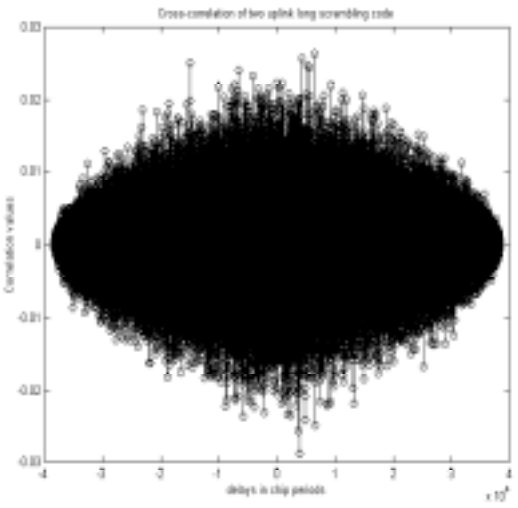

Figure 4.3.3(b): Cross-correlation of two uplink long scrambling codes

As expected the uplink long scrambling code has very good auto- and cross correlation properties. This is the only code that separates the asynchronous uplink users. Due to its good auto-correlation property, the unwanted correlation products from the desired user's multipaths will also be very small.

4.4 Channel Coding

The main purpose of channel coding is to selectively introduce redundancy into the transmitted data and improve the wireless link performance in the process. Channel codes can be used to detect as well as correct errors. The W-CDMA channel coding scheme is a combination of error detection, error correction, along with rate matching, interleaving and transport channels mapping onto/splitting from physical channels [UMTSc]. This section gives a brief introduction on the error detection and error correction schemes recommended for the W-CDMA system.

4.4.1 Error Detection

Error detection is provided by a Cyclic Redundancy Check (CRC) code. The CRC is 24,16,8 or 0 bits. The entire transmitted frame is used to compute the parity bits. Any of the following cyclic generator polynomials can be used to construct the parity bits:

$$\begin{aligned} g_{24}(D) &= D^{24} + D^{23} + D^6 + D^5 + D + 1 \\ g_{16}(D) &= D^{16} + D^{12} + D^5 + D + 1 \\ g_8(D) &= D^8 + D^7 + D^4 + D^3 + D + 1 \end{aligned} \qquad (4.4.1.1)$$

A detailed description of the error detection scheme can be found in [UMTSc].

4.4.2 Error Correction

Two alternative error correction coding schemes have been specified for the W-CDMA system. They are

- Convolutional Coding
- Turbo Coding

For standard services that require a Bit Error Rate (BER) of up to 10^{-3}, which is the case for voice applications, convolutional coding is to be applied. The constraint length for the proposed convolutional coding schemes is 9. Both rate 1/2 and 1/3 convolutional coding has been specified. For high-quality services that require BER from 10^{-3} to 10^{-6}, turbo coding is required. The feasibility of applying a 4-state Serial Concatenated Convolutional Code (SCCC) is being investigated by different standardization bodies. Reference [UMTSc] provides a detailed description of the error correction coding schemes along with the rate matching, interleaving and transport channel mapping.

4.5 Summary

In this chapter, we presented a short background on the generation of the uplink W-CDMA transmitting signal. We discussed about the designated uplink physical channels and their specific frame-slot format at the beginning. We then described the specific modulation and spreading techniques for the dedicated physical channel. For this, we discussed the generation of the uplink spreading and scrambling codes, which are used in latter simulations. We also looked in the auto and cross correlation properties of these codes, which are crucial to justify the system performance in a qualitative manner. Even though our system does not incorporate channel coding, we looked into the proposed coding scheme for future reference. The information provided in this chapter is used extensively in the later chapters to develop our space-time processing simulation testbed.

Chapter 5

System Modeling and Analysis

In the previous chapters, we presented the necessary background for 2-D RAKE receiver structures, spatio-temporal channel models and the current W-CDMA uplink signal format. To integrate all these concepts in an orderly fashion, a mathematical formulation of the system is needed. In this chapter, we characterize the system by building mathematical models of different system components. This modeling is essential for understanding the functionality of the system as well as for analyzing the system performance. In addition, these models aid in building the simulation testbed of a base-station 2-D RAKE receiver for W-CDMA, which we will present in the next chapter. Also, a mathematical description of the system helps validate the simulation results.

We first formulate the transmitted signal in accordance with the W-CDMA uplink signal format. Then, the spatio-temporal channel is characterized by a simple parametric model. We then incorporated these models in building up a complete mathematical description of a pilot symbol assisted (PSA) coherent 2-D RAKE receiver at the base station. When necessary, the details of the functional block diagrams of different system components are included. Finally, we make a qualitative measure of the system by deriving its optimum output signal to interference plus noise ratio (SINR) performance.

The chapter is organized as follows: In section 5.1 we presented the W-CDMA uplink transmitter model. Section 5.2 gives a brief description of the spatio-temporal parametric channel model. In Section 5.3, the PSA 2-D RAKE receiver is analyzed using the input signal and channel models developed in the previous two sections. In section 5.4, we derived the optimum

output SINR performance of this space-time processing system. Finally a summary is given in section 5.5.

5.1 Transmitter Model

The block diagram of the W-CDMA uplink transmitter for the *i*th user as described in section 4.2, is shown in Figure 5.1.1.

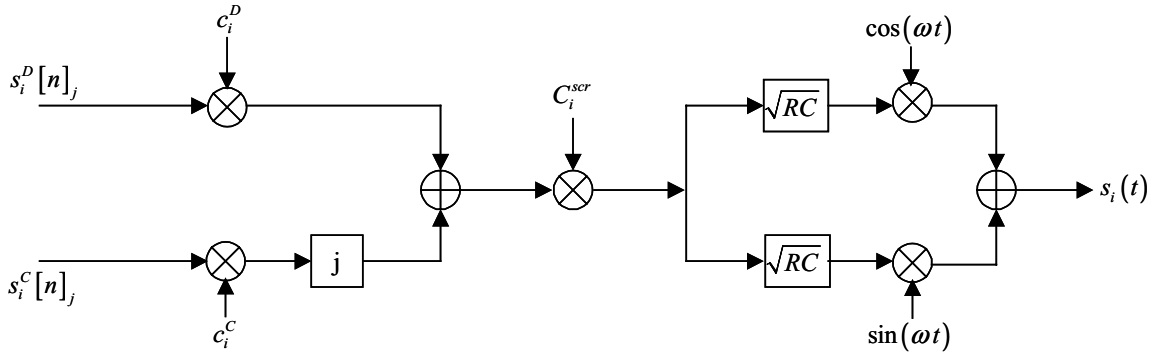

Figure 5.1.1: W-CDMA uplink transmitter model

For simplicity only one data channel (DPDCH) is shown even though the W-CDMA uplink transmitter can support up to six DPDCH. The sequences $b_i^D[n]$ and $b_i^C[n]$ are the channel coded data and control bits of the *i*th user respectively. In this development, these are the signals of interest, so the previous blocks such as coding and interleaving do no appear in the figure. They are mapped into the *I* and *Q* branches and subsequently spreaded by two different channelization code sequence $\mathbf{c}_i^D$ and $\mathbf{c}_i^C$, respectively. These codes commonly known as Orthogonal Variable Spreading Factor (OVSF) codes are orthogonal to each other and user specific. After channelization the two spreaded sequences are weighted by two different gain factors and combined orthogonally to form the baseband QPSK signal.

For simplicity of analysis, we will assume that the data and control channel have the same bit rate and the spreading factor. Then the $G_i \times 1$ spreaded chip sequence vector for the *n*th bit, $\mathbf{v}_i[n]$ can be expressed as

$$\mathbf{v}_i[n] = \mathbf{v}_i\left((n-1)G_i ... nG_i\right) = \beta_i^D b_i^D[n]\mathbf{c}_i^D + j\,\beta_i^C b_i^C[n]\mathbf{c}_i^C;\ n = 1,2...N_{Frame} \qquad (5.1.1)$$

where n is the bit index, G_i is the ith user's spreading factor which is also the length of the channelization code vectors, $\mathbf{c}_i^D$ and $\mathbf{c}_i^C$ and β_i^D, β_i^D are the gain factor for ith user's DPDCH and DPCCH respectively. The spreaded signal is further multiplied by a complex scrambling code, $\mathbf{c}_i^{scr}$ with a periodicity of one frame. The resulting signal is

$$\begin{aligned}\mathbf{s}_i[n] &= \mathbf{v}_i[n]\,diag\left(\mathbf{c}_i^{scr}\left((n-1)G...nG\right)\right) \\ &= \left(\beta_i^D b_i^D[n]\mathbf{c}_i^D + j\beta_i^C b_i^C[n]\mathbf{c}_i^C\right)diag\left(\mathbf{c}_i^{scr}[n]\right);\ n=1,2...N_{Frame}\end{aligned} \tag{5.1.2}$$

where $diag(\cdot)$ is the diagonalization operation with the elements of $\mathbf{c}_i^{scr}[n]$ along the main diagonal. The baseband discrete time signal is then pulse shaped by a root raised cosine filter and upconverted to form the transmitted waveform from the ith user as below

$$\begin{aligned}s_i(t) &= \sum_{n=1}^{N_{Frame}} \mathbf{s}_i[n]c_i(t-nT_b)\exp(j\omega_c t+\phi_i) \\ &= \sum_{n=1}^{N_{Frame}} \beta_i^D b_i^D[n]\sum_{k=1}^{G_i} c_i^D(k)c_i^{scr}\left((n-1)G_i+k\right)g\left(t-\left(nG_i+k\right)T_c\right)\cos\left(\omega_c t+\phi_i\right) \\ &\quad -\beta_i^C b_i^C[n]\sum_{k=1}^{G_i} c_i^C(k)c_i^{scr}\left((n-1)G_i+k\right)g\left(t-\left(nG_i+k\right)T_c\right)\sin\left(\omega_c t+\phi_i\right)\end{aligned} \tag{5.1.3}$$

where $g(t)$ is the chip pulse shaping waveform, T_b and T_c are the bit and chip duration respectively, ω_c is the angular carrier frequency and ϕ_i is an unknown carrier phase. The transmitted signal is propagated through the channel characterized in the next section.

5.2 Channel Description

The spatio-temporal channel models described in Chapter 3 provides a statistical description of the multipaths channel parameters such as channel gain, propagation delays, angle of arrivals (AOA) etc. However, for the purpose of analysis, a simple parametric model represented by a summation of delta functions associated with different amplitudes, time delays and AOA is more useful. Each of these delta functions corresponds to a resolvable multipath in a frequency selective fading channel, as is the case for a W-CDMA signal. Thus the channel impulse response formed in this manner provides a mean description of the statistically distributed channel parameters in both space and time.

An important parameter that characterizes the spatial channel is the angle spread, Δ defined as the spread of the AOA of the discrete multipath components. In other words, each of the delta functions in the channel impulse response is in reality a combination of a number of delta functions (subpaths), which arrive very closely in time but may have different directions. The range of the AOA of these subpaths is characterized by the angle spread. As we will see, this parameter has an important effect on different array processing and combining techniques.

As mentioned earlier, a W-CDMA system undergoes frequency selective fading when the relative multipaths delays are more than a chip period. This time dispersiveness property of the channel is characterized by the delay spread defined in a similar way as the angle spread. That is, delay spread is a measure of spread of the multipaths in time domain. Thus, it will determine the performance of time domain processing schemes such as RAKE combining.

The time-varying property of the channel model is defined by the doppler spread. For the spatio-temporal channel models, an accurate description of doppler power spectrum is still to be formulated. However in this analysis and in our simulation we will be assuming a Rayleigh faded temporal characteristics of the channel since it gives a close enough power spectrum to the models in chapter 3 [Ert98], [Pet96].

Let us consider an N-element linear antenna array at the receiver. The channel impulse response of the ith user can be expressed as

$$\mathbf{h}_i(t) = \sum_{l=1}^{L_i} \alpha_{l,i}(t)\,\mathbf{a}(\theta_{l,i})\,\delta(t-\tau_{l,i}) \tag{5.2.1}$$

where L_i is the number of resolvable multipaths from the ith user each characterized by a complex path amplitude $\alpha_{l,i}(t)$ and a path delay $\tau_{l,i}$. The $N\times 1$ array response vector or the steering vector $\mathbf{a}(\theta_{l,i})$ is defined as

$$\mathbf{a}(\theta_{l,i}) = \left[\begin{array}{cccc} 1 & e^{-j2\pi\frac{d}{\lambda}\sin(\theta_{l,i}+\Delta_i)} & . \;\; . & e^{-j2\pi\frac{d}{\lambda}(N-1)\sin(\theta_{l,i}+\Delta_i)} \end{array}\right]^T \tag{5.2.2}$$

where d is the element spacing and $\theta_{l,i}$ is the AOA of the lth path from ith user and Δ_i is the angle spread of the ith user . In the analysis, we will use the narrowband assumption for array processing which states that the envelope of the plane wave propagating across the array remains essentially constant if the bandwidth of either the signal or the antenna is small compared to the

carrier frequency. For the wideband case, this assumption is also valid provided that the time taken by the wavefront to pass across the array is small compared to the chip period T_c. Equation (5.2.1) can be rearranged as

$$\mathbf{h}_i(t) = \sum_{l=1}^{L_i} \mathbf{a}_{l,i}(t)\,\delta\left(t - \tau_{l,i}\right) \tag{5.2.3}$$

where $\mathbf{a}_{l,i}(t) = \alpha_{l,i}(t)\,\mathbf{a}\left(\theta_{l,i}\right)$ is called the spatial signature vector or the channel vector of the *i*th user. Thus this channel model is equivalent to a tapped delay line filter with the power spectrum defining the time varying filter coefficients.

5.3 Receiver Model

The receiver portion at the base station intended to detect the *i*th user in the uplink is shown in Figure 5.3.1.

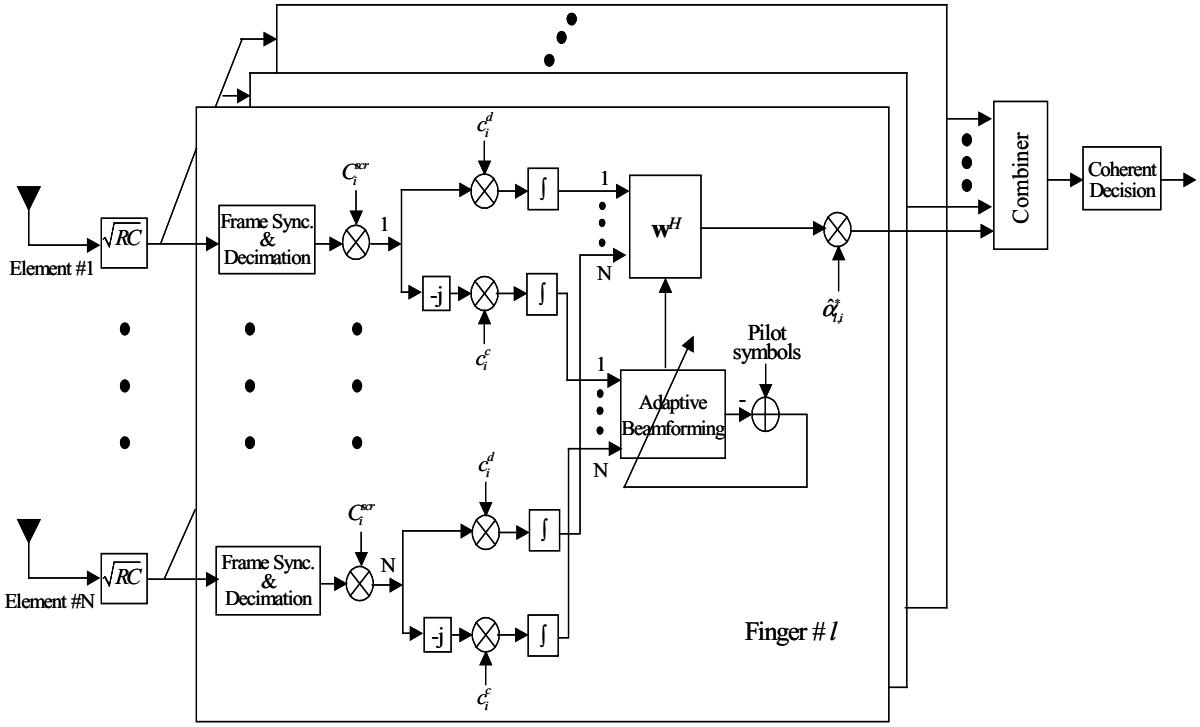

Figure 5.3.1: Base station antenna array receiver model

The base station uses an *N* element antenna array receiver to demodulate the desired user's signal. After downconversion and lowpass filtering, the baseband received signal is processed by a bank of *M* space-time processors each assigned to one of the resolvable multipaths. To detect

the *l*th path, the signals at different antenna elements are first time aligned to the *l*th path delay and discretized to form the chip samples. Then a descrambling operation is performed at each element of the antenna array followed by the despreading using the data and the control channel channelization codes. An adaptive beamforming network then takes the despreaded control channel symbols as the input and calculates the beamformer weights using the pilot symbols in the control channel as the reference signal. Typically gradient-based algorithms such as Least-Mean Square (LMS) algorithm or the standard Recursive Least Square (RLS) algorithm are considered. The weights are updated in each slot of the W-CDMA frame and used on both the data and control channel symbols for beamforming. The outputs of the *M* beamformer are then coherently combined (MRC RAKE combining) by the modified channel gain through the beamformer and hard limited to get the coherent symbol decision.

The total received $N\times1$ signal vector at the base station antenna array is given by

$$\mathbf{x}(t) = \sum_{i=1}^{K}\sum_{l=1}^{L_i}\mathbf{a}_{l,i}(t)s_i(t-\tau_{l,i}) + \boldsymbol{\eta}(t) \tag{5.3.1}$$

where K is the total number of users in the system and $\boldsymbol{\eta}(t)$ is the $N\times1$ complex additive Gaussian noise vector with zero mean and a variance of $\sigma_n^2 = N_0/2$. All the other symbols have the same meaning as in section 5.1 and 5.2. It is assumed that the noise vector is spatially and temporally white, i.e., $E\{\boldsymbol{\eta}(t_1)\boldsymbol{\eta}^H(t_2)\} = \sigma_n^2\delta(t_1-t_2)$, where $(\cdot)^H$ is the Hermitian (conjugate transpose) operator.

Without loss of generality, let us consider the operation of the receiver for the *l*th path of *i*th user. After downconversion, the received signal is synchronized to the *l*th multipath delay $\tau_{l,i}$. and low-pass filtered (root raised cosine matched filtering). The resulting discrete signal can be expressed as

$$\mathbf{X}_{l,i}[n] = \mathbf{A}_{l,i}[n]\,diag(\mathbf{s}_i[n]) + \mathbf{I}[n] + \mathbf{M}[n] + \mathbf{N}[n]; \quad n = 1,2,...,N_{Frame} \tag{5.3.2}$$

where again n is the bit index, $\mathbf{X}_{l,i}[n]$ and $\mathbf{N}[n]$ are $N\times G_i$ received chip sample matrix and sampled noise matrix respectively, $\mathbf{A}_{l,i}[n]$ is the $N\times G_i$ discrete channel matrix for the *l*th path of user i, $\mathbf{s}_i[n]$ is the $G_i\times1$ transmitted chip sequence vector for the user i as given by (5.1.2). The

$N \times G_i$ matrices, $\mathbf{I}[n]$ and $\mathbf{M}[n]$ are the user's self interference due to multipaths and the multiple access interference (MAI) from all the other users and they are expressed as

$$\begin{aligned}\mathbf{I}[n] &= \sum_{\substack{l'=1 \\ l' \neq l}}^{L_i} \mathbf{A}_{l',i}[n]\, diag\left(\mathbf{s}_i\left[n - \left\lfloor \frac{\tau_{l',i} - \tau_{l,i}}{T_c} \right\rfloor\right]\right) \\ \mathbf{M}[n] &= \sum_{\substack{i'=1 \\ i' \neq i}}^{K} \sum_{l=1}^{L_{i'}} \mathbf{A}_{l,i'}[n]\, diag\left(\mathbf{s}_{i'}\left[n - \left\lfloor \frac{\tau_{l,i'} - \tau_{l,i}}{T_c} \right\rfloor\right]\right)\end{aligned} \tag{5.3.3}$$

Substituting (5.1.2) in (5.3.3) and treating the summation of $\mathbf{I}[n]$, $\mathbf{M}[n]$ and $\mathbf{N}[n]$ as a single interference plus noise matrix, $\hat{\mathbf{N}}[n]$, the received discrete chip samples for nth bit

$$\mathbf{X}_{l,i}[n] = \mathbf{A}_{l,i}[n]\, diag\left(\left(\beta_i^D b_i^D[n]\mathbf{c}_i^D + j\beta_i^C b_i^C[n]\mathbf{c}_i^C\right) diag\left(\mathbf{c}_i^{scr}[n]\right)\right) + \hat{\mathbf{N}}[n] \tag{5.3.4}$$

At each antenna element, the signal is descrambled by the ith user's scrambling code sequence, $\mathbf{c}_i^{scr}$ as below

$$\mathbf{X}_{l,i}^{dscr}[n] = \mathbf{X}_{l,i}[n]\, diag\left(\left(\mathbf{c}_i^{scr}\right)^*\right) = \mathbf{A}_{l,i}[n]\, diag\left(b_i^D[n]\mathbf{c}_i^D + j b_i^C[n]\mathbf{c}_i^C\right) + \hat{\mathbf{N}}_{dscr}[n] \tag{5.3.5}$$

where it is assumed that the amplitudes of the complex scrambling sequence, $\mathbf{c}_i^{scr}[n]$ is normalized to unity. The resulting $N \times G_i$ interference plus noise matrix after descrambling, $\hat{\mathbf{N}}_{dcsr}[n]$ is given by

$$\begin{aligned}\hat{\mathbf{N}}_{dscr}[n] &= \mathbf{I}_{dscr}[n] + \mathbf{M}_{dcsr}[n] + \mathbf{N}_{dscr}[n] \\ &= \mathbf{I}[n]\, diag\left(\mathbf{c}_i^{scr}[n]\right) + \mathbf{M}[n]\, diag\left(\mathbf{c}_i^{scr}[n]\right) + \mathbf{N}[n]\, diag\left(\mathbf{c}_i^{scr}[n]\right)\end{aligned} \tag{5.3.6}$$

As shown in chapter 4, the W-CDMA uplink long scrambling code, $\mathbf{c}_i^{scr}$ has very good auto- and cross correlation properties. That means, the auto and cross correlation function of $\mathbf{c}_i^{scr}$ can be approximated as

$$E\left\{c_i^{scr}[p]\left(c_{i'}^{scr}[q]\right)^*\right\} \cong \delta_{i,i'}(p-q); \quad p,q = 1,2,\ldots,C_{frame}; \quad i \neq i' \tag{5.3.7}$$

Then this has the effect of making the elements of the descrambled interference plus noise matrix, $\hat{\mathbf{N}}_{dcsr}[n]$ uncorrelated. Subsequent despreading of the resultant signal by the $G_i \times 1$ data and control channelization code vectors, $\mathbf{c}_i^D$ and $\mathbf{c}_i^C$, respectively, collapses the chip samples over

a code length into one data and control channel bit. The resulting despreaded data and control bits can be expressed as

$$\begin{aligned}\mathbf{x}_{l,i}^{D}[n] &= \frac{1}{G_i}\mathbf{X}_{dscr}[n]\mathbf{c}_i^{D} = \mathbf{a}_{l,i}[n]\beta_i^{D}b_i^{D}[n] + \hat{\boldsymbol{\eta}}_l^{D}[n] \\ \mathbf{x}_{l,i}^{C}[n] &= \frac{1}{G_i}(-j)\mathbf{X}_{dscr}[n]\mathbf{c}_i^{C} = \mathbf{a}_{l,i}[n]\beta_i^{C}b_i^{C}[n] + \hat{\boldsymbol{\eta}}_l^{C}[n]\end{aligned} \tag{5.3.8}$$

where $\mathbf{a}_{l,i}[n] = \alpha_{l,i}[n]\mathbf{a}(\theta_{l,i})$ is the $N\times1$ channel vector for the nth bit, $\hat{\boldsymbol{\eta}}_l^{D}[n]$ and $\hat{\boldsymbol{\eta}}_l^{C}[n]$ are $N\times1$ total interference plus noise vectors for the nth bit associated with data and control channel, respectively. It is intuitive from the previous statements that the elements of the interference plus noise vectors will also be uncorrelated. Also, it is shown analytically in [Ann99] and by simulation in [Nag96b] that when the number of user is large (heavily loaded system), autocorrelation matrices of these interference plus noise vectors are close to scaled identity matrices, which is what we expect if they are composed of independent elements. That is

$$\begin{aligned}\mathbf{R}_{uu}^{D}[n] &= E\left\{\hat{\boldsymbol{\eta}}_l^{D}[n]\left(\hat{\boldsymbol{\eta}}_l^{D}[n]\right)^{H}\right\} \cong \sigma_{\hat{\boldsymbol{\eta}}_l^{D}}^{2}\mathbf{I} \\ \mathbf{R}_{uu}^{C}[n] &= E\left\{\hat{\boldsymbol{\eta}}_l^{C}[n]\left(\hat{\boldsymbol{\eta}}_l^{C}[n]\right)^{H}\right\} \cong \sigma_{\hat{\boldsymbol{\eta}}_l^{C}}^{2}\mathbf{I}\end{aligned} \tag{5.3.9}$$

where $\sigma_{\hat{\boldsymbol{\eta}}_l^{D}}^{2}$ and $\sigma_{\hat{\boldsymbol{\eta}}_l^{C}}^{2}$ are the variances of $\hat{\boldsymbol{\eta}}_l^{D}[n]$ and $\hat{\boldsymbol{\eta}}_l^{C}[n]$ respectively and $\mathbf{I}$ is an $N\times N$ identity matrix. The despreaded control channel signal has a factor of $-j$ in its expression indicating the fact that it was mapped into the Q-branch in the original transmitted signal

As mentioned in chapter 4, the current W-CDMA uplink signal format defines pilot bits in the control channel [ETS00]. Therefore, any beamformer that uses the pilot bits as the reference signal should take the despreaded control channel bits as the input. We considered three different pilot symbol assisted (PSA) beamforming techniques: Minimum Mean Squared Error (MMSE) based Direct Matrix Inversion (DMI) beamforming, Least Mean Square (LMS) and Recursive Least Square (RLS) adaptive beamforming. They are explained in the following sections.

5.3.1 Direct Matrix Inversion (DMI) beamforming

The DMI beamformer minimizes the mean squared error between the beamformer output and the reference signal [Mon80], [Ert98b]. Denoting the reference signal as $d[n]$ and the input

signal to the N-element beamformer as $\mathbf{x}[n]$, the optimum weight vector estimate is given by the Wiener-Hopf (W-H) equation as below

$$\hat{\mathbf{w}}_{OPT} = \hat{\mathbf{R}}_{xx}^{-1}\hat{\mathbf{r}}_{xd} \tag{5.3.1.1}$$

where the $N \times N$ matrix, $\hat{\mathbf{R}}_{xx}$ is an windowed estimate of the sample autocorrelation matrix, $\mathbf{R}_{xx}$ and is usually given by

$$\hat{\mathbf{R}}_{xx}[i] = \sum_{n=1}^{i} \lambda^{i-n}\mathbf{x}[n]\mathbf{x}^{H}[n]; \quad 1 \le n \le i \tag{5.3.1.2}$$

where λ is a weighting factor or forgetting factor defined over the interval (0,1]. The value of λ determines how much past information will be used to calculate the sample correlation matrix. For a nonstationary fading channel, λ is usually less than 1, which defines an exponential window, thus ensuring that the data in the distant past is forgotten in order to account for the statistical variation of the data samples. For fading channels, λ is chosen so that the window length extends over the coherence time of the channel, i.e., the time over which the fading can be considered correlated. For a stationary channel, λ is taken as 1.

The $N \times 1$ vector, $\hat{\mathbf{r}}_{xd}$ in (5.3.1.1) is an estimate of the sample crosscorrelation vector between $\mathbf{x}[n]$ and $d[n]$ and is defined in the same way as $\hat{\mathbf{R}}_{xx}$, i.e.,

$$\hat{\mathbf{r}}_{xd}[i] = \sum_{n=1}^{i} \lambda^{i-n}\mathbf{x}[n]d^{*}[n]; \quad 1 \le n \le i \tag{5.3.1.3}$$

where the symbols have the same meaning as before. Equations (5.3.1.2) and (5.3.1.3) can be written in a recursive fashion as below

$$\begin{aligned}
\hat{\mathbf{R}}_{xx}[i] &= \lambda\left[\sum_{n=1}^{i-1} \lambda^{i-1-n}\mathbf{x}[n]\mathbf{x}^{H}[n]\right] + \mathbf{x}[i]\mathbf{x}^{H}[i] = \lambda\hat{\mathbf{R}}_{xx}[i-1] + \mathbf{x}[i]\mathbf{x}^{H}[i] \\
\hat{\mathbf{r}}_{xd}[i] &= \lambda\left[\sum_{n=1}^{i-1} \lambda^{i-1-n}\mathbf{x}[n]d^{*}[n]\right] + \mathbf{x}[i]d^{*}[i] = \lambda\hat{\mathbf{r}}_{xd}[i-1] + \mathbf{x}[i]d^{*}[i]
\end{aligned} \tag{5.3.1.4}$$

As mentioned earlier, the despreaded control channel signal, $\mathbf{x}_{l,i}^{C}[n]$ as given in (5.3.8) is the input to the lth beamformer designated for the ith user. The reference signal, $d[n]$ is the pilot in the control channel of the uplink W-CDMA signal [ETS00]. For each slot of a frame, the

weight vectors are calculated using the pilot bits for that slot. The auto and cross correlation estimates at the end of a slot are used to update the estimates for the next slot according to (5.3.1.4). Thus if N_d is the number of pilot bits per slot, then the weight vector of the lth beamformer for the jth slot is given by

$$\mathbf{w}_l^j = \left(\hat{\mathbf{R}}_{x_c x_c}^j [N_d]\right)^{-1} \hat{\mathbf{r}}_{x_c d}^j [N_d]; \quad j = 1,2,...,15 \tag{5.3.1.5}$$

where

$$\begin{aligned}
\hat{\mathbf{R}}_{x_c x_c}^j [N_d] &= \hat{\mathbf{R}}_{x_c x_c}^{j-1} [N_d] + \sum_{n=(j-1)N_d+1}^{jN_d} \lambda^{jN_d-n} \mathbf{x}_{l,i}^C [n] \left(\mathbf{x}_{l,i}^C [n]\right)^H = \hat{\mathbf{R}}_{x_c x_c}^{j-1} [N_d] + \lambda \hat{\mathbf{R}}_{x_c x_c}^j [N_d - 1] + \mathbf{x}_{l,i}^C [N_d] \left(\mathbf{x}_{l,i}^C [N_d]\right)^H \\
\hat{\mathbf{r}}_{x_c d}^j [N_d] &= \hat{\mathbf{r}}_{x_c d}^{j-1} [N_d] + \sum_{n=(j-1)N_d+1}^{jN_d} \lambda^{jN_d-n} \mathbf{x}_{l,i}^C [n] \left(d^j [n]\right)^* = \hat{\mathbf{r}}_{x_c d}^{j-1} [N_d] + \lambda \hat{\mathbf{r}}_{x_c d}^j [N_d - 1] + \mathbf{x}_{l,i}^C [N_d] \left(d^j [N_d]\right)^*
\end{aligned} \tag{5.3.1.6}$$

where $d^j[n]$, n=1,2,…,N_d are the pilot bits for the jth slot.

5.3.2 Least Mean Square (LMS) Adaptive beamforming

The DMI method as described in section 5.3.1 requires the inversion of the autocorrelation matrix $\mathbf{R}_{xx}$, which involves a significant amount of computation. An attractive solution to this problem is the use of Least Mean Square (LMS) adaptive algorithm, which is a member of the so-called stochastic gradient descent algorithms [Hay91]. The basic idea of the LMS algorithm is that it tries to get an instantaneous (symbol by symbol) estimate of the gradient vector of the cost function, which in this case is the Mean Squared error (MSE) between the reference signal and the beamformer output. In this respect, the LMS algorithm differs from the steepest descent method of solving the W-H equation in that the gradient vector estimation does not require a large windowed estimate of the correlation functions [Hay91]. In other words, the algorithm uses a one-symbol data window to get a noisy estimate of these functions and consequently adapts to the incoming data in order to converge to the optimum Wiener solution given by (5.3.1.1)

The weight vector update using the LMS algorithm is given by the following recursive formula

$$\hat{\mathbf{w}}[n+1] = \hat{\mathbf{w}}[n] + \mu \mathbf{x}[n] e^*[n] \tag{5.3.2.1}$$

where $\mathbf{x}[n]$ is the beamformer input. $e[n]$ is the estimation error between the beamformer output and the reference signal, $d[n]$, and is represented as

$$e[n] = d[n] - \hat{\mathbf{w}}[n]^H \mathbf{x}[n] \tag{5.3.2.2}$$

The parameter μ in (5.3.2.1) is a small positive constant that defines the step size of the incremental correction of the weight vector. The convergence of the algorithm towards the optimum weight vector depends on the selection of μ. A larger value of μ drives the algorithm faster towards convergence but has the risk of not achieving the minimum value of the cost function and instability. On the other hand, a smaller value of μ increases the probability of reaching the minimal point but it suffers from slower convergence.

Referring to the W-CDMA frame format, the antenna weight vectors are updated in each slot using the pilot bits for that slot. The weight vector calculated at the end of a slot is used as the initial weight vector for the weight updation in the next slot. Thus the weight update equation for the jth slot can be represented as

$$\begin{aligned} &\mathbf{w}_l^j[1] = \mathbf{w}^{j-1}[N_d] \\ &\mathbf{w}_l^j[n+1] = \mathbf{w}^j[n] + \mu \mathbf{x}_{l,i}^C\left[(j-1)N_d + n\right]\left(e^j[n]\right)^*; \quad n = 1,2,...,N_d \end{aligned} \tag{5.3.2.3}$$

where as in section (5.3.1), N_d is the number of pilot bits per slot and $\mathbf{x}_{l.i}{}^C[n]$ is the beamformer input given by the despreaded control channel signal in (5.3.8). The error signal for the jth slot, $e^j[n]$ is expressed as below

$$e^j[n] = d^j[n] - \left(\mathbf{w}_l^j[n]\right)^H \mathbf{x}_{l,i}^C\left[(j-1)N_d + n\right]; \quad n = 1,2,...,N_d \tag{5.3.2.4}$$

5.3.3 Recursive Least-Square (RLS) Adaptive Beamforming

The RLS algorithm is a recursive technique that gives an approximate least-square (LS) estimate of the antenna weight vectors. Thus the cost function of the RLS algorithm is the sum of the squared errors over a sample window as opposed to the ensemble average of the squared error (MSE) in the LMS algorithm [Hay91].

The key feature of the RLS algorithm is an iterative technique that estimates the inverse of the windowed autocorrelation function, $\mathbf{R}_{xx}$. The steps of the RLS algorithm are given below

$$\begin{aligned}
\mathbf{k}[n] &= \frac{\lambda^{-1}\mathbf{P}[n-1]\mathbf{x}_c[n]}{1+\lambda^{-1}\mathbf{x}_c^H[n]\lambda^{-1}\mathbf{P}[n-1]\mathbf{x}_c[n]} \\
\alpha[n] &= d[n]-\hat{\mathbf{w}}^H[n-1]\mathbf{x}_c[n] \\
\hat{\mathbf{w}}[n] &= \hat{\mathbf{w}}[n-1]+\mathbf{k}[n]\alpha^*[n] \\
\mathbf{P}[n] &= \lambda^{-1}\mathbf{P}[n-1]-\lambda^{-1}\mathbf{k}[n]\mathbf{x}_c^H[n]\mathbf{P}[n-1]
\end{aligned} \tag{5.3.3.1}$$

where $\mathbf{x}[n]$, $d[n]$ and λ have the same meaning as in sections (5.3.1) and (5.3.2). The $N\times N$ matrix, $\mathbf{P}[n]$ which is updated recursively in the algorithm, is an estimate of the inverse of the autocorrelation matrix, $\mathbf{R}_{xx}[n]$. The initial value of $\mathbf{P}[n]$ is usually set as

$$\mathbf{P}[0] = \delta^{-1}\mathbf{I} \tag{5.3.3.2}$$

where $\mathbf{I}$ is the $N\times N$ identity matrix and δ is a small positive constant. As in the case of the LMS algorithm, the antenna weight vectors are updated in each slot using the pilot bits for that slot and the weights calculated at the end of a slot are used to initialize the algorithm in the next slot.

In all the three beamforming techniques described above, the weight vectors are calculated on a slot by slot basis either by taking all the pilot bits in a slot to form the correlation estimates as in DMI or by updating the weights recursively with each pilot bits in the slot as in LMS or RLS. Thus the weight vector associated with a particular control channel slot can be used to beamform both the corresponding data and control channel slot. Continuing from Equation (5.3.9), the output of the lth beamformer for the jth data and control channel slot can be expressed as

$$\begin{aligned}
z_{l,i}^D[n]_j &= \left(\mathbf{w}_l^j\right)^H \mathbf{x}_{l,i}^D(n)_j \\
z_{l,i}^C[n]_j &= \left(\mathbf{w}_l^j\right)^H \mathbf{x}_{l,i}^C(n)_j ; n = (j-1)N_d,...,jN_d,\ j = 1,...,\frac{N_{frame}}{N_d}
\end{aligned} \tag{5.3.10}$$

where again j is the slot index, $\mathbf{w}_l^j$ is the weight vector for the jth slot and $\mathbf{x}_{l,i}^D[n]_j$ and $\mathbf{x}_{l,i}^C[n]_j$ are the despreaded data and control channel bits respectively for the jth slot given by (5.3.6). Substituting (5.3.6) in (5.3.7)

$$
\begin{aligned}
z_{l,i}^{D}[n]_j &= \left(\mathbf{w}_l^j\right)^H \mathbf{a}_{l,i}[n]\beta_i^D b_i^D[n] + \left(\mathbf{w}_l^j\right)^H \hat{\boldsymbol{\eta}}_l^D[n] \\
z_{l,i}^{C}[n]_j &= \left(\mathbf{w}_l^j\right)^H \mathbf{a}_{l,i}[n]\beta_i^C b_i^C[n] + \left(\mathbf{w}_l^j\right)^H \hat{\boldsymbol{\eta}}_l^C[n]
\end{aligned}
\tag{5.3.11}
$$

In the receiver, each RAKE finger is associated with a beamformer dedicated to a specific spatio-temporal multipath. Thus, to coherently combine all the beamformer outputs the channel gains for all these paths need to be estimated. The modified channel gain at the beamformer output is given by

$$
\hat{\alpha}_{l,i}[n]_j = \left(\mathbf{w}_l^j\right)^H \mathbf{a}_{l,i}[n];\ n = (j-1)N_d, ..., jN_d,\ l = 1,2,...,M \tag{5.3.12}
$$

where $\mathbf{a}_{l,i}[n] = \alpha_{l,i}[n]\mathbf{a}(\theta_{l,i})$ is the $N\times 1$ channel vector for the nth bit and M is the number of RAKE fingers used in the receiver. In practice, this modified channel gain for each path is estimated by some sort of weighted average of the pilot bits in a single or multiple control channel slots [And98]. The output of the MRC coherent RAKE combiner is then expressed as

$$
\begin{aligned}
z_i^D[n]_j &= \sum_{l=1}^{M} z_{l,i}^D[n]_j \left(\hat{\alpha}_{l,i}[n]_j\right)^* \\
z_i^C[n]_j &= \sum_{l=1}^{M} z_{l,i}^C[n]_j \left(\hat{\alpha}_{l,i}[n]_j\right)^*;\quad n = (j-1)N_d, ..., jN_d
\end{aligned}
\tag{5.3.13}
$$

where the respective symbols have the same meaning as described before. The soft decisions, $z_i^D[n]$ and $z_i^D[n]$ are then hard-limited to get coherent decisions for the uncoded data and control channel bits.

5.4 Generalized Optimum Output SINR Analysis

In this section, the output SINR expression of the 2-D RAKE receiver employing a general optimum beamformer is derived. The approach followed here is similar to the one used in [Ann99] and [Ert98a]. The assumptions made here will be to be validated in our future research.

The optimum weight vectors for the lth beamformer is well known to be given by [Hay91]

$$
\begin{aligned}
\mathbf{w}_{l,OPT}^D &= \gamma_l^D \left(\mathbf{R}_{uu}^D[n]\right)^{-1} \mathbf{a}_{l,i}[n] \\
\mathbf{w}_{l,OPT}^C &= \gamma_l^D \left(\mathbf{R}_{uu}^C[n]\right)^{-1} \mathbf{a}_{l,i}[n]
\end{aligned}
\tag{5.4.1}
$$

where γ_l^D and γ_l^C are arbitrary constants, $\mathbf{R}_{uu}^D[n]$ and $\mathbf{R}_{uu}^C[n]$ are the data and control interference plus noise correlation matrices respectively given as (5.3.9) and $\mathbf{a}_{l,i}[n]$ and the channel vector defined in (5.3.9). In the case, if $\mathbf{R}_{uu}^D[n]$ and $\mathbf{R}_{uu}^C[n]$ can be approximated by identity matrices, the optimum weight vectors become

$$\begin{aligned}\mathbf{w}_{l.OPT}^D &\cong \gamma_l^D \sigma_{\hat{\boldsymbol{\eta}}_l^D}^2 \mathbf{a}_{l,i}[n] \\ \mathbf{w}_{l.OPT}^C &\cong \gamma_l^C \sigma_{\hat{\boldsymbol{\eta}}_l^C}^2 \mathbf{a}_{l,i}[n]\end{aligned} \tag{5.4.2}$$

As can be seen when the interference and noise is white, the solution becomes the MRC diversity combining.

Substituting (5.4.1) in (5.3.11), the lth beamformer output can be expressed as

$$\begin{aligned}z_{l,i}^D[n] &= \left(\gamma_l^D\right)^* \mathbf{a}_{l,i}^H[n]\left(\mathbf{R}_{uu}^D[n]^{-1}\right)^H \mathbf{a}_{l,i}[n]\beta_i^D b_i^D[n] + \left(\gamma_l^D\right)^* \mathbf{a}_{l,i}^H[n]\left(\mathbf{R}_{uu}^D[n]^{-1}\right)^H \hat{\boldsymbol{\eta}}_l^D[n] \\ z_{l,i}^C[n] &= \left(\gamma_l^C\right)^* \mathbf{a}_{l,i}^H[n]\left(\mathbf{R}_{uu}^C[n]^{-1}\right)^H \mathbf{a}_{l,i}[n]\beta_i^C b_i^C[n] + \left(\gamma_l^C\right)^* \mathbf{a}_{l,i}^H[n]\left(\mathbf{R}_{uu}^C[n]^{-1}\right)^H \hat{\boldsymbol{\eta}}_l^C[n]\end{aligned} \tag{5.4.3}$$

According to (5.3.12), the weights of the RAKE combiner is then

$$\begin{aligned}\hat{\alpha}_{l,i}^D[n] &= \left(\mathbf{w}_{l,OPT}^D\right)^H \mathbf{a}_{l,i}[n] = \left(\gamma_l^D\right)^* \mathbf{a}_{l,i}^H[n]\left(\mathbf{R}_{uu}^D[n]^{-1}\right)^H \mathbf{a}_{l,i}[n] \\ \hat{\alpha}_{l,i}^C[n] &= \left(\mathbf{w}_{l,OPT}^C\right)^H \mathbf{a}_{l,i}[n] = \left(\gamma_l^C\right)^* \mathbf{a}_{l,i}^H[n]\left(\mathbf{R}_{uu}^C[n]^{-1}\right)^H \mathbf{a}_{l,i}[n]\end{aligned} \tag{5.4.4}$$

Substituting (5.4.3) and (5.4.4) in (5.3.10), the output of the RAKE combiner is then

$$\begin{aligned}z_i^D[n] &= \sum_{l=1}^M z_{l,i}^D[n]\left(\hat{\alpha}_{l,i}[n]\right)^* = \sum_{l=1}^M \left|\gamma_l^D\right|^2 \left\|\mathbf{a}_{l,i}[n]\right\|^4 \beta_i^D b_i^D[n] + \sum_{l=1}^M \hat{\eta}_l'^D[n] \\ z_i^C[n] &= \sum_{l=1}^M z_{l,i}^C[n]\left(\hat{\alpha}_{l,i}[n]\right)^* = \sum_{l=1}^M \left|\gamma_l^C\right|^2 \left\|\mathbf{a}_{l,i}[n]\right\|^4 \beta_i^C b_i^C[n] + \sum_{l=1}^M \hat{\eta}_l'^C[n]\end{aligned} \tag{5.4.5}$$

where the noise and interference terms $\hat{\eta}_l'^D[n]$ and $\hat{\eta}_l'^C[n]$ are given by

$$\begin{aligned}\hat{\eta}_l'^D[n] &= \left|\gamma^D\right|^2 \mathbf{a}_{l,i}^H[n]\left(\mathbf{R}_{uu}^D[n]^{-1}\right)^H \hat{\boldsymbol{\eta}}_l^D[n]\mathbf{a}_{l,i}^H[n]\mathbf{R}_{uu}^D[n]^{-1}\mathbf{a}_{l,i}[n] \\ \hat{\eta}_l'^C[n] &= \left|\gamma^C\right|^2 \mathbf{a}_{l,i}^H[n]\left(\mathbf{R}_{uu}^C[n]^{-1}\right)^H \hat{\boldsymbol{\eta}}_l^C[n]\mathbf{a}_{l,i}^H[n]\mathbf{R}_{uu}^C[n]^{-1}\mathbf{a}_{l,i}[n]\end{aligned} \tag{5.4.6}$$

The output signal to noise plus interference ratio (SINR) then is given by

$$SINR_{OPT}^{D} = \frac{\beta_i^D E\left\{\left|b_i^D\right|^2\right\}\sum_{l=1}^{M}\left|\gamma_l^D\right|^2\left\|\mathbf{a}_{l,i}[n]\right\|^4}{E\left\{\left|\sum_{l=1}^{M}\hat{\eta}_l'^D[n]\right|^2\right\}}; SINR_{OPT}^{C} = \frac{\beta_i^C E\left\{\left|b_i^C\right|^2\right\}\sum_{l=1}^{M}\left|\gamma_l^C\right|^2\left\|\mathbf{a}_{l,i}[n]\right\|^4}{E\left\{\left|\sum_{l=1}^{M}\hat{\eta}_l'^C[n]\right|^2\right\}} \quad (5.4.7)$$

5.5 Summary

In this chapter, we developed the mathematical model of our proposed space-time processing system for W-CDMA. The formulation started with a model of the W-CDMA uplink transmitter. A simple characterization of the spatio-temporal channel suitable for the analytical purpose is presented. Using these two formulations we then extensively analyze a PSA coherent space-time RAKE receiver intended for the base station. In the following chapter, we will create a simulation environment to test the receiver and quantify its performance.

Chapter 6

Simulation Results and Discussion

In the previous chapter, we present a detailed mathematical description of our proposed PSA space-time (2-D) RAKE receiver for the W-CDMA system. We formulate the W-CDMA transmitter model and the spatio-temporal channel model and use those to analyze the receiver. In doing so, we get a qualitative measure of the performance of a 2-D RAKE receiver in a frequency selective multipath channel with MAI. In this chapter, we quantify the performance by simulating the PSA 2-D RAKE receivers in the GBSB circular and elliptical channel with the uplink W-CDMA signal standard. We consider the LMS, DMI and RLS based PSA beamforming techniques with varying number of antenna elements. We also consider MRC coherent RAKE receiver with different number of fingers. We compare the performance of these different PSA 2-D RAKE receivers with the conventional (1-D) RAKE receivers and the conventional PSA based beamformer. We simulate the receiver operation in channel conditions that show the performance trade-off between array processing and RAKE combining. Performances are compared in terms of three parameters: antenna elements, RAKE fingers and beamforming algorithms. Both the BER versus number of users and the BER versus Eb/No performances are considered.

The chapter is organized as follows: In section 6.1, we present the simulation set up for the proposed system. We describe the transmitter specifications for the W-CDMA used in the simulation. In section 6.2, the multipath channel generation is discussed. Section 6.3 presents the block diagram of the receiver used in the simulation. Section 6.4 provides the parameters to create the simulation environment. In section 6.5, we present the simulation results along with the relevant discussion. Finally we conclude the chapter with a brief summary in section 6.5.

6.1 Simulation Set Up

6.1.1 Transmitter Specifications

The W-CDMA uplink physical channels have a frame/slot structure as described in chapter 4. The frame length is 10 ms and it comprises of 15 slots with duration of 0.667 ms each. The uncoded DPDCH and DPDCH bits are channel coded by a convolutional encoder and subsequently mapped into I and Q channels respectively. In the simulation, we assume that the channel coding is already performed so that the signals of interest are the encoded DPDCH and DPCCH bits. The encoded DPDCH bits are Binary Phase Shift Keying (BPSK) modulated and grouped into 80 symbols to form one DPDCH slot so that the resulting data symbol rate is 120 ksps. Similarly, the encoded DPCCH bits are also BPSK modulated to form the antipodal signal. Each DPCCH slot has 8 pilot symbols time multiplexed with 2 TPC symbols resulting in a control symbol rate of 15 ksps. The uplink frame/slot parameters are listed in Table 6.1.

Table 6.1: Uplink W-CDMA Frame-Slot parameters

Frame duration		10ms
Frame rate		100 frames/sec
Slots/frame		15
Slot duration		0.667ms
Slot rate		1500 slots/sec
Symbol/slot	DPDCH	80
	DPCCH	10
DPCCH slot field*	Pilot	8
	TPC	2
	TFCI	0
	FBI	0

*DPCCH slot fields are described in Chapter 4

It is assumed that each uplink user has only one DPDCH even though the maximum possible DPDCH that can be assigned to a particular user is six. The spreading factor (SF) for each user's DPDCH is taken to be 32. The SF for the DPCCH is always set at 256. For spreading, orthogonal variable spreading factor (OVSF) codes are used which are explained in chapter 4. Each uplink user's DPDCH is spreaded by a length 32 OVSF code, $C_{32,9}$, where the 1st

index is the level in the code tree and the 2nd index is the code number in that particular level. The spreading code for DPCCH is a length 256 sequence of all 1's. Both the DPDCH and DPCCH gain factors are set at 1. The spreaded I and Q channels are QPSK modulated and the resulting complex chip sequence has a rate of 3.84 Mcps. A user specific complex long scrambling code with a repetition period of 38400 chips (1 frame) is used to multiply the QPSK chip sequence. The scrambling code is generated uniquely for a specific code user and is described in details in chapter 4. Each scrambled chip samples are then upsampled by a factor of 4. Finally, to confine the spreaded wideband signal within the 5 MHz allocated bandwidth for uplink, a square-root raised cosine Nyquist transmitter filter with a rolloff factor of 0.22 is applied. The resulting pulse-shaped signal is the transmitted baseband signal from an uplink user. The major transmitter parameters used in simulation are listed in Table 6.2.

Table 6.2: Uplink W-CDMA transmitter parameters for simulation

Dedicated Physical channels	DPDCH	1
	DPCCH	1
Data modulation	DPDCH	BPSK
	DPCCH	BPSK
Spreading Factor	DPDCH	32
	DPCCH	256
Spreading code (OVSF)*	DPDCH	$C_{32,9}$
	DPCCH	$C_{256,1}$
Symbol Rate	DPDCH	120 ksps
	DPCCH	15 ksps
Gain Factor	DPDCH	1.0
	DPCCH	1.0
Spreading (chip) modulation		Dual Channel QPSK
Scrambling code		Uplink long scrambling code
Chip rate		3.84 Mcps
Oversampling factor		4 samples/chip
Pulse shaping		Root RC with roll-off 0.22
Carrier frequency		1.92 GHz

*OVSF codes $C_{SF,k}$ are described in chapter 4

6.2 Multipath Channel Generation

6.2.1 Microcellular Environment

Microcells correspond to small cells with high user density and are usually defined in a dense urban area. The base station antenna heights are relatively low and users are located within 1 km surrounding the base station. As mentioned in chapter 3, in such environments, elliptical channel models are more applicable. Figure 6.2.1 depicts a microcellular scenario with the elliptical channel model used to generate the resolvable multipath rays from the user.

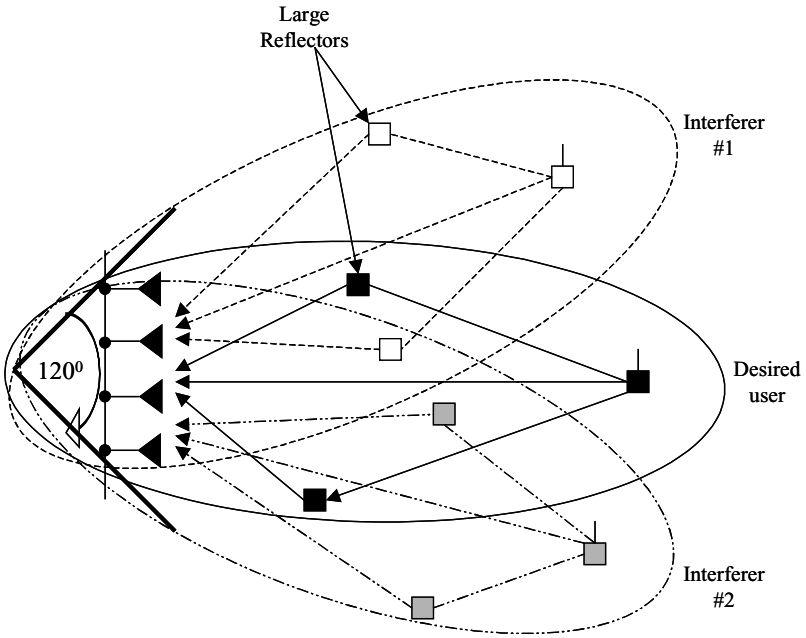

Figure 6.2.1: Multipath propagation scenario for microcellular environments

In Figure 6.2.1, a three-sectored base station with a linear antenna array for each 120^0 sector is considered. The element spacing is set at 0.5λ where λ is the wavelength of the transmitted W-CDMA waveform with a carrier frequency of 1.92 GHz. All the users are located within 1km distance from the base station. Each user has an elliptical region of uniformly distributed large reflectors surrounding it and the base station. The boundary of the elliptical reflector region for a user is determined by the maximum multipath delay from that user relative to its LOS path delay. The LOS path delay of a user is determined by its distance from the base station. As mentioned in chapter 3, the maximum multipath delay (relative to LOS) for the

ETSI's Vehicular A outdoor channel is 2.5 μs which corresponds to approximately eight W-CDMA chip periods (1 chip period ≈ 0.3 μs). Therefore, in simulation the maximum relative multipath delay for all the users are set at 8 chip periods. A large reflector in an elliptical region contributes one resolvable multipath from the corresponding user. Resolvable multipaths are considered to be those paths whose relative delays are greater than a chip period. The delays, amplitudes and AOA of these paths are calculated using the procedure described in chapter 3. The fractional multipath delays are rounded up to integer chip samples. Only the distance dependent path loss is assumed and no long term fading is considered. The path loss exponent is taken to be 3.5. Perfect power control assumption for all the uplink users is validated by fixing their LOS power to a fixed level. Small scale fading due to the local scatteres is incorporated by assuming that each resolvable path undergoes independent Rayleigh fading. Ideally the samples of the fading envelope should be generated at the W-CDMA chip rate of 3.84 Mcps. However to make the simulation faster, the fading is generated at the rate of DPDCH data symbols (120 ksps). The velocity of the mobiles are kept in a range of 30~40 mph (48~65 kmph) which corresponds to a maximum doppler frequency of 86~115 Hz. This velocity range is realistic in a typical urban environment for which the elliptical model is applicable. It is also assumed that the users are moving in a direction directly away from the base station so that the LOS path from each user experiences the maximum doppler spread. The doppler spread of the other multipaths from a user depend on their AOA at the base station with respect to the LOS path. For perfect synchronization of the uplink user's LOS path, the distance of all the users from the base station should be kept as the same.

6.2.2 Macrocellular Environment

Macrocells correspond to large cells where base station has relatively high antenna. The propagation path length can be up to several miles. Typically users are considered to be within 10 km of the base station. Circular channel models are more appropriate in such environments, which depicts suburban and rural multipath propagation scenario. As described in chapter 3, each user has a circular region of large reflectors surrounding it. The radius of the circle is again determined by the maximum multipath delay relative to the LOS path delay. In accordance with the ETSI's vehicular A channel, the maximum relative multipath delay for all the users are again set to be 8 W-CDMA chip period in simulation. All the other assumptions are similar to the

elliptical channel described in the previous section, expect now the velocity range is 60~70 mph (96~113) which corresponds to a maximum Doppler frequency range of 180~200 Hz. The reasoning for this is that highways for fast moving vehicles typically run in rural and suburban areas. A macrocelluar scenario employing circular reflector region around each user is shown in Figure 6.2.2.

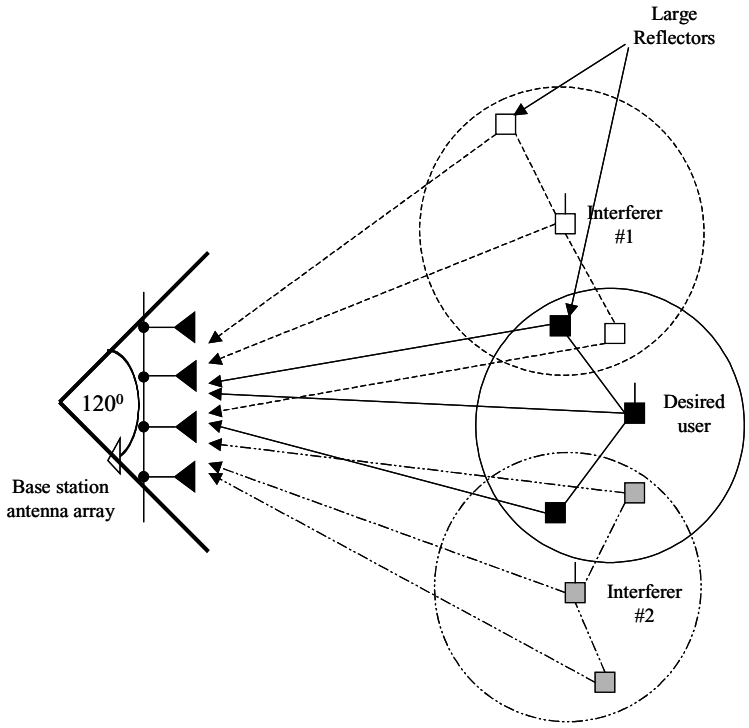

Figure 6.2.2: Multipath propagation model for macrocellular environment

6.3 Receiver Operational Block

The processing block diagram of a PSA 2-D RAKE receiver used for simulation is shown in Figure 6.3.1. The receiver operation is explained in details in chapter 5. The main assumption we make in simulating the receiver is perfect channel estimation. That means the multipath channel delays, gains, phases and AOAs are assumed to be known in the receiver. Thus the synchronization and channel estimation blocks are not shown in Figure 6.3. Also all the control channel bits (both pilot and TPC) are assumed to be known in the receiver. In a practical system, the control channel signal level is usually estimated before applying it to any pilot symbol assisted operation such as channel estimation or beamforming. Thus, instead of using the known pilot bits directly as the reference signal for beamforming, a modified version of the pilot

bits are often employed. In the simulation, we did this modification by multiplying the pilot bits with the instantaneous complex channel gain, which is assumed to be known. Thus the reference signal for PSA beamforming is the product of known pilot bits and the instantaneous channel coefficient. Another practical issue in the receiver is that one complete DPCCH frame needs to be demodulated first to extract the information about the SF for DPDCH. This is due to the fact the TFCI bits, which extend over the whole frame, carry the information about variable data rate and the corresponding variable SF. Thus the data in DPDCH needs to be buffered for a full frame time before despreading. As mentioned in chapter 5, in our system beamformer weights calculated with one DPCCH slot is applied to the corresponding DPDCH slot. In this case, the data in DPDCH need to be buffered only for one slot. For simulation purposes, it does not make any difference in the performance of the receiver. Synchronization of frame, code (both scrambling and spreading) and symbol timing are assumed to be perfect.

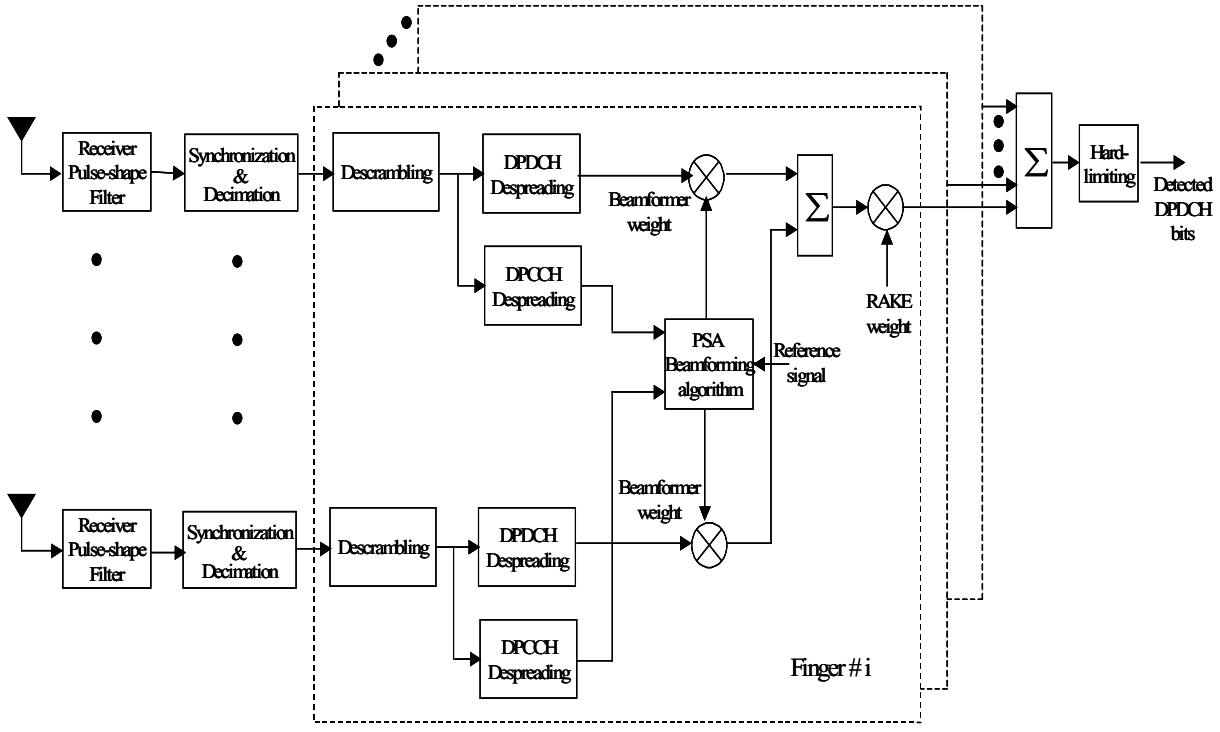

Figure 6.3.1: Block diagram of a PSA 2-D RAKE receiver used for simulation

6.4 Simulation Environment

In the simulation, the maximum number of users considered is 12, each having a SF of 32 (data rate=120 kbps). As the PSA 2-D RAKE receiver is a single user receiver, only one user is the desired one and all the others are interferers. The users are distributed uniformly in a 120^0 sector. The distances of all the users are kept at 800 m from the base station for microcellular elliptical channel and 8 km for macrocellular circular channel. Thus the receive timing of the user's LOS path are synchronous. Also, the received power of LOS components all the users are fixed at 1 W, thereby ensuring perfect power control. Each user has six resolvable multipaths (including the LOS) with different delays, gains and AOAs generated by the elliptical and circular channel model. A Rayleigh fading simulator is used to incorporate the independent fading that each multipath experiences. For both the elliptical and circular channel the velocity of all the users are kept at 100 kmph (62 mph) which corresponds to a maximum Doppler frequency of 178 Hz. This is done to simulate an extreme case scenario where all the users are moving directly away from the base station. The 2-D RAKE receiver adopts a linear antenna array of 2, 4 and 6 elements and a RAKE receiver with 3,4 and 6 fingers. The step size parameter, μ, for LMS algorithm is chosen as 0.001 and the weighting/forgetting factor, λ, for both DMI and RLS algorithm is taken to be 0.99. The initial antenna weight vectors for both the LMS and RLS algorithms are chosen to be a zero vector. For each Monte-Carlo simulation 50 different channel snapshots are generated and the performance results over all the iterations are averaged.

6.5 Simulation Results

6.5.1 BER performance Versus Number of Users

The first set of performance curves that we present is the BER vs. number of users of the 2-D RAKE receivers as a function of antenna elements and RAKE fingers. As already mentioned, we consider three different PSA beamforming techniques, i.e., LMS, DMI and RLS algorithms in the simulation of the 2-D RAKE receiver. We consider 2, 4 and 6-element antenna arrays along with 3,4 and 6-finger RAKE receivers. For comparison we also plot the corresponding curves for single element (1-D) RAKE receivers and single finger (conventional) beamformer. It is assumed that the Eb/No is fixed at 5dB. We compare the performance in both the macrocellular circular channel and the microcellular elliptical channel. From these

performance curves, we intend to demonstrate the interference suppression capability of the beamformer in a 2-D RAKE receiver.

6.5.1.1 Macrocellular Circular Channel Environment

6.5.1.1.1 LMS Beamforming

Figure 6.5.1 shows the BER performance of a 2-D RAKE receiver for varying number of users in a macrocelluar circular channel environment. The receiver uses a 2-element adaptive LMS beamformer for each finger of the RAKE receiver. The number of RAKE fingers can be 1,3,4 and 6. As can seen, with the increase of RAKE fingers the performance of both the 1-D RAKE and 2-D RAKE improves. However, the performance improvement for the 2-D RAKE is more pronounced than the 1-D RAKE for the corresponding number of finger. For example, a 3-finger 2-D RAKE receiver can outperform both the 3 and 4-finger 1-D RAKE receiver for same number of users and similar channel condition. This performance enhancement comes at the expense of increasing the number of antenna elements by 1 and performing the extra spatial domain processing. Also, can be seen that the relative performance improvement between the 1-D and the 2-D RAKE receiver increases with the number of RAKE fingers. That is, the performance improvement between a 6-finger 1-D RAKE and a 6-finger 2-D RAKE is higher than that of between the 3and 4-finger1-D and 2-D RAKE receivers.

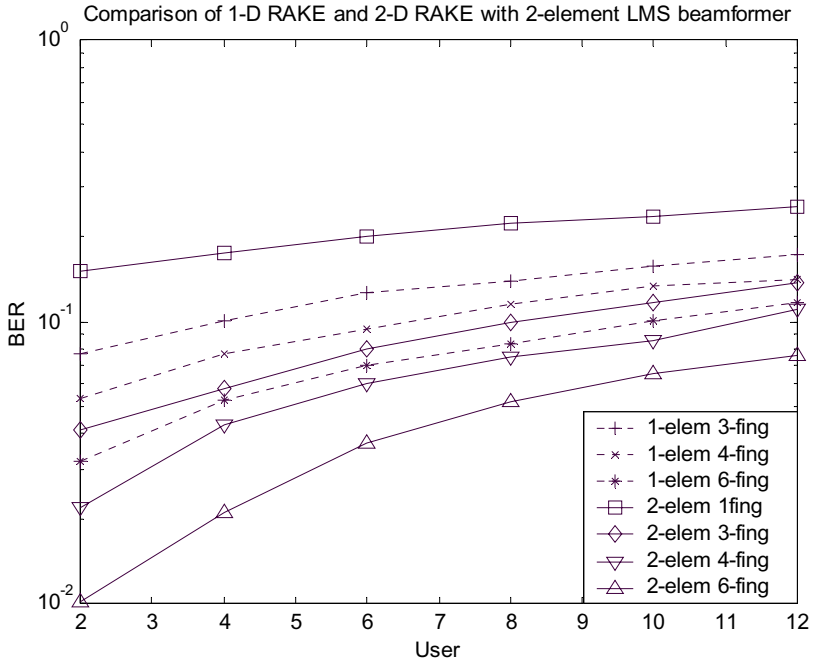

Figure 6.5.1: BER performance of a 2-D RAKE receiver with 2-element LMS beamformer

Another interesting observation from Figure 6.5.1 is that the 1-finger 2-D RAKE receiver, which is just a 2-element LMS beamformer, performs worse than all the 1-D RAKE receivers. The reason, which is already mentioned in chapter 3, is twofold. First the circular channel model offers less angular separation between the multipath components; meaning that the beamformers directed to different multipath components will not perform as well as they would have if the multipath components have more angular separation. Secondly, it was shown in chapter 3, that the relative power levels of the multipaths are close to each other in the power-delay profile of the circular channel model, which obviously improves the performance of a RAKE receiver. This is also the reason, that the both the 1-D and 2-D RAKE receiver shows a substantial improvement in performance when the number of RAKE finger is increased. This is the so-called RAKE-array performance tradeoff with respect to the multipath channel characteristics. As, we will see later, the situation will be reversed in the microcellular elliptical channel environment. The BER performance for a 4-element 2-D RAKE with LMS beamforming is shown in Figure 6.5.2.

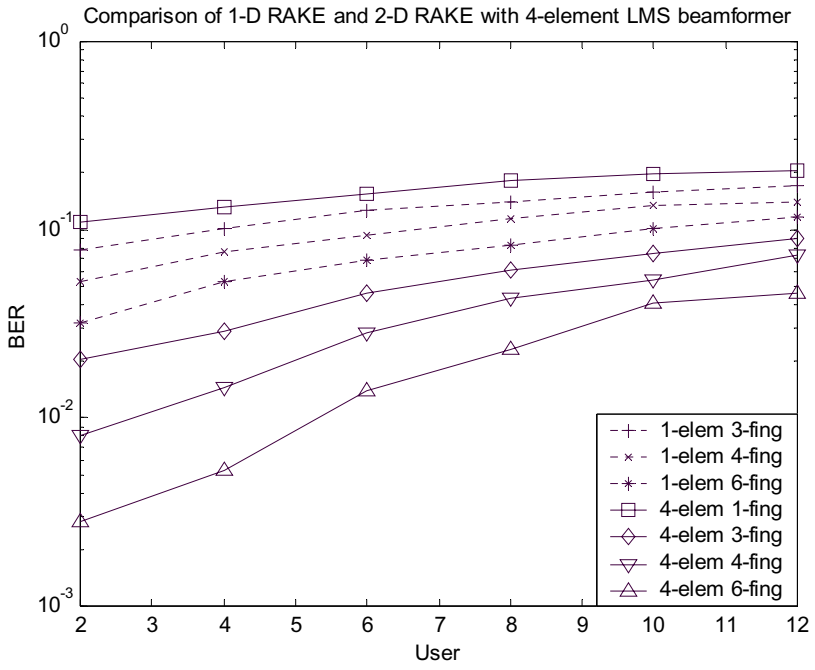

Figure 6.5.2: BER performance of a 2-D RAKE receiver with 4-element LMS beamformer

Again, the curves follow the same trend as those for the 2-element 2-D RAKE receiver, i.e., performance of both of them improves with the RAKE fingers and the relative performance improvement between the 1-D and the 2-D RAKE for the corresponding RAKE finger increases

with the number of finger. As can be expected, the increase of antenna element from 2 to 4 improves performance over the 2-element case. Indeed, a 3-finger 2-D RAKE outperforms the 3, 4 and 6 finger 1-D RAKE receivers. With the increase of RAKE fingers substantial improvement in performance of the 2-D RAKE receiver can be achieved. Also it can be seen that the performance of the single finger 4-element antenna array is better than that of the single finger 2-element array in Figure 6.5.2. Similar curves for 6-element 2-D RAKE receiver are shown in Figure 6.5.3. The behavior of the curves are similar to those for 2 and 4-element cases. As expected, the performance is better due to increased spatial domain processing. It can be seen that the curve for single finger 6-element LMS beamformer closely matches to that for single element 3-finger RAKE receiver. That is, with the assumed channel conditions, a conventional 6-element LMS beamformer and a conventional 3-finger RAKE receiver will give similar performance.

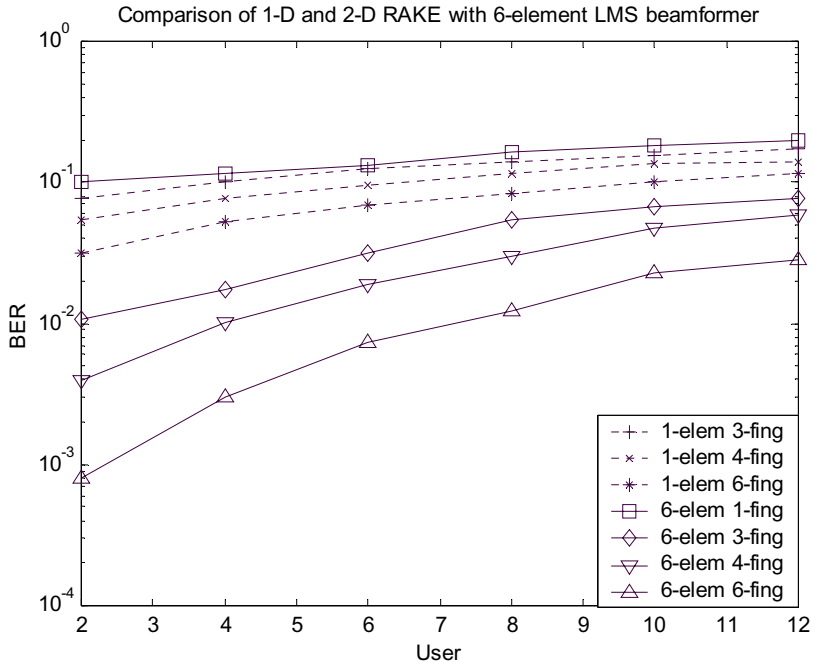

Figure 6.5.3: BER performance of a 2-D RAKE receiver with 6-element LMS beamformer

6.5.1.1.2 DMI beamforming

The BER performance curves as a function of users for 2, 4 and 6-element 2-D RAKE receivers employing the DMI beamforming are shown in Figure 6.5.4, 6.5.5 and 6.5.6, respectively.

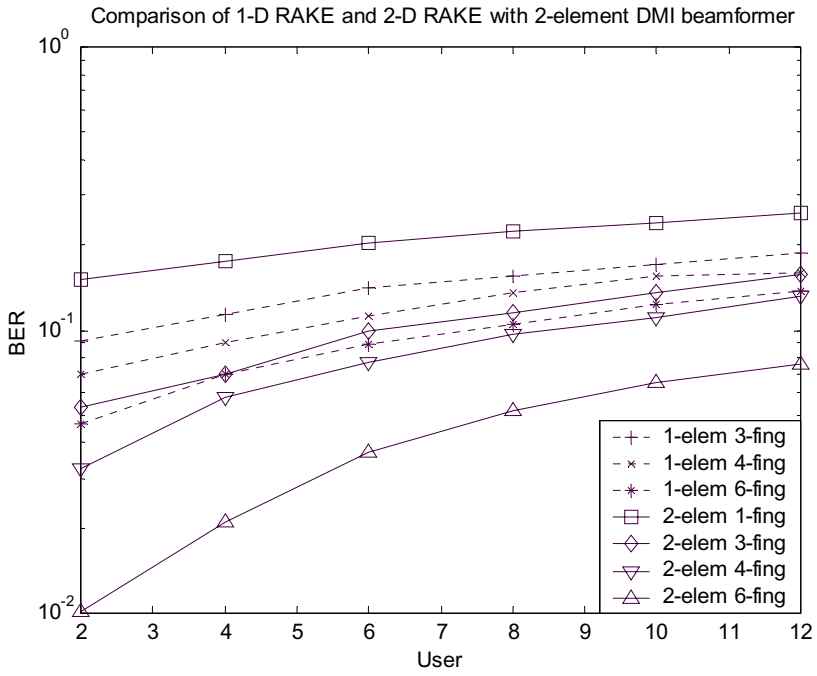

Figure 6.5.4: BER performance of a 2-D RAKE receiver with 2-element DMI beamformer

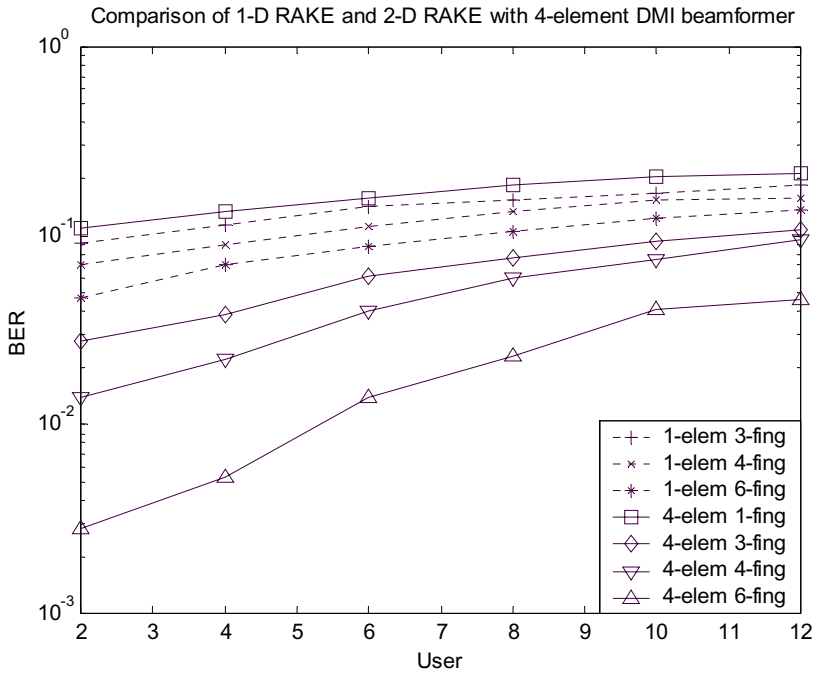

Figure 6.5.5: BER performance of a 2-D RAKE receiver with 4-element DMI beamformer

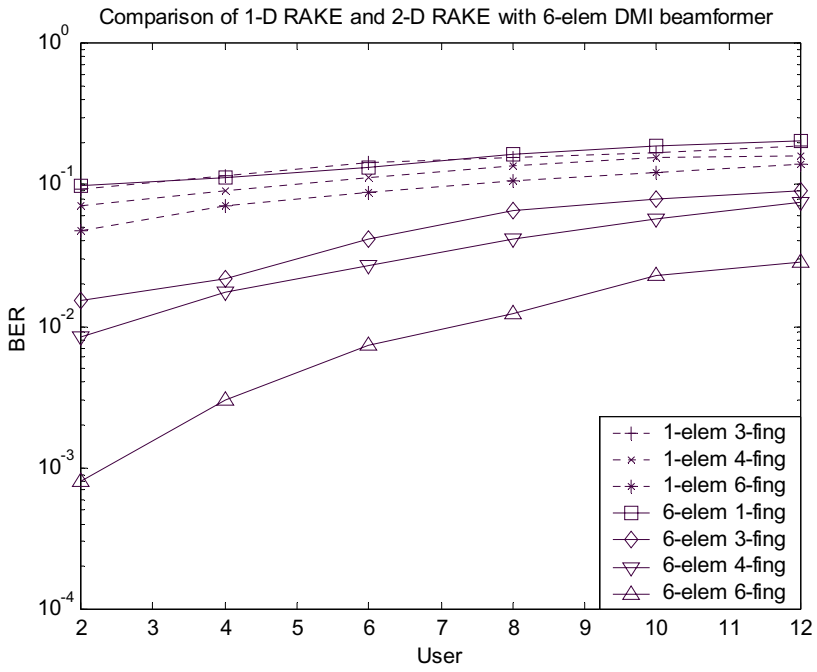

Figure 6.5.6: BER performance of a 2-D RAKE receiver with 6-element DMI beamformer

The behavior of the curves are very similar to those for 2-D RAKE receiver with LMS beamformer. The performance of the 2-D RAKE receiver improves with the increase of both the antenna elements and the RAKE fingers. As already explained for the case of LMS, due to the characteristics of the circular channel model, performance improvement with RAKE fingers is better than that with the antenna elements. In almost all the cases the 2-D RAKE receiver outperforms both the single element RAKE receiver and the single finger antenna array.

6.5.1.1.3 RLS beamforming

The BER vs. user performance curves for a RLS based 2-D RAKE receiver with 2, 4 and 6-element antenna array are shown in Figure 6.5.7, 6.5.8, 6.5.9, respectively. Again the trends of the curves are the same as those for the LMS and the DMI 2-D RAKE receivers, i.e., the performance improves with the increase in either the antenna elements and RAKE fingers. For the case of RLS we observe that the curves are not as smooth as those for LMS and DMI. The reason behind this is that in a rapidly time varying channel, as is the case in our simulation, it is very difficult to fix a suitable value for the forgetting factor λ. As mentioned in chapter 5, the most obvious choice of λ should be the channel coherence time, which we did not use in the

simulation. Also it is more appropriate to choose different values of λ for different beamformer connected to different fingers of the RAKE receiver.

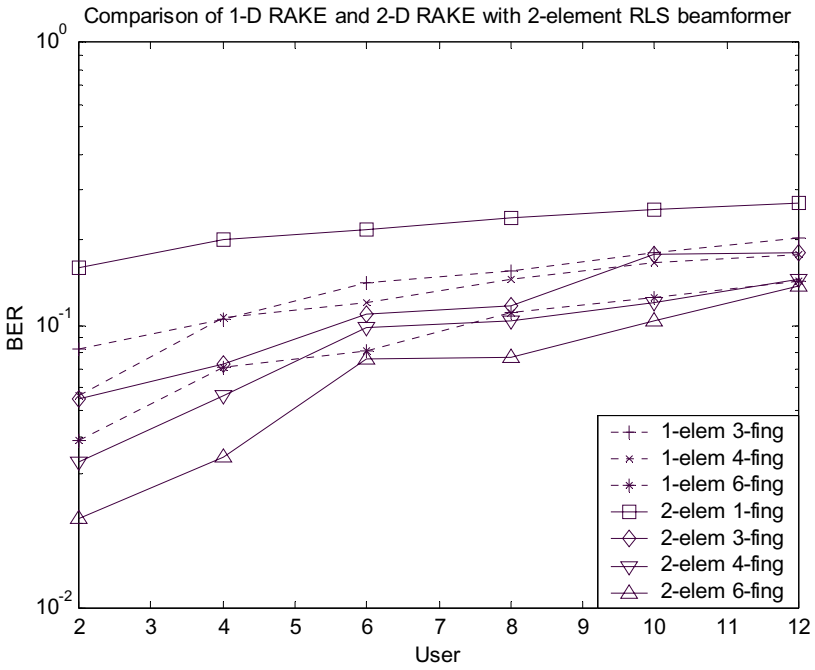

Figure 6.5.7: BER performance of a 2-D RAKE receiver with 2-element RLS beamformer

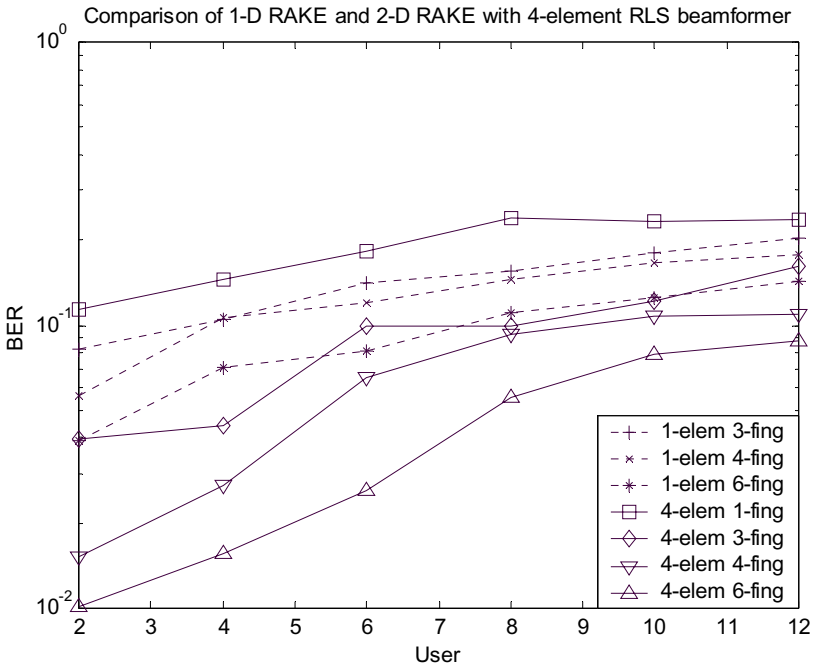

Figure 6.5.8: BER performance of a 2-D RAKE receiver with 4-element RLS beamformer

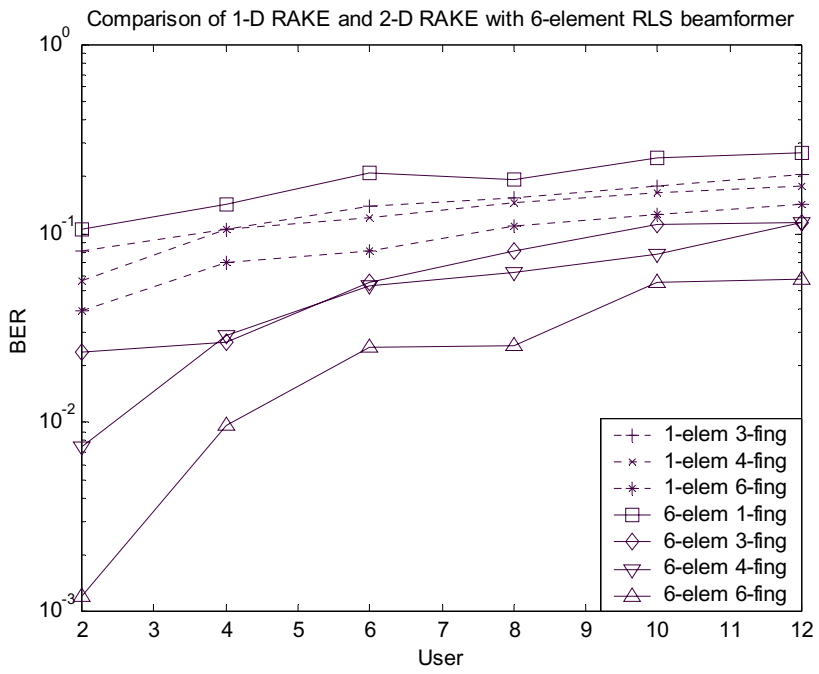

Figure 6.5.9: BER performance of a 2-D RAKE receiver with 6-element RLS beamformer

To summarize the performance of a 2-D RAKE receiver with the circular channel model, it can be definitely said that the processing in the spatial domain (in this case beamforming) improves the performance over that of a single element RAKE receiver. The degree of performance enhancement depends on the number of antenna elements and the number of RAKE fingers. It was shown that in most cases a 2-element 2-D RAKE is able to achieve performance close enough to a 1-D RAKE receiver with arbitrary number of fingers. Increasing the number of elements will of course give better performance but at the same time increases the computational burden. Also, it was seen that when the channel condition is similar to that modeled by a circular channel, increasing the number of antenna elements is not as effective as increasing the number of RAKE fingers, i.e., RAKE combining gives better performance than array processing.

6.5.1.2 Microcellular Elliptical Channel Environment

6.5.1.2.1 LMS Beamforming

In the elliptical channel model, the multipath AOA range at the base station can be can be anywhere between 0 and 360^0. Antenna arrays should give better performance in such channel conditions. Also as mentioned in Chapter 3, in the power delay profile of the elliptical

channel, the relative power levels of the multipath components show significant variation. Increasing hte RAKE fingers will not improve the performance if the relative multipaths power levels die down quickly. Compared to the performance in the circular channel as described in the previous section, this is the other end of the RAKE-array trade-off where antenna array performance dominates over the RAKE receiver performance. Figure 6.5.10 shows the BER performance vs. users of a 2-element 2-D RAKE receiver employing LMS Beamforming in the elliptical channel environment.

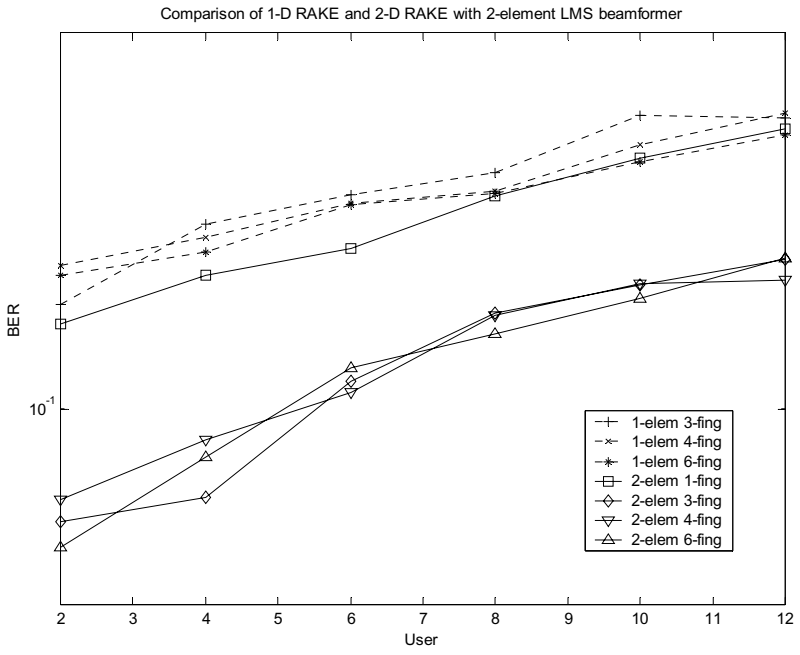

Figure 6.5.10: BER performance of a 2-D RAKE receiver with 2-element LMS beamformer

The first observation that can be made form Figure 6.5.10 is that, increasing the number of RAKE fingers for both the 1-D RAKE and 2-D RAKE does not improve performance that much. The curves for different number of RAKE fingers are very close to each other for a fixed number of antenna elements. The second observation is that the introduction of array processing improves the performance quite significantly. In fact, just a single finger 2-element LMS beamformer is able to outperform all the 1-D RAKE receivers. With the 2-D RAKE receivers substantial enhancement in performance can be achieved due to added spatial processing. Similar performance curves for 4- and 6-element cases are shown in Figures 6.5.11 and 6.5.12, respectively.

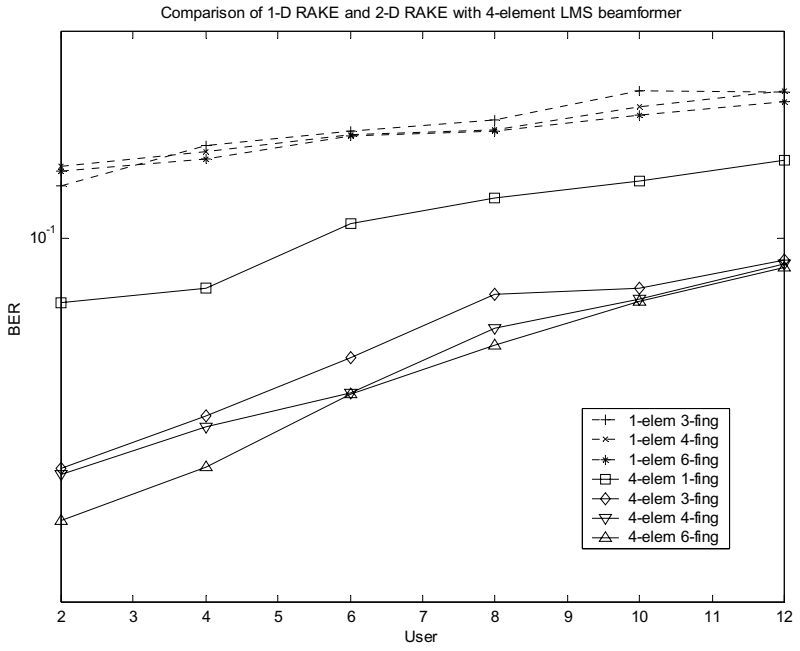

Figure 6.5.11: BER performance of a 2-D RAKE receiver with 4-element LMS beamformer

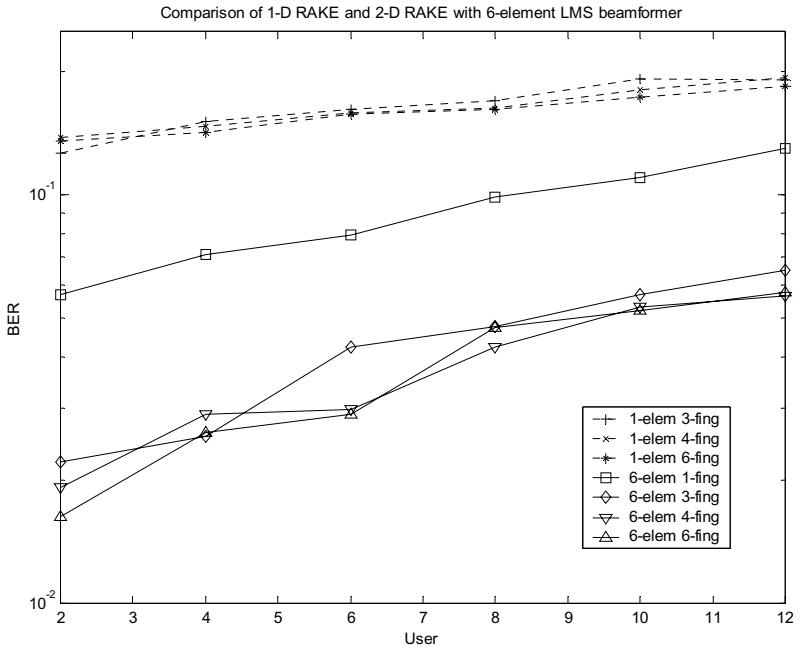

Figure 6.5.12: BER performance of a 2-D RAKE receiver with 6-element LMS beamformer

It can be clearly seen that, in both the cases, with the increase of antenna elements performance improves. A simple 4-element or 6-element LMS beamformer outperforms all the

single element RAKE receivers by a large margin. Again the 2-D RAKE receivers substantially outperform both the single element RAKE receiver and single finger antenna array.

6.5.1.2.2 DMI Beamforming

The BER performance curves as a function of the number of users for the DMI beamforming based 2-D RAKE receiver employing 2, 4 and 6-element antenna arrays are shown in Figures 6.5.13, 6.5.14 and 6.5.15, respectively. The curves have the same behavior as those with LMS beamforming. That I,s with additional antenna elements substantial performance improvement can be achieved but with additional RAKE fingers performance improvement is marginal.

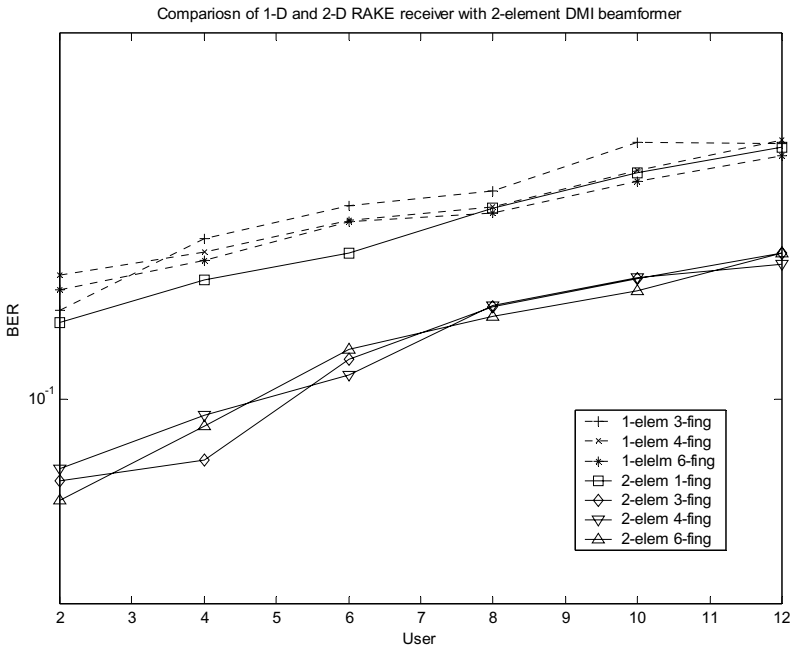

Figure 6.5.13: BER performance of a 2-D RAKE receiver with 2-element DMI beamformer

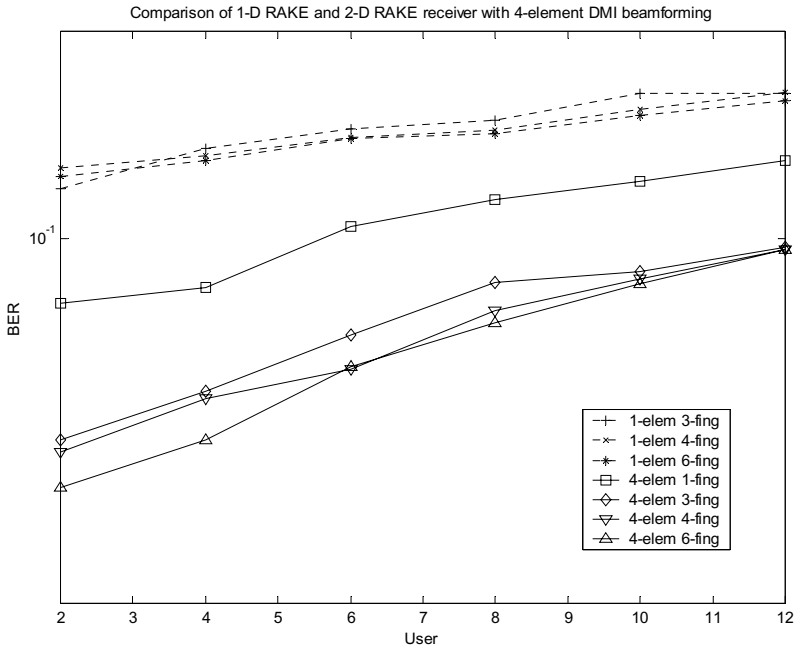

Figure 6.5.14: BER performance of a 2-D RAKE receiver with 4-element DMI beamformer

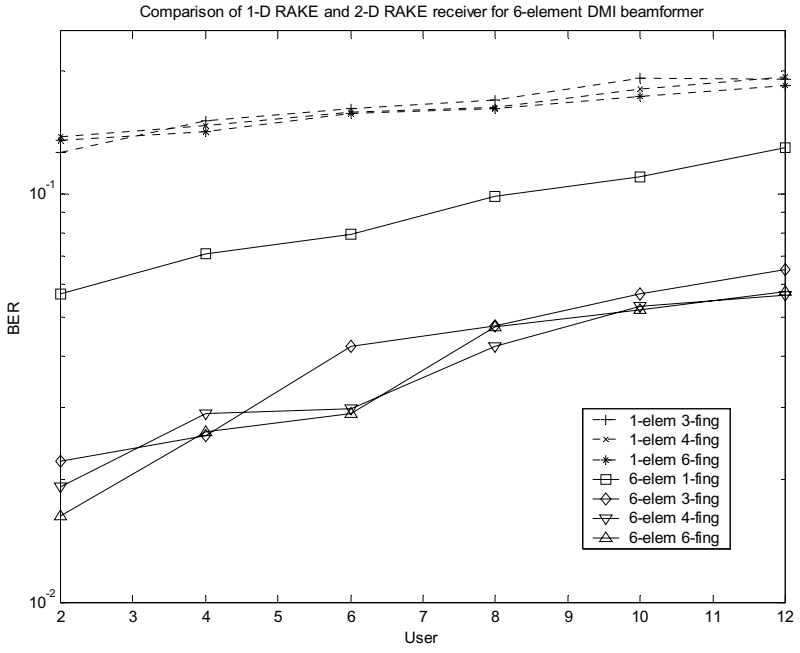

Figure 6.5.15: BER performance of a 2-D RAKE receiver with 6-element DMI beamformer

6.5.1.2.3 RLS Beamforming

The BER performance curves as a function of users for the RLS beamforming based 2-D RAKE receiver employing 2, 4 and 6-element antenna arrays are shown in Figures 6.5.16, 6.5.17 and 6.5.18, respectively. The curves also have same trends as those for LMS and DMI beamforming. As was the case in the circular channel model, the problem with RLS beamforming is to set the weighting factor, λ, to a value suitable for fast fading channel. Also, the Doppler spread of the multipaths depends on their AOA, which varies over a large range for the elliptical channel model. So, to get consistent BER values for the elliptical channel, a very large number of channel snapshopts needs to be incorporated for each Monte-Carlo simulation. The same argument holds for the LMS and the DMI cases.

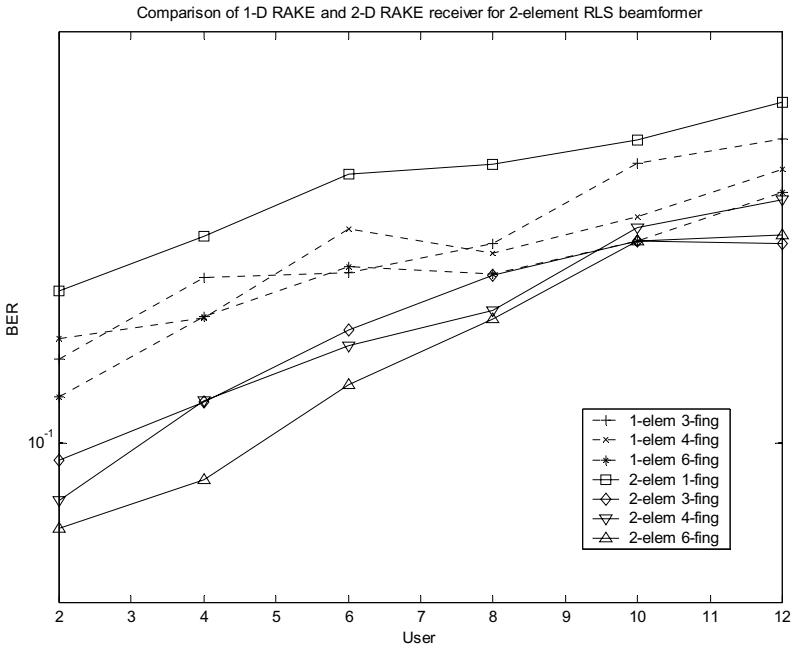

Figure 6.5.16: BER performance of a 2-D RAKE receiver with 2-element RLS beamformer

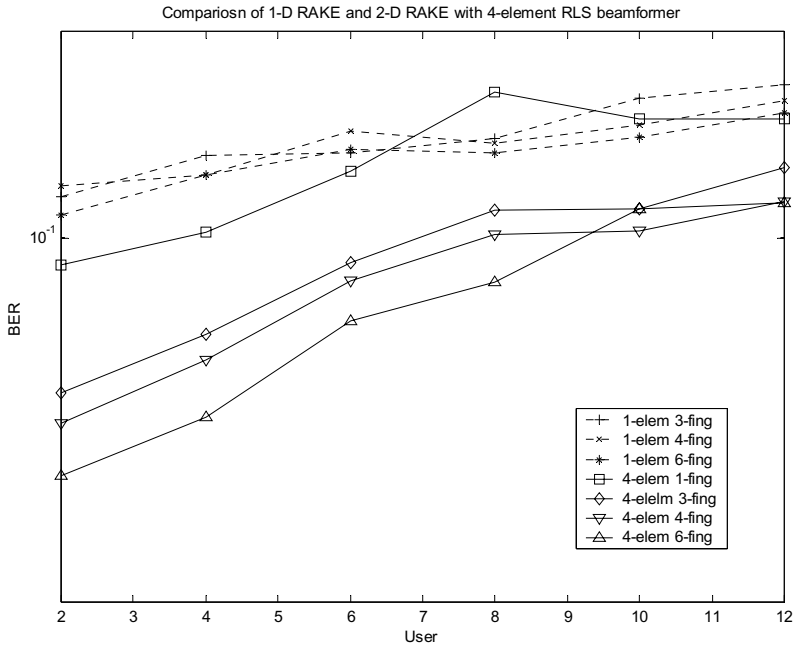

Figure 6.5.17: BER performance of a 2-D RAKE receiver with 4-element RLS beamformer

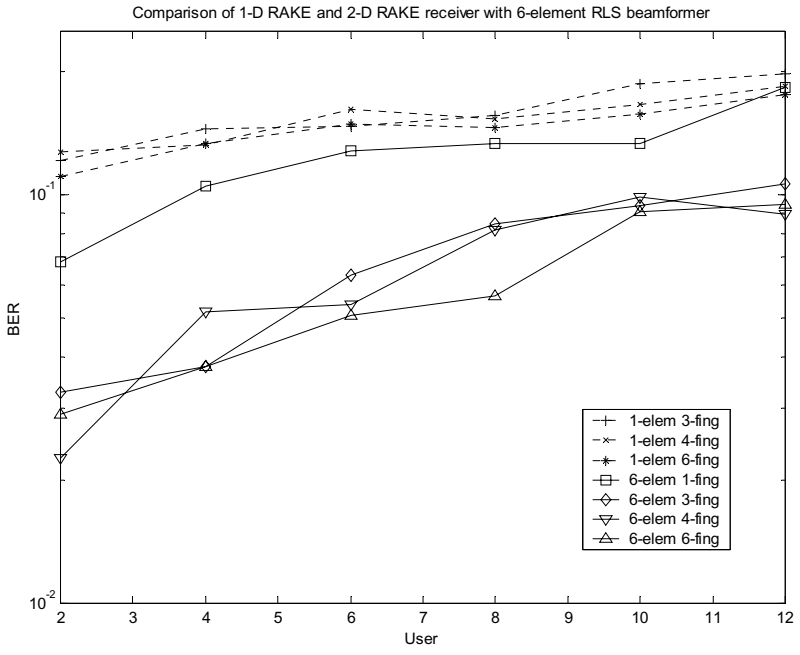

Figure 6.5.18: BER performance of a 2-D RAKE receiver with 6-element RLS beamformer

To summarize the performance of a 2-D RAKE receiver with the elliptical channel model is more improved by spatial array processing than temporal RAKE processing. The degree of performance enhancement depends on the number of antenna elements and the number of RAKE fingers. It was seen that, increasing the number of antenna elements is more effective than increasing the number of RAKE fingers.

6.5.2 BER performance vs. Eb/No

The second set of results that we present is the BER performance curves as a function of Eb/No for the 2-D RAKE receivers with varying number of antenna elements and RAKE fingers. For each set of antenna elements we considered two distinct cases. In the first case, the number of users is kept the same as the number of antenna elements i.e., the underloaded case while in the second case it is doubled, i.e., the overloaded case. Again the users are assumed to be uniformly distributed in a 120^0 sector. As in the case of BER vs. user plots, we compare the performance of the 2-D RAKE receiver with the conventional 1-D RAKE receiver and the conventional beamformer. Also, the performance comparison among different PSA beamforming techniques is provided.

6.5.2.1 Macrocellular Circular Channel Environment

6.5.2.1.1 LMS beamforming

Figure 6.5.19 shows the BER vs. Eb/No plots for a 2-D RAKE receiver employing a 2-element LMS beamformer in the circular channel model and the 2-user scenario. As can be seen, the performance of the 2-D RAKE receivers are much better than both the 1-D RAKE receiver and the conventional 2-element LMS beamformer. For example, a 2-element, 3-finger, 2-D RAKE receiver can match the performance of a 6-finger 1-D RAKE receiver. Similar to the case in the BER vs. user plots, with the increase of RAKE fingers, the performance of both the 1-D RAKE and the 2-D RAKE receiver improves substantially for the circular channel model. Also it can be seen that the conventional 2-element LMS beamformer performs worse than both the 1-D and the 2-D RAKE receivers, the reason is given in section 6.5.1.1.1.

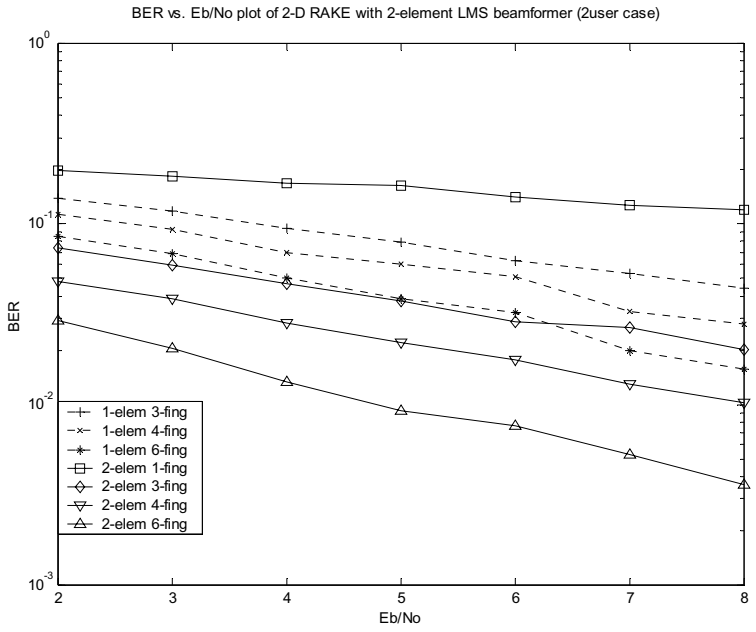

Figure 6.5.19: BER vs. Eb/No for a 2-element LMS 2-D RAKE receiver with 2-user scenario

The BER performance curves for an overloaded 4-user scenario is shown in Figure 6.5.20.

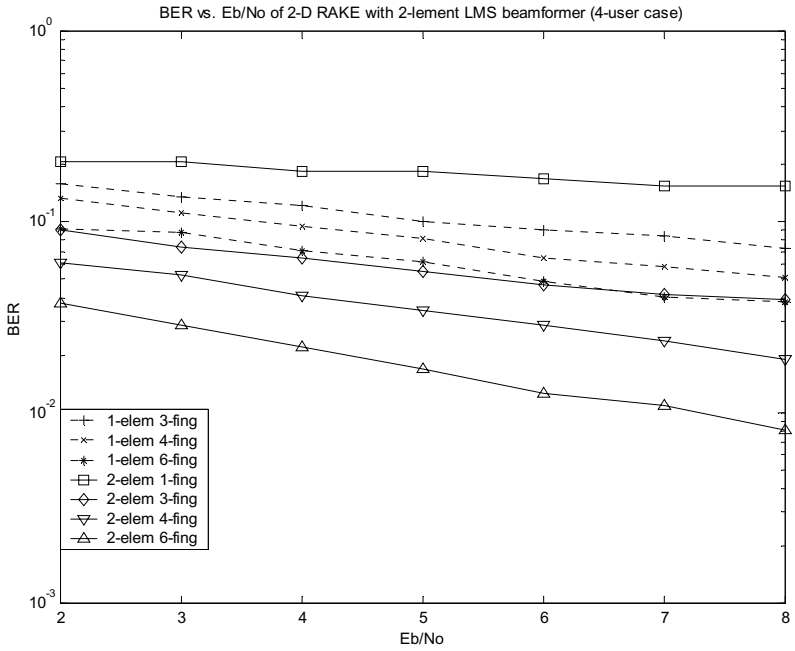

Figure 6.5.20: BER vs. Eb/No for a 2-element LMS 2-D RAKE receiver with 4-user scenario

Comparing Figure 6.5.20 with Figure 6.5.19, it can be seen that even in the overloaded case, the 2-D RAKE receiver maintains approximately the same relative performance with the 1-D RAKE receiver as with the underloaded case. This can be attributed to the interference suppression capability of a 2-D RAKE receiver. Similar curves for a 4-element LMS based 2-D RAKE receiver with 4 and 8 users are shown in Figures 6.5.21 and 6.5.22, respectively. As can be seen, with the increase of antenna elements to 4, the performance of the 2-D RAKE receiver naturally improves over the 2-element case. Also, the relative performance between the 1-D and 2-D RAKE receiver improves for the overloaded case. That is, in the overloaded case the 2-D RAKE receiver is able to support more users. Another observation is that, the single finger 4-element LMS beamformer now exhibits equivalent performance to that of a 1-D RAKE receiver with 3-fingers.

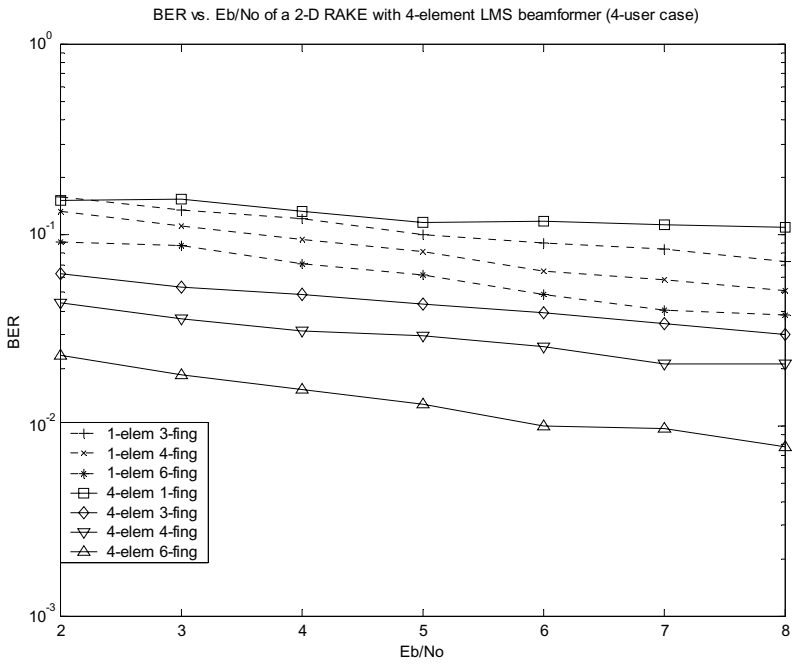

Figure 6.5.21: BER vs. Eb/No for a 4-element LMS 2-D RAKE receiver with 4-user scenario

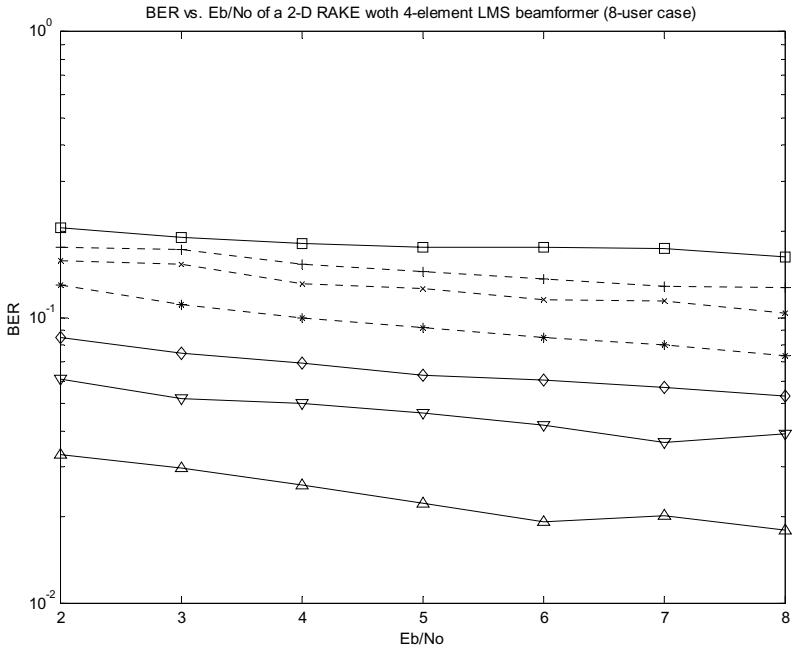

Figure 6.5.22: BER vs. Eb/No for a 4-element LMS 2-D RAKE receiver with 8-user scenario

The BER vs. Eb/No performance curves for the 6-element LMS based 2-D RAKE receivers with 6 and 12 users are shown in Figures 6.5.23 and 6.5.24, respectively. The curves follow the same trend as those for the 2 and 4-element cases. The absolute performance for each of them increases because of the additional spatial processing.

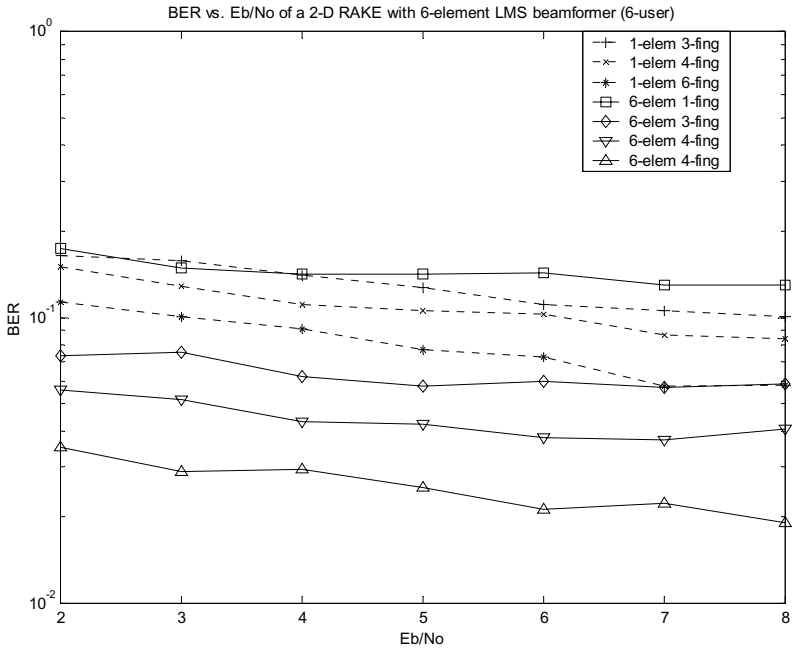

Figure 6.5.23: BER vs. Eb/No for a 6-element LMS 2-D RAKE receiver with 6-user scenario

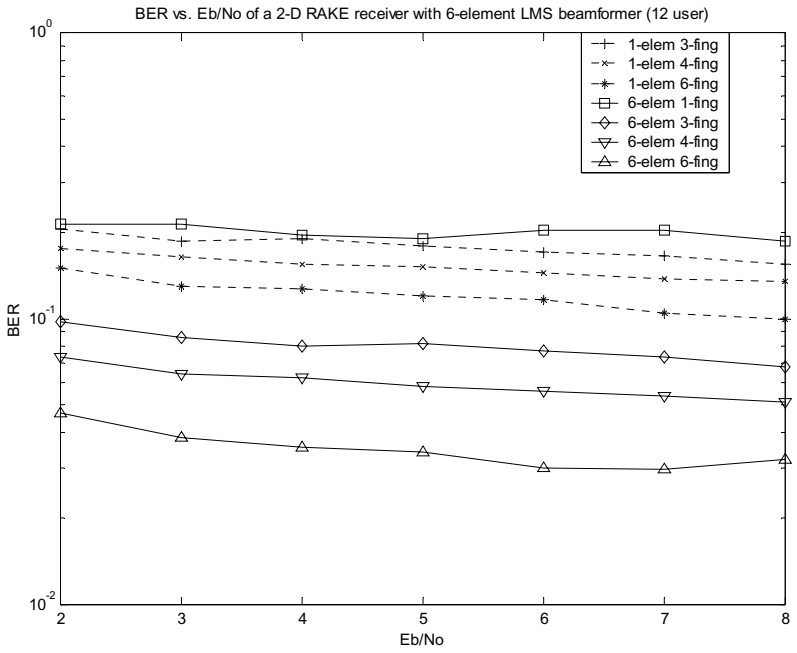

Figure 6.5.24: BER vs. Eb/No for a 6-element LMS 2-D RAKE receiver with 12-user scenario

6.5.2.1.2 DMI beamforming

Figure 6.5.25 through 6.5.30 show the BER performance curves as a function of Eb/No for the DMI beamforming based 2-D RAKE receiver with 2,4 and 6 antenna elements in both the underloading and the overloading scenarios. The curves have the same general trend as those for the LMS case.

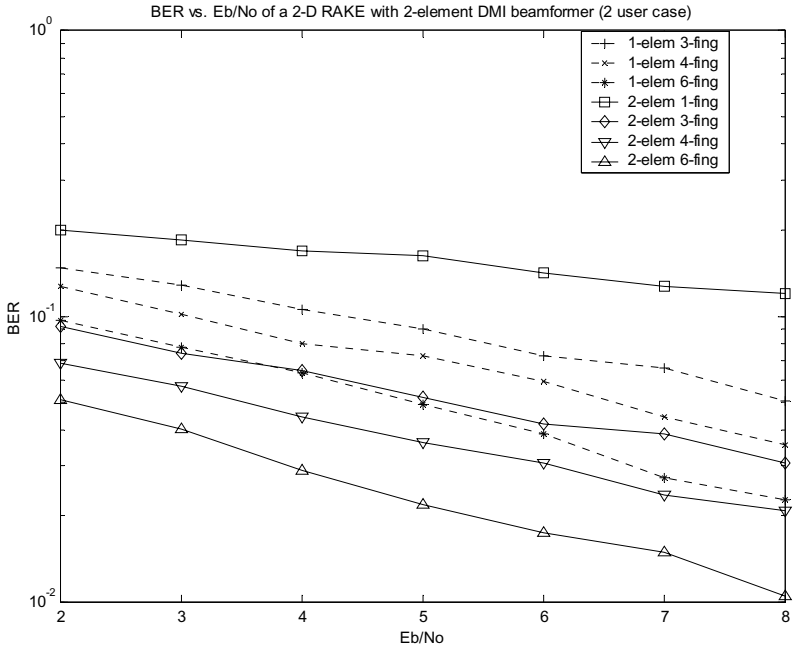

Figure 6.5.25: BER vs. Eb/No for a 2-element DMI 2-D RAKE receiver with 2-user scenario

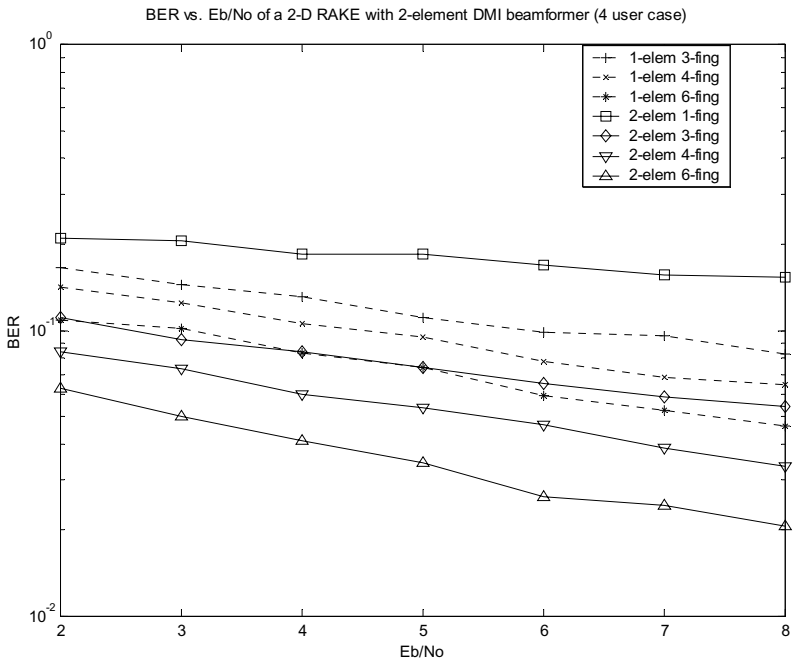

Figure 6.5.26: BER vs. Eb/No for a 2-element DMI 2-D RAKE receiver with 4-user scenario

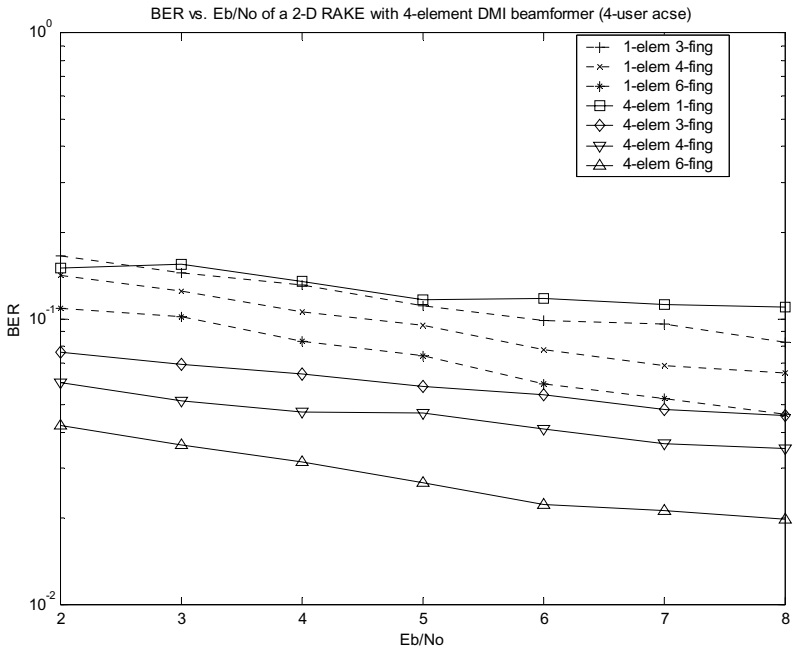

Figure 6.5.27: BER vs. Eb/No for a 4-element DMI 2-D RAKE receiver with 4-user scenario

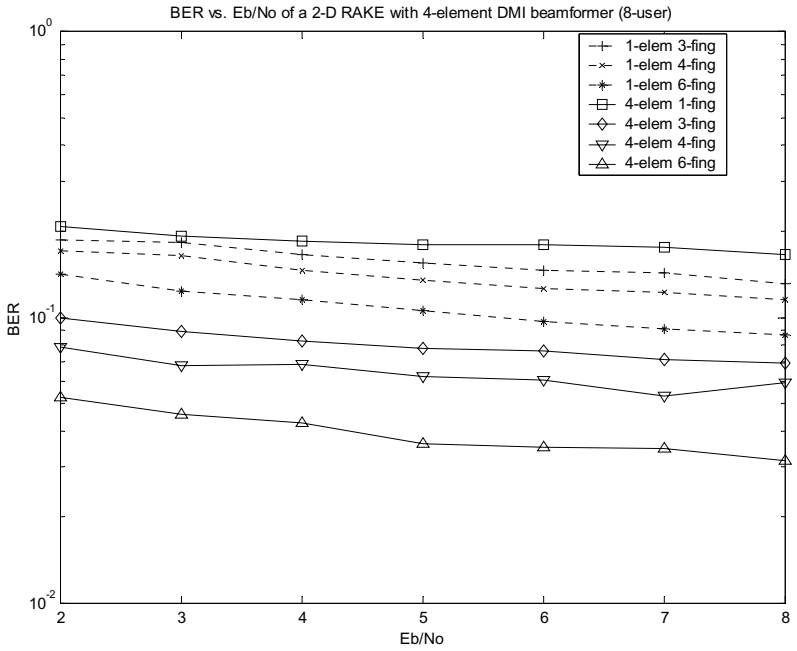

Figure 6.5.28: BER vs. Eb/No for a 4-element DMI 2-D RAKE receiver with 8-user scenario

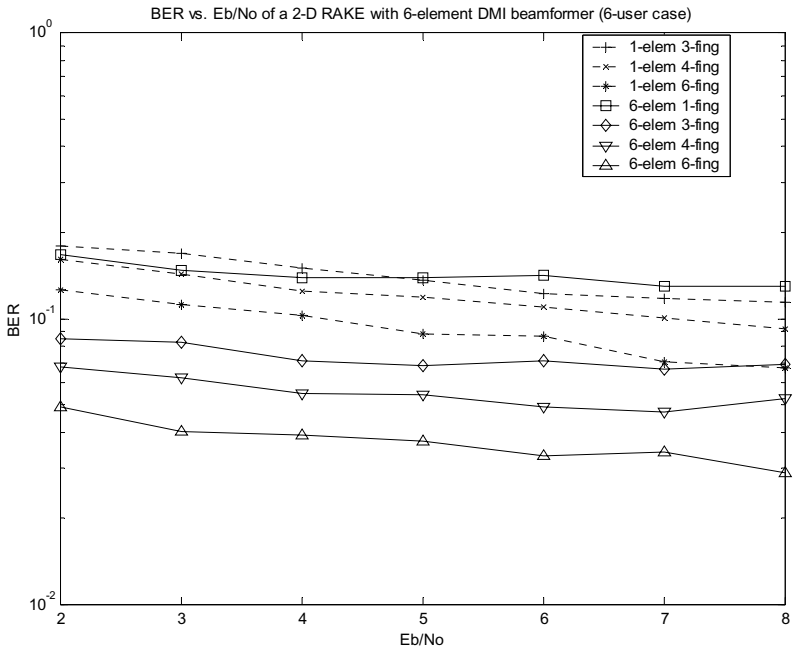

Figure 6.5.29: BER vs. Eb/No for a 6-element DMI 2-D RAKE receiver with 6-user scenario

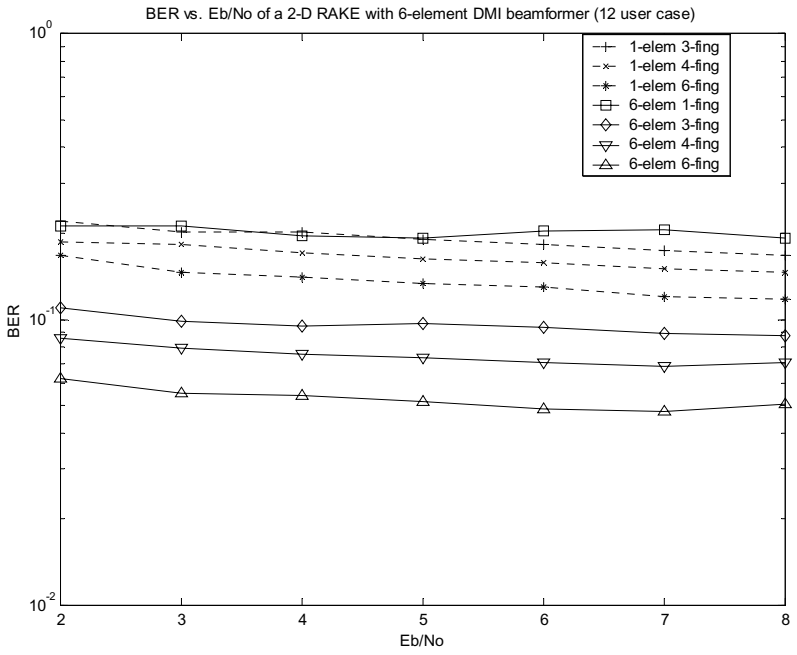

Figure 6.5.30: BER vs. Eb/No for a 6-element DMI 2-D RAKE receiver with 12-user scenario

6.5.2.1.3 RLS beamforming

Figures 6.5.31 through 6.5.36 show the BER performance curves as a function of Eb/No for the RLS beamforming based 2-D RAKE receiver with 2, 4 and 6 antenna elements in both the underloading and the overloading scenarios. The curves also have the same general trend as those for the LMS and DMI beamforming cases.

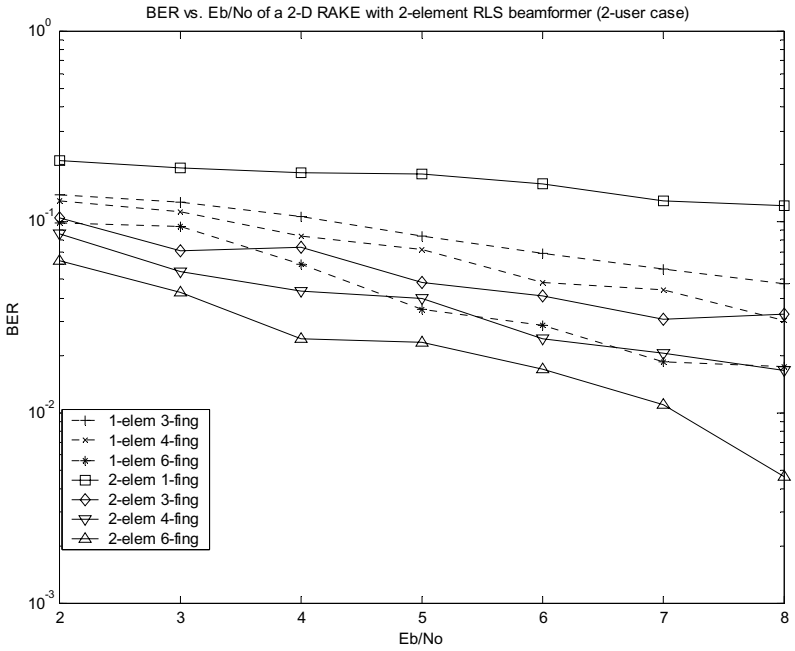

Figure 6.5.31: BER vs. Eb/No for a 2-element RLS 2-D RAKE receiver with 2-user scenario

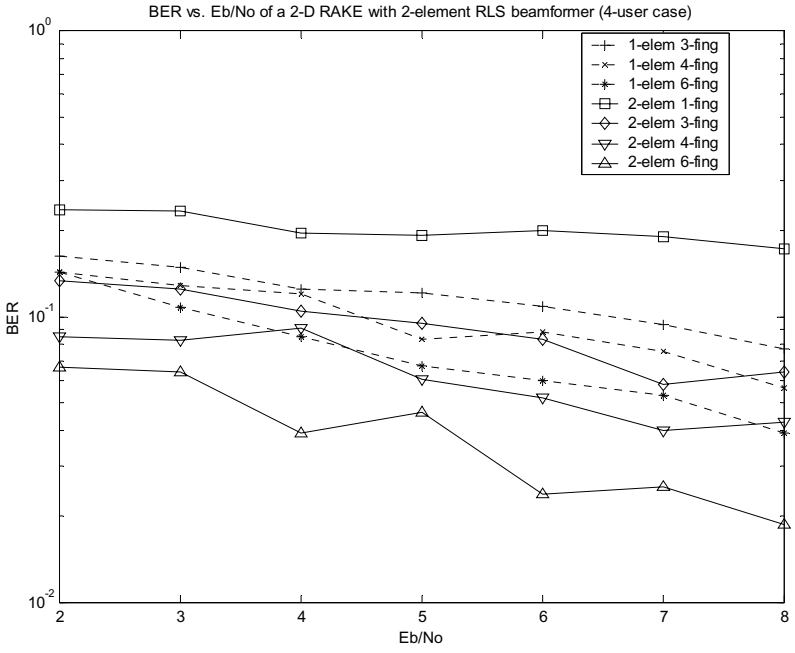

Figure 6.5.32: BER vs. Eb/No for a 2-element RLS 2-D RAKE receiver with 4-user scenario

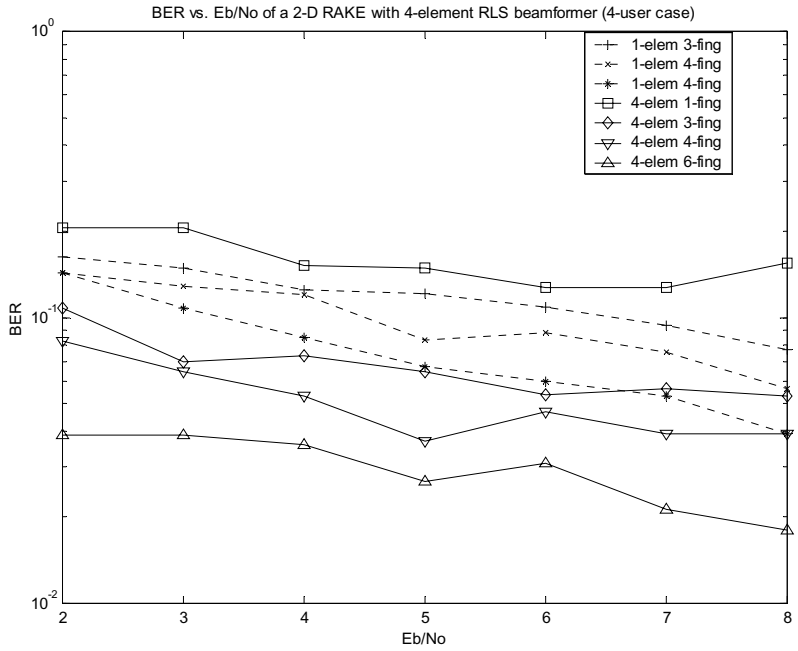

Figure 6.5.33: BER vs. Eb/No for a 4-element RLS 2-D RAKE receiver with 4-user scenario

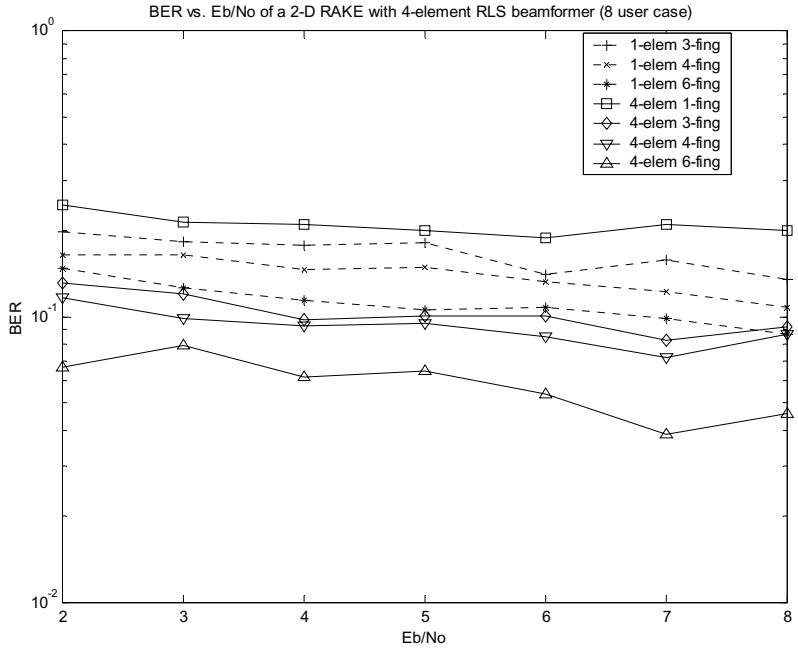

Figure 6.5.34: BER vs. Eb/No for a 4-element RLS 2-D RAKE receiver with 8-user scenario

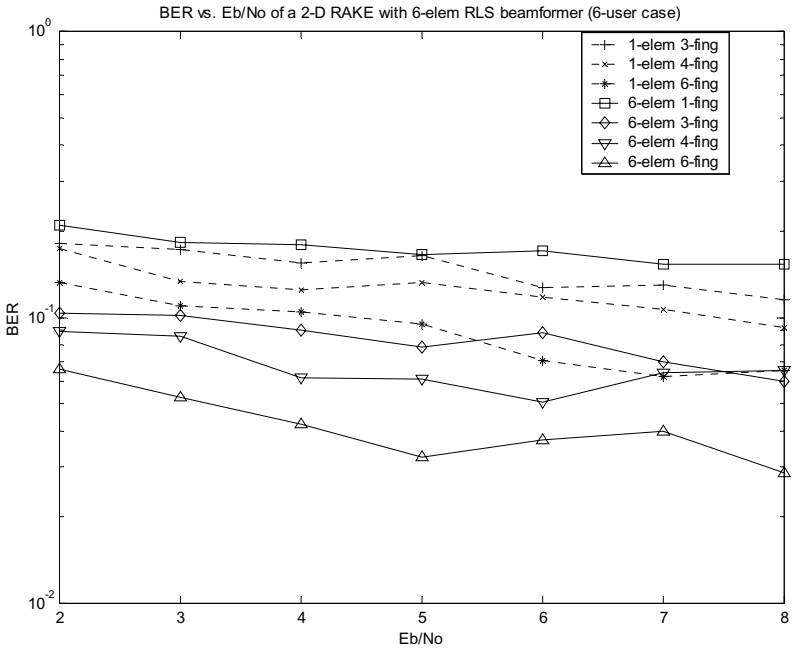

Figure 6.5.35: BER vs. Eb/No for a 6-element RLS 2-D RAKE receiver with 6-user scenario

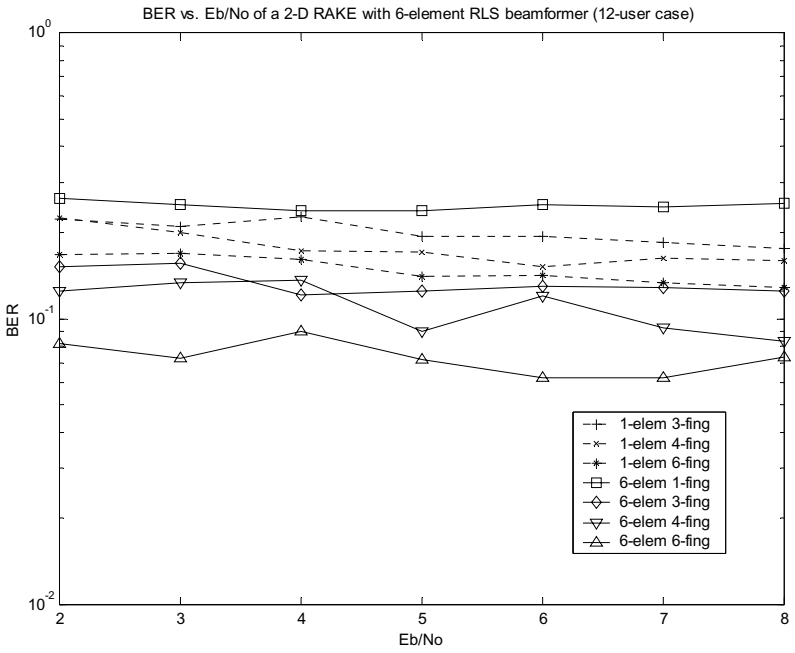

Figure 6.5.36: BER vs. Eb/No for a 6-element RLS 2-D RAKE receiver with 12-user scenario

6.5.2.2 Microcellular Elliptical Channel Environment

6.5.2.2.1 LMS beamforming

Figure 6.5.37 shows the BER vs. Eb/No plots of an LMS based 2-element 2-D RAKE receiver for 2 user scenario. As already mentioned in section 6.5.1.2.1, in the elliptical channel, increasing the number of RAKE fingers does not significantly improve the performance of both the 1-D and 2-D RAKE receiver. However, due to the large range of AOA, use of the antenna array in this type of channel will be beneficial. Indeed, a 2-element conventional beamformer closely matches the performance of a conventional 1-D RAKE receiver with 3, 4 and 6 fingers. And the 2-D RAKE receiver outperforms both the conventional beamformer and the conventional 1-D RAKE by a significant margin.

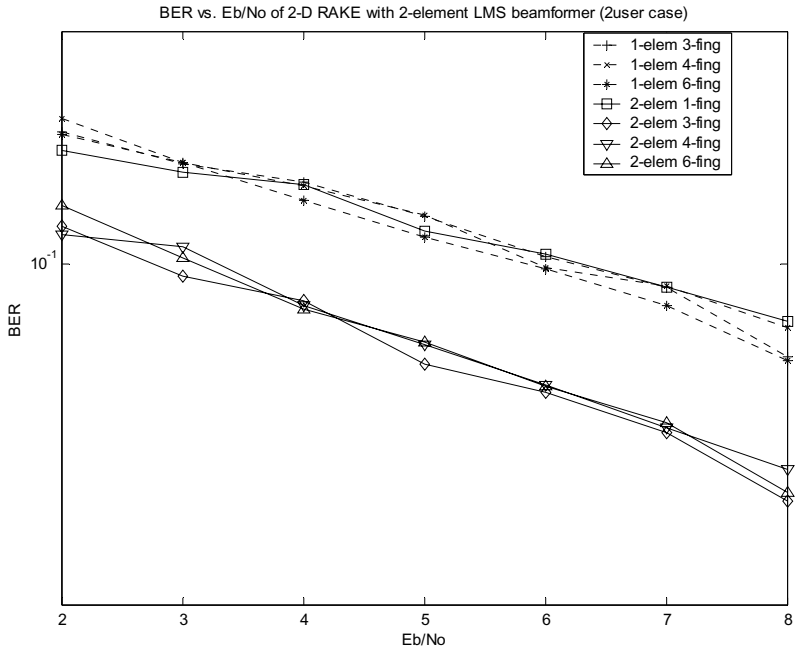

Figure 6.5.37: BER vs. Eb/No for a 2-element LMS 2-D RAKE receiver with 2-user scenario

For the overloaded case, i.e., when the number of user is 4, the BER vs. Eb/No performance curves for a 2-element 2-D RAKE receiver are shown in Figure 6.5.38.

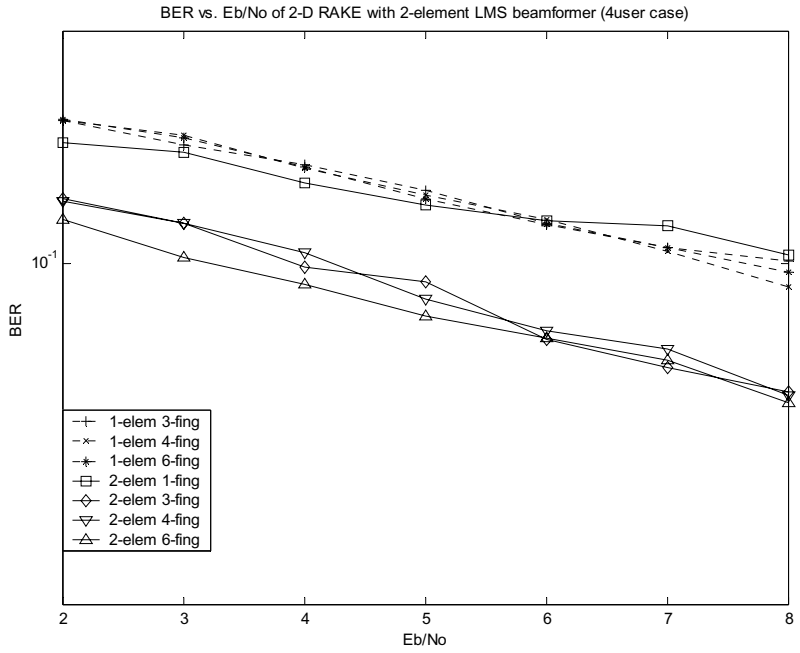

Figure 6.5.38: BER vs. Eb/No for a 2-element LMS 2-D RAKE receiver with 4-user scenario

As can be seen even in this overloaded case, the 2-D RAKE outperforms the 1-D RAKE receivers by a significant margin. This is due to the interference suppression capability of the beamformers in the 2-D RAKE receiver. Also, due to the same reason, in the overloaded case, the 2-element LMS beamformer gives slightly better performance than the 1-D RAKE receiver. Similar curves for a 4 element, LMS based, 2-D based RAKE receiver for 4 and 8 user scenarios are shown in Figures 6.5.39 and 6.5.40, respectively. As expected, due to the increase of the number of antenna elements and hence the added spatial processing, the performance of both the 2-D RAKE receiver and the conventional beamformer increases over the 2-element case. The conventional 4-element beamformer now outperforms all the 1-D RAKE receivers with 3, 4 and 6-fingers. Also from Figure 6.5.40, it can be seen that in the overloaded case the relative performance between the 1-D RAKE and the 2-D RAKE receivers are similar to that of the underloaded case in Figure 6.5.39. That is, in the overloaded case, 2-D RAKE still outperforms the 1-D RAKE by a margin very close to that in the underloaded case.

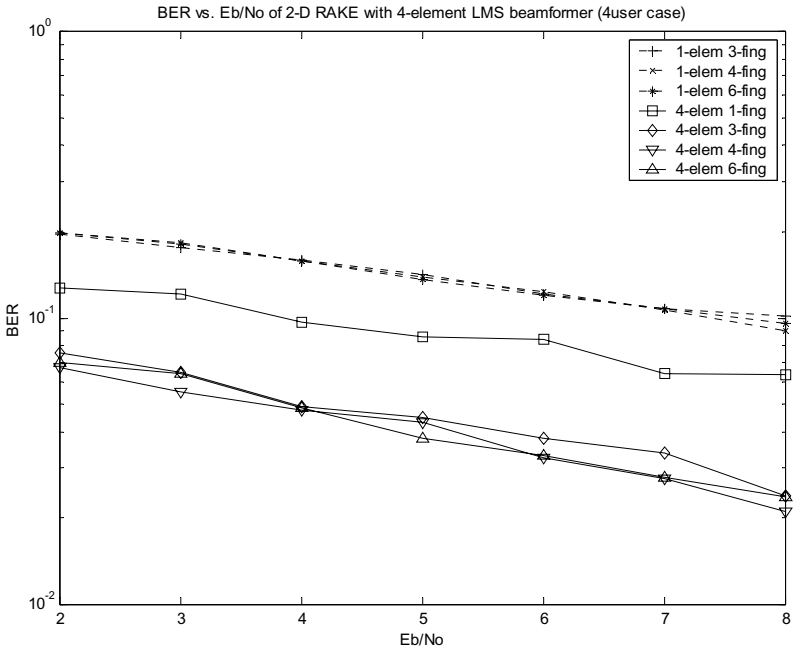

Figure 6.5.39: BER vs. Eb/No for a 4-element LMS 2-D RAKE receiver with 4-user scenario

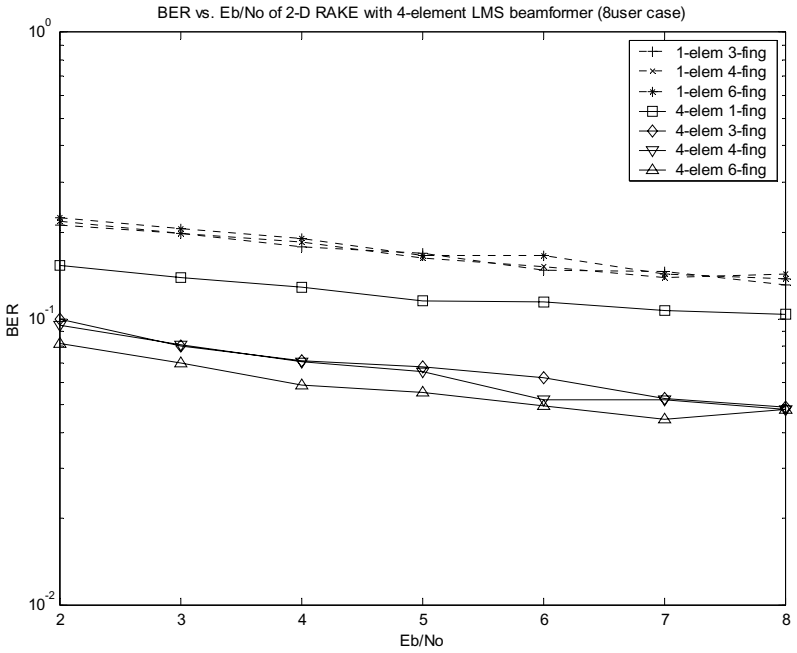

Figure 6.5.40: BER vs. Eb/No for a 4-element LMS 2-D RAKE receiver with 8-user scenario

6.5.2.2.2 DMI beamforming

Figures 6.5.41 through 6.5.44 show the BER performance curves as a function of Eb/No for the DMI beamforming based 2-D RAKE receiver with 2 and 4 antenna elements in both the underloading and the overloading scenarios. The curves have the same general trend as those for the LMS case.

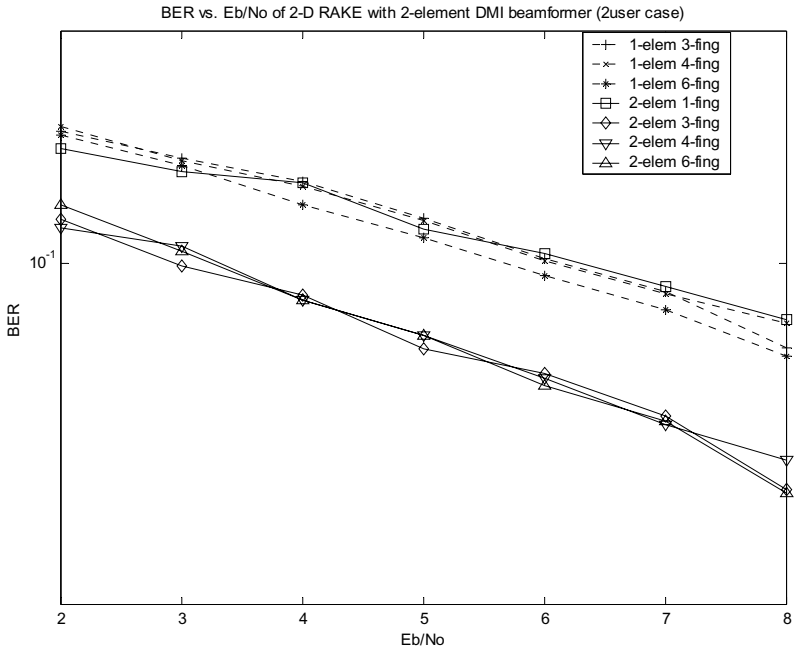

Figure 6.5.41: BER vs. Eb/No for a 2-element DMI 2-D RAKE receiver with 2-user scenario

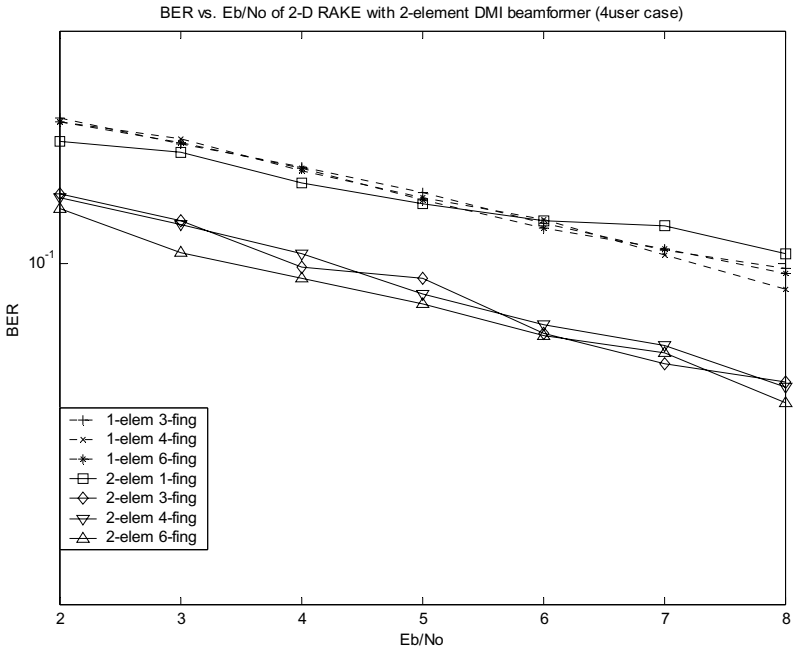

Figure 6.5.42: BER vs. Eb/No for a 2-element DMI 2-D RAKE receiver with 4-user scenario

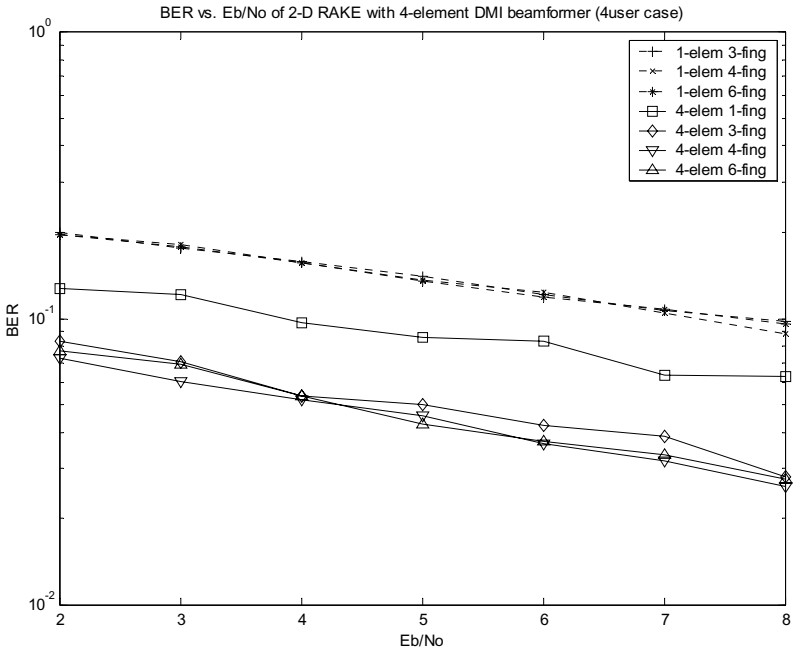

Figure 6.5.43: BER vs. Eb/No for a 4-element DMI 2-D RAKE receiver with 4-user scenario

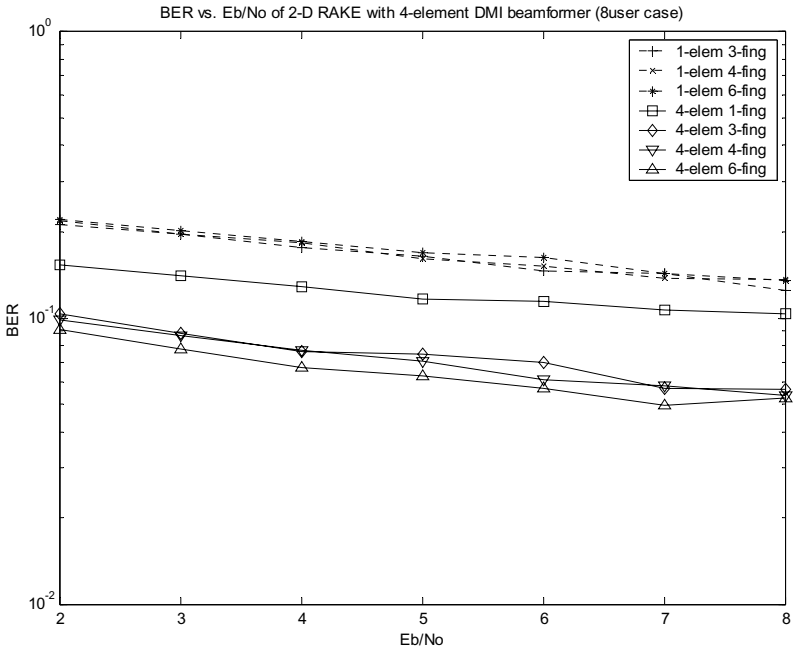

Figure 6.5.44: BER vs. Eb/No for a 4-element DMI 2-D RAKE receiver with 8-user scenario

6.5.2.2.3 RLS beamforming

Figures 6.5.45 through 6.5.48 show the BER performance curves as a function of Eb/No for the DMI beamforming based 2-D RAKE receiver with 2 and 4 antenna elements in both the underloading and the overloading scenarios. The curves have the same general trend as those for the LMS and the DMI cases.

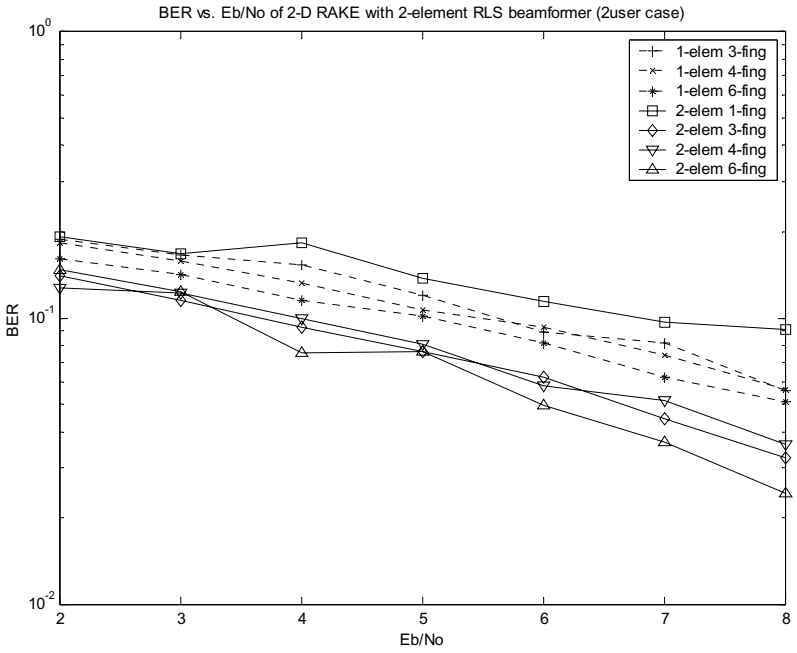

Figure 6.5.45: BER vs. Eb/No for a 2-element RLS 2-D RAKE receiver with 2-user scenario

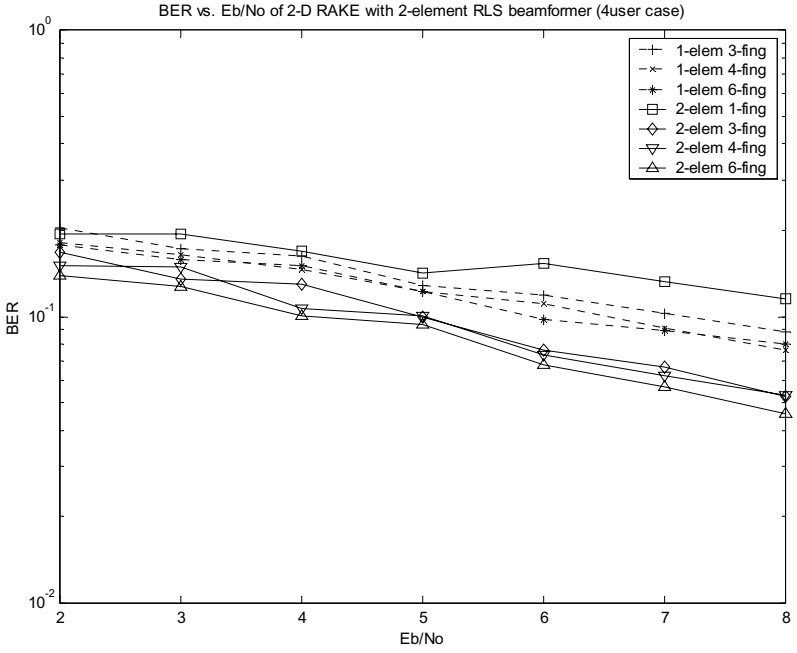

Figure 6.5.46: BER vs. Eb/No for a 2-element RLS 2-D RAKE receiver with 4-user scenario

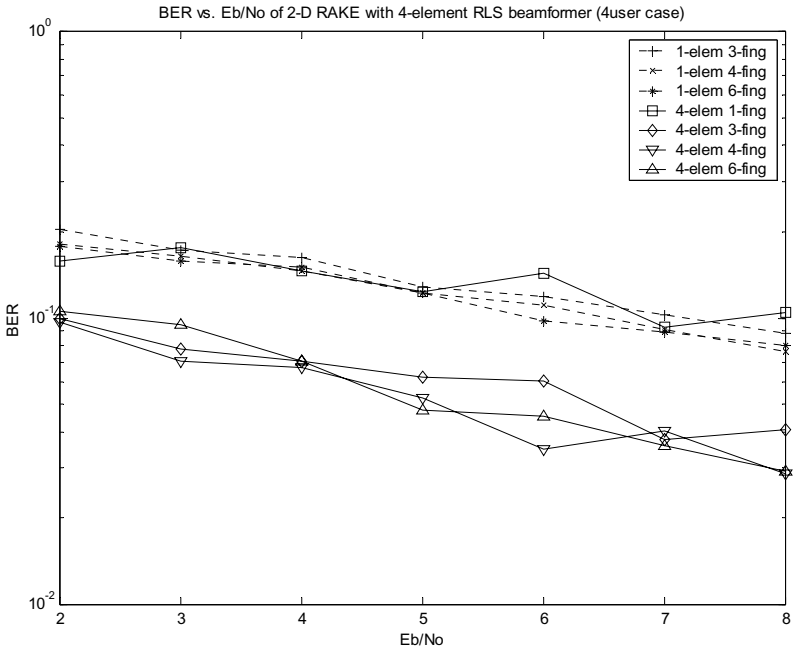

Figure 6.5.47: BER vs. Eb/No for a 4-element RLS 2-D RAKE receiver with 4-user scenario

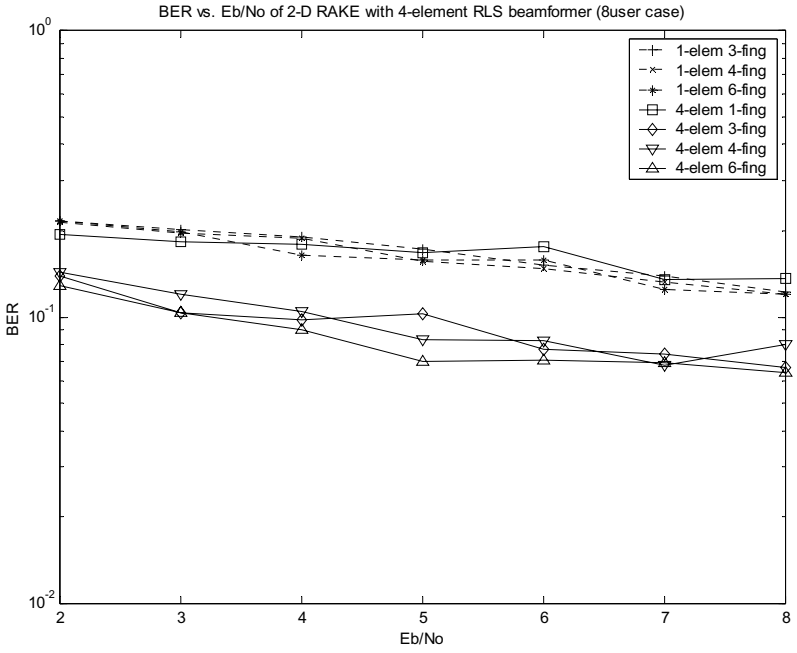

Figure 6.5.48: BER vs. Eb/No for a 4-element RLS 2-D RAKE receiver with 8-user scenario

6.6 Summary

In this chapter, we present the simulation results of different PSA 2-D RAKE receivers in both the macrocellular circular channel and the microcellular elliptical channel. We provide the BER vs. user and the BER vs. Eb/No performances of the LMS, DMI and RLS based 2-D RAKE receivers as a function of number of antenna elements and number of RAKE fingers. We compare the performance curves of the 2-D RAKE receiver with both the conventional 1-D RAKE receiver and the conventional beamformer. From the comparisons, we conclude that in almost all the cases, the 2-D RAKE receiver outperforms both the conventional 1-D RAKE and the conventional beamformer by a significant margin. We also see that, RAKE combining gives improved performance in the circular channel, while the beamforming suits better in the elliptical channel. Also we see that, all the PSA beamforming techniques employed in the 2-D RAKE receiver perform very similar in both the channels.

Chapter 7

Conclusions and Future Work

In this thesis, we investigate the performance of three different PSA coherent 2-D RAKE receivers intended for the uplink of the W-CDMA system. First, we present a detailed mathematical analysis of these PSA 2-D RAKE receivers with the uplink W-CDMA signal format. Then we set up a computer simulation test bed to compare the performance of these receivers in two different GBSB statistical channel environments with multipath Rayleigh fading. The BER performance versus both the number of users and Eb/No of all these receivers are compared with varying number of spatial and temporal processing parameters (e.g., number of antenna elements and RAKE fingers). It is shown that, in most of the cases, a combination of a beamformer with a small number of elements and a RAKE combiner is sufficient to outperform both the single element RAKE receiver and the single finger beamformer. It is also shown that, depending on the channel conditions; there is a performance tradeoff between the beamformer and the RAKE combiner of the 2-D RAKE receiver. The beamformer works well when the multipath AOA range is large, while the RAKE receiver shows better performance when many dominant multipaths are present in the channel. We compare the performance of the three PSA beamforming techniques used in the 2-D RAKE receiver, i.e., DMI, LMS and RLS adaptive beamforming. In most of the cases, the performance is very close to each other. We also derived the output SINR expression of a 2-D RAKE receiver using the generalized expression of an optimum beamformer. In this thesis, a detailed literature survey on different space-time processing techniques intended for CDMA is also provided.

7.1 Future Work

Based on the work that we have done in this thesis, a number of interesting research direction can be pursued in the future. These are outlined below.

1. Since the W-CDMA has pilot symbols defined in the uplink, we only concentrated on the PSA based beamforming techniques. It will be interesting to compare the performance of the blind beamforming based 2-D RAKE receivers with the PSA 2-D RAKE receiver.

2. Even though these receivers are attractive in terms of performance, their complexity may be too high to make them feasible for implementation in a base station. It will definitely be useful to show the complexity trade-offs of a 2-D RAKE receiver with the 1-D RAKE receiver and the conventional antenna array.

3. In Chapter 5, we derived the generalized optimum SINR expression for a 2-D RAKE receiver. However, we need to validate the expression and the assumptions that we made through simulation. Also, that analysis may be extended to derive the BER expression for the 2-D RAKE receiver.

4. In the simulation, we assumed that all the users have the same SF and hence the same data rate. It will be interesting, to shows the interference suppression performance of the antenna array for variable data rate users, which the W-CDMA is intended to support. Also, we assume perfect power control but the performance of 2-D RAKE receiver for imperfect power control scenario should be interesting.

5. For vector channel models, we used the GBSB elliptical and circular channel models. Even though they are more realistic than the simple parametric channel models, it would be even better if the performance is evaluated using measurement-based channel model.

6. Finally, all the 2-D RAKE receivers proposed for the W-CDMA are designed for the uplink. The downlink still remains to be explored even though space-time processing for the downlink is not very computationally practical.

REFERENCES

[Ada96] F. Adachi, K. Ohno, A Higashi, T. Dohi, and Y. Okumura, "Coherent multicode DS-CDMA mobile radio access," *IEICE Trans. Commun.*, vol. E79-B, no. 9, pp. 1316-1325, Sept 1996.

[Ann99] Monica Dell'Anna and A. Hamid Aghvami, "Performance of Optimum and Suboptimum Combining at the Antenna Array of a W-CDMA System," *IEEE J. Select. Areas Commun.*, Vol. 17, No. 12, pp. 2123-2137, Dec. 1999.

[Ber96] X Bernstein and A. M. Haimovic, "Space-Time Processing for Increased Capacity of Wireless CDMA," in *Proc.ICC'96*, vol. I, pp. 597-601.

[Ert98a] R. Ertel, P. Cardieri, K. Sowerby, T. Rappaport, and J. Reed, "Overview of spatial channel models for antenna array communication systems," *IEEE Personal Communications Magazine*, pp. 10-22, Feb. 1998.

[Ert98b] R. B. Ertel and J. H. Reed, *Antenna Array Systems: Propagation and Performance.* PhD thesis, Virginia Polytechnic Institute and State University, July 1999.

[ETS97] ETSI, "Selection procedures for the choice of radio transmission technologies of the UMTS (UMTS 30.03 version 3.1.0)," Eur. Telecommunications Standards Institute, Sophia Antipolis, Cedex, France, Nov 1997.

[God97] L. C. Godara, "Application of Antenna Arrays to Mobile Communications, Part II: Beamforming and Direction-of-Arrival Considerations," in *Proc. IEEE*, vol. 85, No. 8, pp. 1195-1245, Aug. 1997.

[Gro90] U. Grob, A. L. Welti, Z. Zollinger, R. Kung, and H. Kaufmann, "Micro-Cellular Direct Sequence Spread-Spectrum Radio System Using N-path RAKE receiver," *IEEE J. Select. Areas Commun.*, vol. JSAC-8(5), pp. 772-780, May 1990.

[Hay91] S. Haykin, *Adaptive Filter Theory.* Englewood Cliffs, NJ: Prentice Hall, 1991.

[Hig95] A. Higashi and T. Matsumoto, "Combined Adaptive RAKE Diversity (ARD and CODING for DPSK DS/CDMA mobile Radio," *IEEE J. Select. Areas Commun*., vol. JSAC-11(7), pp. 1076-1084, Sept. 1993.

[Kan90] R. E. Kane, K. S. Gong, and R. R. Kurth, "Performance of a RAKE Demodulator with Pre-Decision Multipath Thresholding," in *Proc. MILCOM '90*, pp. 1025-1029, May 1990.

[Kri96] H. Krim and M. Viberg, "Two decades of array signal processing research: the parametric approach," *IEEE Signal Processing Magazine*, 13(4):67-94, July 1996.

[Lib96] J. C. Liberti, Jr. and T. S. Rappaport, *Analysis of CDMA Cellular Radio Systems Employing Adaptive Antennas.* PhD thesis, Virginia Polytechnic Institute and State University, Sept. 1995.

[Lit96] J. Litva and T. K.-Y. Lo, *Digital Beamforming in Wireless Communications.* Boston, MA: Artech House Publishers, 1996.

[Mon80] R. A. Monzingo and T. W. Miller, *Introduction to Adaptive Arrays.* New York: John Wiley & Sons, 1980.

[Nag94a] A. Naguib and A. Paulraj, "Performance of CDMA Cellular Networks with Base-Station Antenna Arrays," in *Proc. International Zurich Seminar on Digital Communications*, (Zurich, Switzerland), pp 87-100, Mar. 1994.

[Nag94b] A. F. Naguib, A. Paulraj, and T. Kailath, "Capacity Improvement with Base-Station Antenna Array in Cellular CDMA," *IEEE Trans. Veh. Tech.*, vol. VT-43(3), pp. 691-698, Aug. 1994.

[Nag96a] A. F. Naguib and A. Paulraj, *Adaptive Antennas for CDMA Wireless Networks.* PhD thesis, Stanford University, Aug 1996.

[Nag96b] A. F. Naguib and A. Paulraj, "Performance of Cellular CDMA with M-ary Orthogonal Modulation and Cell Site Antenna Arrays," *IEEE J. Select. Areas Commun.*, vol. 14-(9), pp. 1770-1783, Dec. 1996.

[Olip99] M. W. Oliphant, "The Mobile Phone Meets the Internet," *IEEE Spectrum*, pp. 20-28, Aug. 1999.

[Pad94] R. Padovani, " The capacity of CDMA Cellular: Reverse Link Field Test Results," in *Proc. International Zurich Seminar on Digital Communications*, (Zurich, Switzerland), pp. 56-66, March 1994.

[Pro95] J. G. Proakis, *Digital Communications.* McGraw-Hill, third ed., 1995.

[Pri58] R. Price and P. E. Green, "A communication technique for multipath channels," *Proceedings of the IRE*, vol.2 pp. 555-570, Mar. 1958.

[Pau97] A. Paulraj and C. B. Papadias, "Space-time processing for wireless communications," *IEEE Trans. Veh. Technol.*, vol. 43, pp.691-697, Aug. 1994.

[Pet96] P. Petrus, J. H. Reed, and T. S. Rappaport, "Geometrically based statistical channel model for macrocellular mobile environments," in *Proc., IEEE Veh. Tech. Conf.,* pp. 844-848, Apr. 1996.

[Qua92] Qualcomm Inc., *Wideband Spread Spectrum Digital Cellular System*, April 1992. Proposed EIA/TIA Interim Standard.

[Sal87] A. A. M. Saleh, and R. A. Valenzula, " A Statistical model for Indoor Multipath Propagation," *IEEE J. Select. Areas Commun.*,vol. JSAC-5, No.2, pp. 128-137, Feb. 1987.

[Spe97] Q. Spencer, M. Rice, B. Jeffs, and M. Jensen, "A statistical model for angle of arrival in indoor multipath propagation," in *Proc., IEEE Veh. Tech. Conf.*, 1997.

[Sua93] B. Suard, A. Naguib, G. Xu, and A. Paulraj, "Performance Analysis of CDMA Mobile Communication Systems using Antenna Arrays," in *Proc. ICASSP'93*, vol. VI, (Minneapolis, MN), pp. 153-156, Apr. 1993.

[Tan97] S. Tanaka, M. Sawasashi, and F. Adachi, "Pilot symbol-assisted decision-directed coherent adaptive array diversity for DS-CDMA mobile radio reverse link," *IEICE Trans. Commun.*, vol. E80-A, pp.2445-2454, Dec. 1997.

[Tan00] S. Tanaka, M. Sawasashi, and F. Adachi, "Experiments on Coherent Adaptive Anrenna Array Diversity for Wideband DS-CDMA Mobile Radio," *IEEE J. Select. Areas Commun.*, Vol. 18, No. 8, pp. 1495-1504, Aug. 2000.

[Tho96] J. S. Thompson, P. M. Grant, and B. Mulgrew, "Smart Antenna Arrays for CDMA Syatems," *IEEE Pers. Commun.*, vol. 3, no. 5, pp. 16-25, Oct. 1996.

[UMTSa] Universal Mobile Telecommunications System, "Physical channels and mapping of transport channels onto physical channels (FDD)," TS 25.211 v3.2.0 (2000-03).

[UMTSb] Universal Mobile Telecommunications System, "Spreading and modulation (FDD)," TS 25.213 v3.2.0 (2000-03).

[UMTSc] Universal Mobile Telecommunications System, "Multiplexing and channel coding (FDD)," TS 25.212 v3.2.0 (2000-03).

[Vee88] B. D. Veen and K. M. Buckley, "Beamforming: A Versatile Approach to Spatial Filtering," *IEEE ASSP Mag.,* April 1998, pp. 4-24.

[Zen99] M. Zeng, A. Annamalai, and V. K. Bhargava, "Recent Advances in Cellular Wireless Communications," *IEEE Communications Magazine*, vol. 37, No. 9, Sept 1999.

VITA

Kazi A. Zahid was born on May 1, 1973 in Chittagong, Bangladesh. He received his Bachelor of Science Degree in Electrical and Electronic Engineering in July 1997 from Bangladesh University of Engineering and Technology, Dhaka, Bangladesh. He worked as a lecturer in the EEE Department of his alma mater for a year. He started to pursue his M.S. in Virginia Tech from Fall 1998. In August 1999, he joined the Mobile and Portable Radio Research Group, where he worked with Dr. J. H. Reed in the area of space-time processing for the W-CDMA system.